**RAA 2021** Vol. **21** No. **5**, 107(38pp) doi: 10.1088/1674-4527/21/5/107

*http://www.raa-journal.org* *http://iopscience.iop.org/raa*

***R**esearch in*
***A**stronomy and*
***A**strophysics*

# The FAST Galactic Plane Pulsar Snapshot survey: I. Project design and pulsar discoveries*

J. L. Han[1,2,3], Chen Wang[1,2], P. F. Wang[1,2], Tao Wang[1,3], D. J. Zhou[1,3], Jing-Hai Sun[1,2], Yi Yan[1,3], Wei-Qi Su[1,3], Wei-Cong Jing[1,3], Xue Chen[1,3], X. Y. Gao[1,2], Li-Gang Hou[1,2], Jun Xu[1,2], K. J. Lee[1,4], Na Wang[6,7], Peng Jiang[1,2], Ren-Xin Xu[5], Jun Yan[1,2], Heng-Qian Gan[1,2], Xin Guan[1,2], Wen-Jun Huang[8], Jin-Chen Jiang[4,5], Hui Li[1,2], Yun-Peng Men[4,5], Chun Sun[1,2], Bo-Jun Wang[4,5], H. G. Wang[8], Shuang-Qiang Wang[6,7], Jin-Tao Xie[6,7], Heng Xu[4,5], Rui Yao[1,2], Xiao-Peng You[9], D. J. Yu[1,2], Jian-Ping Yuan[6,7], Rai Yuen[6,7], Chun-Feng Zhang[4,5] and Yan Zhu[1,2]

[1] National Astronomical Observatories, Chinese Academy of Sciences, Beijing 100101, China; *hjl@nao.cas.cn; wangchen@nao.cas.cn*
[2] CAS Key Laboratory of FAST, NAOC, Chinese Academy of Sciences, Beijing 100101, China
[3] School of Astronomy, University of Chinese Academy of Sciences, Beijing 100049, China
[4] Kavli Institute for Astronomy and Astrophysics, Peking University, Beijing 100871, China
[5] Department of Astronomy, Peking University, Beijing 100871, China
[6] Xinjiang Astronomical Observatory, Chinese Academy of Sciences, Urumqi 830011, China
[7] Key Laboratory of Radio Astronomy, Chinese Academy of Sciences, Nanjing 210008, China
[8] Department of Astronomy, Guangzhou University, Guangzhou 510006, China
[9] School of Physical Science and Technology, Southwest University, Chongqing 400715, China

Received 2021 January 14; accepted 2021 April 20

**Abstract** Discovery of pulsars is one of the main goals for large radio telescopes. The Five-hundred-meter Aperture Spherical radio Telescope (FAST), that incorporates an L-band 19-beam receiver with a system temperature of about 20 K, is the most sensitive radio telescope utilized for discovering pulsars. We designed the *snapshot* observation mode for a FAST key science project, the Galactic Plane Pulsar Snapshot (GPPS) survey, in which every four nearby pointings can observe *a cover* of a sky patch of 0.1575 square degrees through beam-switching of the L-band 19-beam receiver. The integration time for each pointing is 300 seconds so that the GPPS observations for a cover can be made in 21 minutes. The goal of the GPPS survey is to discover pulsars within the Galactic latitude of $\pm 10^\circ$ from the Galactic plane, and the highest priority is given to the inner Galaxy within $\pm 5^\circ$. Up to now, the GPPS survey has discovered 201 pulsars, including currently the faintest pulsars which cannot be detected by other telescopes, pulsars with extremely high dispersion measures (DMs) which challenge the currently widely used models for the Galactic electron density distribution, pulsars coincident with supernova remnants, 40 millisecond pulsars, 16 binary pulsars, some nulling and mode-changing pulsars and rotating radio transients (RRATs). The follow-up observations for confirmation of new pulsars have polarization-signals recorded for polarization profiles of the pulsars. Re-detection of previously known pulsars in the survey data also leads to significant improvements in parameters for 64 pulsars. The GPPS survey discoveries are published and will be updated at `http://zmtt.bao.ac.cn/GPPS/`.

**Key words:** pulsars: general

## 1 INTRODUCTION

Pulsars are fantastic objects with many physically extreme properties that are not understood yet. It is widely believed that they are degenerate stars consisting of neutrons but their internal content and structure are hitherto not known (Özel & Freire 2016). Inside neutron stars, neutrons could be mixed with quarks or strangeons (Alcock et al. 1986; Xu 2003; Wu et al. 2020). Such physics can be observationally

* News and views on this paper

constrained by the discovery of pulsars with high masses (e.g. Demorest et al. 2010; Antoniadis et al. 2013; Cromartie et al. 2020) or short spin periods (Backer et al. 1982; Hessels et al. 2006). Pulsars have strong magnetic fields, in general around $10^{12}$ G, but $10^{13} - 10^{14}$ G in magnetars (Kaspi & Beloborodov 2017) or $10^{8} - 10^{9}$ G in millisecond pulsars (MSPs). Their emission can be continuous but may null for some periods (e.g. Wang et al. 2007, 2020b) or show a giant pulse occasionally (e.g. Jessner et al. 2010; McKee et al. 2019). The pulse profiles can have one peak, two peaks or many peaks (e.g. Rankin 1993; Lyne & Manchester 1988; Manchester & Han 2004), which may be generated in different regions of the magnetosphere and come from different parts of an emission beam (Cordes 1978; Thorsett 1991; Phinney 1992; Mitra & Deshpande 1999; Han & Manchester 2001). The profiles can be highly polarized, even 100% linearly polarized, and the polarization angle swings follow S-curves (e.g. Lyne & Manchester 1988; Han et al. 2009). The circular polarization has diverse behaviors, often with reversed senses for the central profile peak but keeping one sense for the shoulder components (Han et al. 1998). The periodic emission of pulses from some MSPs is very stable, with long-term stability even better than atomic clocks (Hobbs et al. 2020), while the periods of young pulsars occasionally have a glitch (Lyne et al. 2000; Wang et al. 2000; Yuan et al. 2010; Espinoza et al. 2011).

The discovery of pulsars has been a main task for large telescopes. Immediately after the first discovery (Hewish et al. 1968), many large radio telescopes, such as the Jodrell bank 76 m telescope (Davies et al. 1968, 1973; Clifton & Lyne 1986; Clifton et al. 1992), the Molonglo Observatory Synthesis Telescope (Large & Vaughan 1971; Manchester et al. 1978), the Parkes radio telescope (Robinson et al. 1968; Komesaroff et al. 1973), the 91 m old Green Bank Telescope (Damashek et al. 1978, 1982), and the Arecibo telescope (e.g. Hulse & Taylor 1974; Cordes et al. 2006), have been used for pulsar hunting sooner or later. The new Green Bank Telescope (GBT, Hessels et al. 2008; Boyles et al. 2013; Stovall et al. 2014) and the Giant Metrewave Radio Telescope (GMRT, Bhattacharyya et al. 2016; Surnis et al. 2018; Bhattacharyya et al. 2019) also joined in the efforts later. It has been very clear that instrument improvements are the key to finding more pulsars. The first pulsar discoveries were made by the narrow-band signal recording at that time (e.g. Hewish et al. 1968). Multi-channel signal recording and de-dispersion were big steps forward (e.g. Manchester et al. 1978), leading to many more new discoveries. The fast Fourier transform (FFT) technology for long-time data-recording and folding is an another step (e.g. Komesaroff et al. 1973; Damashek et al. 1978). Later, cooling receivers at the L-band (i.e. the radio frequency band around 1.4 GHz) with a very wide bandwidth certainly made sense for improving the sensitivity, which is the key to detecting distant weak pulsars (Johnston et al. 1992; Manchester et al. 1996; Lyne et al. 1998). Multi-beam receivers, first mounted on the Parkes telescope (Staveley-Smith et al. 1996), can not only speed the survey but also give a much longer integration time so that an unprecedented sensitivity can be achieved. The pulsar survey of the Galactic plane by the Parkes telescope (Manchester et al. 2001; Morris et al. 2002; Kramer et al. 2003; Hobbs et al. 2004; Faulkner et al. 2004; Lorimer et al. 2006a), and later extended to mid to high Galactic latitudes (Burgay et al. 2006; Keith et al. 2010), led to a great increase in pulsar discoveries. Recently, low frequency arrays, which incorporate beam-forming technology, could survey very large sky areas for pulsars concurrently, also leading to more new discoveries, such as the pulsar survey by the Low-Frequency Array (LOFAR, Sanidas et al. 2019). In addition, advances in candidate selection technology, such as sorting and scoring (e.g. Keith et al. 2009; Eatough et al. 2009), image pattern recognition (Zhu et al. 2014) and classification approaches (Lyon et al. 2016), also help pulsar discoveries. Single pulse search technology (Cordes & McLaughlin 2003) led to the discovery of RRATs (McLaughlin et al. 2006) and fast radio bursts (FRBs, Lorimer et al. 2007). In addition, the acceleration search technology (Ransom 2001; Eatough et al. 2013a; Andersen & Ransom 2018) led to discoveries of many binaries such as those in Terzan 5 (e.g. Ransom et al. 2005) and even a millisecond pulsar in a triple system (Ransom et al. 2014).

Up to now, there are about 3000 pulsars in the updated version of the Australia Telescope National Facility (ATNF) Pulsar Catalogue (Manchester et al. 2005). Most of them are located in the Galactic disk (Yao et al. 2017), and a few tens are in the Magellanic clouds (McConnell et al. 1991; Crawford et al. 2001; Manchester et al. 2006; Ridley et al. 2013). Historically, big increases in pulsar numbers always come from dedicated pulsar surveys, mostly on the Galactic disk, for example, the Molonglo2 survey (Manchester et al. 1978) which led to the discovery of 155 pulsars, the Parkes Southern Pulsar Survey (Lyne et al. 1998) which revealed 101 pulsars and the Parkes multi-beam pulsar survey (Manchester et al. 2001; Morris et al. 2002; Kramer et al. 2003; Hobbs et al. 2004; Faulkner et al. 2004; Lorimer et al. 2006a) which discovered more than 700 pulsars. In addition, the Fermi satellite has recorded many Gamma-ray pulsars (Abdo et al. 2013). Currently, many pulsar surveys are still going on, for example, (1) the Deep Multibeam Survey Processing (DMSP)[1] using Parkes telescope, which has discovered 15 new pulsars; (2) the SUrvey for Pulsars and Extragalactic

[1] http://astro.phys.wvu.edu/dmb/

Radio Bursts (SUPERB) using Parkes telescope (Keane et al. 2018; Spiewak et al. 2020); (3) the GBT 350-MHz Drift Scan Survey[2], which has found 35 new pulsars, including 7 MSPs; (4) the Green Bank North Celestial Cap (GBNCC) pulsar survey[3] (Stovall et al. 2014), which has discovered 190 pulsars, including 33 MSPs and 24 RRATs; (5) the LOFAR Pilot Pulsar Survey (LPPS) and the LOFAR Tied-Array All-Sky Survey (LOTAAS)[4], which have revealed 81 new pulsars (Sanidas et al. 2019; Michilli et al. 2020); (6) the GMRT High-resolution Southern Sky Survey for Pulsars and Transients (Bhattacharyya et al. 2016, 2019); (7) the Pulsar ALFA (PALFA) survey[5] by the Arecibo telescope, which has discovered 208 pulsars (e.g. Cordes et al. 2006; Lazarus et al. 2015); (8) the Arecibo 327 MHz Drift Survey[6] which has found 95 pulsars including 10 MSPs and 20 RRATs. Though some discoveries of these surveys have been published in papers (e.g. Ng et al. 2015), many of the newly discovered pulsars are just listed in webpages and not yet formally published.

With many pulsars found already, why do we have to discover more? What new physics or science can be further uncovered? There have been many exciting progresses on pulsar science, such as the discovery of the first pulsars (Hewish et al. 1968) which revealed an extreme matter state in the Universe and one kind of end product of stellar evolution, the discovery of the first binary pulsar (Hulse & Taylor 1975) and double pulsars (Burgay et al. 2003; Lyne et al. 2004) which have been used for experimental tests of predictions from the general relativity of gravitational radiation (Taylor & Weisberg 1989; Kramer et al. 2006) and the discovery of MSPs (Backer et al. 1982; Hessels et al. 2006) which constrains the equation of state of matter. For new surveys, the most important goal is to find exotic pulsars, especially pulsars with a very short spin period or a short orbital period (see e.g. Stovall et al. 2018), or with a large mass (e.g. Demorest et al. 2010; Cromartie et al. 2020) or in a neutron-star black-hole binary (see e.g. Faucher-Giguère & Loeb 2011). Discovery of a pulsar with a spin period of less than 1 ms (e.g. efforts by Han et al. 2004b) or a very massive pulsar (see a complete list of mass measurements in Shao et al. 2020) would constrain the compositions of matters in the interior of neutron stars (e.g. Hu et al. 2020) and have implications for quark or strangeon stars (e.g. Alcock et al. 1986; Xu 2003); discovery of binary pulsars in various orbits can make breakthroughs in the current knowledge of stellar evolution (e.g. Jiang et al. 2015; Tauris et al. 2017; Wang & Liu 2020). Since at least 10 mergers of stellar binary black holes and one merger of binary neutron stars were detected by the advanced Laser Interferometer Gravitational wave Observatory (LIGO, e.g. Abbott et al. 2016, 2019, 2020), it is expected to discover a neutron-star black-hole binary in the near future (e.g. Shao & Li 2018; Chattopadhyay et al. 2021), which can better constrain the theory of gravity and general relativity better than any known double neutron-star binaries (e.g. Kramer et al. 2006; Stovall et al. 2018) or white-dwarf neutron-star binaries (e.g. Freire et al. 2012). Even if the parameters of newly discovered pulsars are within the ranges of known pulsars, more new distant pulsars can be exploited to explore the interstellar medium in a large unexplored region of the Galactic disk such as the farther spiral arms for both the electron density distribution and interstellar magnetic fields (e.g. Han et al. 2002; Yao et al. 2017; Han et al. 2018); more weaker pulsars in the solar vicinity can even probe more detailed properties of the interstellar medium (e.g. Han et al. 2004a; Xu & Han 2019). Discoveries of pulsars in other galaxies (McConnell et al. 1991; Manchester et al. 2006; Ridley et al. 2013; van Leeuwen et al. 2020) can probe the intergalactic medium if the contributions from the Milky Way and the host galaxies can be accounted for properly.

The Five-hundred-meter Aperture Spherical radio Telescope (FAST, Nan 2008; Nan et al. 2011) has the largest collecting area for radio waves, with an aperture of 300 m in diameter. Mounted together with the 19-beam L-band receiver that has a system temperature of about 20 K, FAST is currently the most sensitive radio telescope for discovering pulsars. Construction of FAST was completed in September 2016, and the commissioning was finished in January 2020 (Jiang et al. 2019). During the initial commissioning phase when FAST was not ready to track a source, a drifting survey, the so-called Commensal Radio Astronomy FAST Survey (CRAFTS, Li et al. 2018), discovered 124 pulsars as reported on the webpage[7]. By viewing the plots produced from the search pipeline, Qian et al. (2019) discovered the first FAST pulsar. Already published discoveries from this drift survey include a pulsar with nulling and subpulse drifting (Zhang et al. 2019), an FRB (Zhu et al. 2020) and 11 new pulsars (Cameron et al. 2020). Targeted pulsar searches using FAST have also led to discoveries of a binary millisecond pulsar in the globular cluster M13 (Wang et al. 2020a) and an eclipsing binary millisecond pulsar in M92 (Pan et al. 2020). Obviously FAST has great prospects to discover pulsars (Qian et al. 2020). Based on a simulation, Smits et al. (2009) estimated that 5200 pulsars can be discovered by FAST, which is probably over-optimistic according to Lorimer et al. (2019) and Huang & Wang (2020), and there may be much fewer depending on the emission models. The number of actual discoveries in the Arecibo multibeam

[2] http://astro.phys.wvu.edu/GBTdrift350/
[3] http://astro.phys.wvu.edu/GBNCC/
[4] https://www.astron.nl/lotaas/
[5] http://www.naic.edu/~palfa/newpulsars/
[6] http://www.naic.edu/~deneva/drift-search/
[7] https://crafts.bao.ac.cn/pulsar/

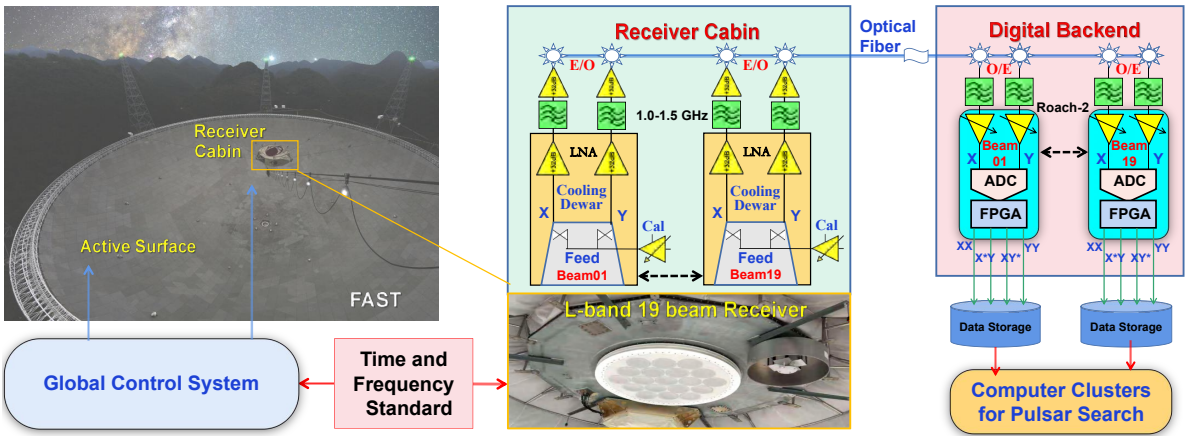


**Fig. 1** The observational system of FAST for the GPPS survey. See details in text.

pulsar survey (Cordes et al. 2006; Lazarus et al. 2015) is much less than what is expected from similar simulations, mainly because there are much fewer pulsars in the outer region of the Galactic disk.

With the advantage of its large collection area and sensitive receivers, FAST is an excellent radio telescope to discover more weak pulsars, distant pulsars or pulsars in binary systems. Because most pulsars were born in the Galactic disk and hence the distribution of pulsars is concentrated in the Galactic plane, we designed the Galactic Plane Pulsar Snapshot (GPPS) survey, and carried out the pulsar survey in the Galactic latitude range of $\pm 10°$ from the Galactic plane, with the highest priority given to the inner Galactic disk within the Galactic latitude of $\pm 5°$. At the end of 2019, the GPPS project was selected by the FAST science committee as one of the five FAST high-priority key science projects for the next few years. In this paper, we briefly introduce the observational system and survey strategy in Section 2, and introduce the observation status and data-processing in Section 3. Discoveries of new pulsars are presented in Section 4. Re-detection of known pulsars and improved parameters are described in Section 5. Some perspectives are discussed in Section 6.

## 2 INSTRUMENTS AND SURVEY DESIGN

The observational system of FAST for the GPPS survey is illustrated in Figure 1, which consists of the FAST facility with an active surface and the mobile receiver cabin controlled by the Global Control System, the L-band 19-beam receiver, the digital backends, the data storage system and the computer cluster for data processing.

### 2.1 The FAST and Receivers

The FAST facility consists of a huge active spherical surface as the main reflector and the mobile receiver cabin (Nan et al. 2011). The reflector has a diameter of 500 m. When FAST observes a source, according to its location in the sky, part of the spherical surface with a diameter of 300 m is deformed from the spherical

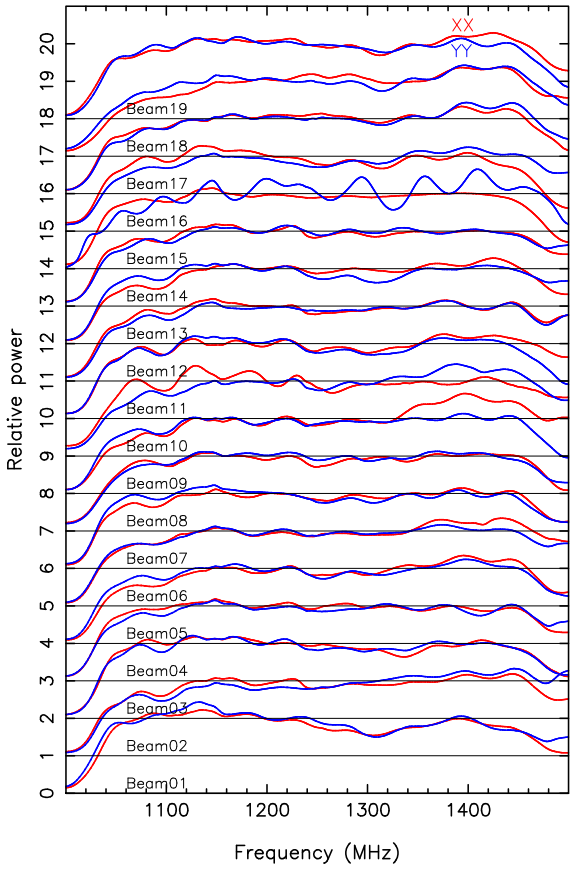


**Fig. 2** The complete bandpass for the L-band 19-beam receivers, represented by the standard deviation of actual data from an example of snapshot observations, after narrow-band and wide-band RFI are efficiently mitigated by using the ArPLS and SumThreshold algorithms (see Zeng et al. 2021, for details). The bandpass spectrum has been measured and is related to the system temperature in some parts of the band by Jiang et al. (2020), and the curves have a mean amplitude around 22 K in general, depending on beam and frequency.

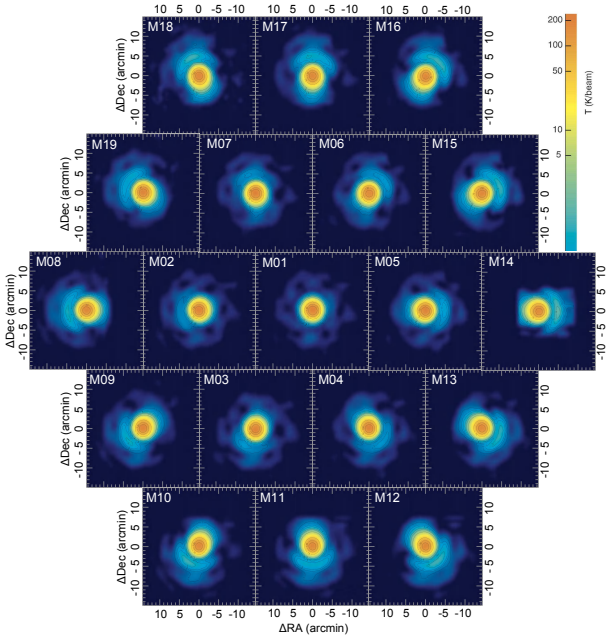


**Fig. 3** Beam pattern of the L-band 19-beam receiver of FAST obtained from the scanning observations of 3C 454.3 and integrated in the frequency range of 1050 – 1450 MHz. A low level of sidelobes is displayed on enhanced log-scales.

surface to a quasi-paraboloidal surface and acts as the main reflector, so that radio waves can focus. This is controlled and monitored by the Global Control System, and is adjusted by the dynamic-support system, currently based on the pre-set standard paraboloid model according to pre-measurements. The deviation from a paraboloid of the so-adjusted surface, as measured by control nodes, is about 3 mm, so that the measured efficiency of the 300 m aperture radio telescope is about 60% at the L-band (Jiang et al. 2019). The receiver cabin, which is suspended and driven by six cables that run over six towers around the huge reflector, can be moved to any designed focus position with an accuracy of about 10 mm. When a radio source moves in the sky, the active part of the main surface and the mobile receiver cabin are simultaneously adjusted, so that the receiver keeps moving and stays at the designed focus of the series of paraboloids. This makes the telescope able to track a radio source properly.

Though the best frequency range to discover distant pulsars several kpc away in the Galactic disk is about 2 to 3 GHz (Xu et al. 2011), currently the best receiver available in the receiver cabin is the L-band 19-beam receiver (Jiang et al. 2020). It formally works in the frequency range from 1050 to 1450 MHz, but in practice radio signals from 1000 to 1500 MHz are all received with a degraded band of only 20 – 40 MHz at each edge, see Figure 2 for the bandpasses of the 19-beam receiver. The bandpasses are all very stable as we have checked the real observational data acquired

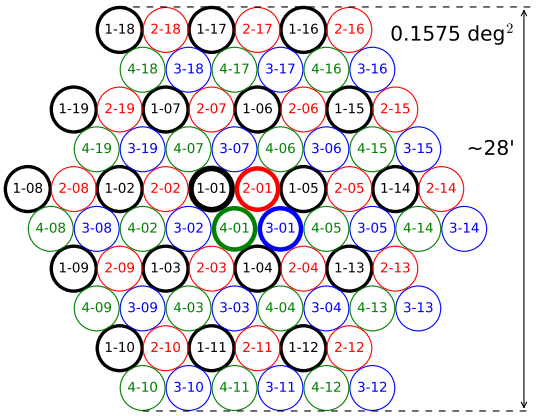


**Fig. 4** A snapshot made by four pointings via three-beam switchings of the 19 beams of the L-band 19-beam receiver of FAST which can survey a *cover* of a sky area of 0.1575 square degrees.

from the GPPS survey after narrow- and wide-band radio frequency interference (RFI) is efficiently mitigated by using the ArPLS and SumThreshold algorithms (see Zeng et al. 2021, for details). The RFI is more serious in daytime, occupying about 10% of the band; while it is much better in the nighttime and RFI could sometimes disappear completely. See figure 24 and figure 25 in Jiang et al. (2020) to ascertain the RFI situation in 2019 at the FAST site.

The receiver feeds illuminate a quasi-parabolic area forming an aperture 300 m in diameter, without spillover radiation due to large reflectors surrounding that area. The beam size is about $3'$ in the L-band, varying with frequency in the range of $2.8'$ for 1440 MHz to $3.5'$ at 1060 MHz (see table 2 in Jiang et al. 2020). The beams of the L-band 19-beam receiver are well organized, and the outer beams have more obvious side lobes and are more aberrated, as illustrated in Figure 3. For any radio source within 26.4° of the zenith, the system temperature is about 20 K and FAST can track the source by the full illumination area with a full gain in $G$ of about 16 K Jy$^{-1}$. The outer beams have a smaller aperture efficiency, with an additional degradation of about 85%. Outside the zenith angle (i.e. $26.4^\circ$ <ZA< $40^\circ$) of the full illumination, the gain and system temperature further degrade due to partial illumination.

Therefore, we conclude that three aspects of FAST, the huge surface, the accurate positioning of the surface and receiver, and the excellent performance of the L-band 19-beam receiver, make FAST the most sensitive radio telescope currently in the world to survey pulsars.

### 2.2 The Snapshot Observation Mode

As mentioned above, the pointing changes of FAST to a new source are realized by adjusting the main surface

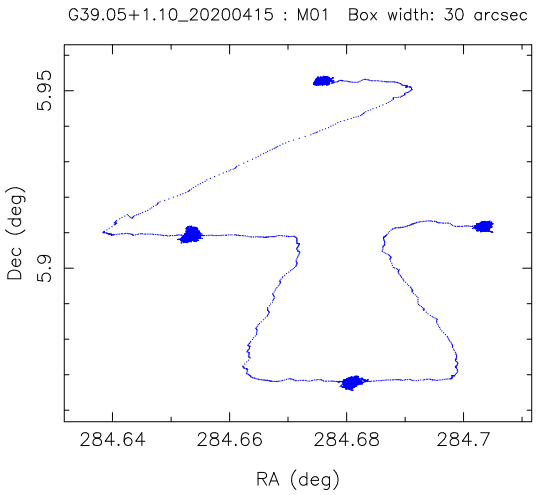


**Fig. 5** An example of the pointing trajectory in the sky of central beam of the L-band 19-beam receiver during GPPS observations of a cover.

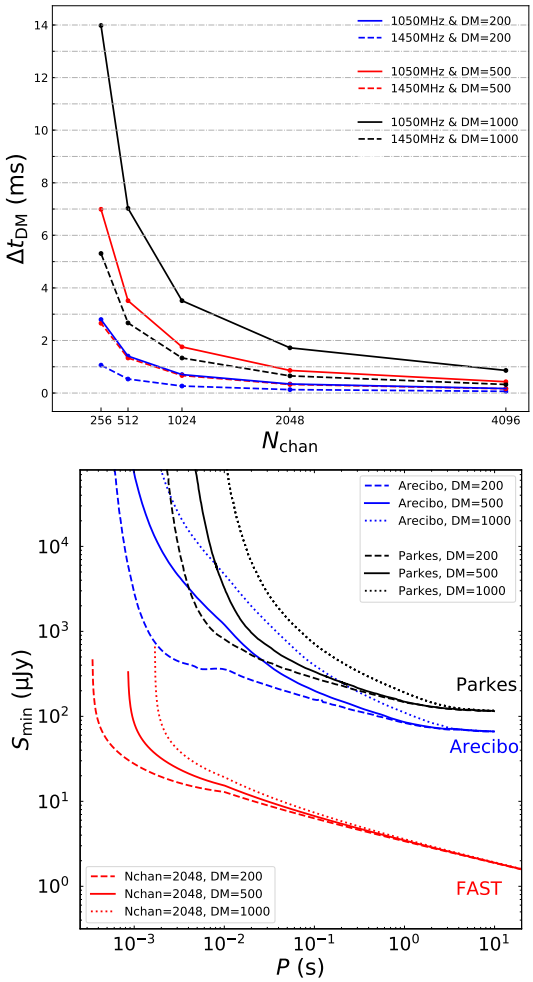


**Fig. 6** *Top*: the channel DM smearing time of two frequency channels at $\nu = 1050$ MHz and 1450 MHz, calculated by $83(DM/100)(\nu/100\ \mathrm{MHz})^{-3}\Delta\nu$ (in ms) for three example DM values. Here $\nu$ and $\Delta\nu$ have the unit of MHz, and $\Delta\nu$ is the channel bandwidth. *Bottom*: the $10\sigma$ detection sensitivity curves of the GPPS survey with parameters listed in Table 1 and an assumed 10% pulse width for a pulsar with a period $P < 10$ ms but declining with $P^{-1/2}$ when the period $P > 10$ ms. The scattering time of $3.2(DM/100)^{3.5}(\nu/100\ \mathrm{MHz})^{-5}\Delta\nu$ (in ms) and the channel DM smearing time as described above has been calculated at $\nu = 1100$ MHz and combined with the sampling time for drawing the sensitivity curves. Compared to the survey sensitivity curves of the Parkes multibeam survey (Manchester et al. 2001) and the Arecibo PALFA survey (Cordes et al. 2006), the FAST GPPS survey is super sensitive, especially for MSPs (see Fig. 13 below).

according to the pre-set standard paraboloid model and by positioning the receiver cabin at the designed focus. This takes a few minutes for the mechanical movements and cable stabilization. The pointing accuracy of FAST is better than $8''$ (Jiang et al. 2020), according to real measurements for strong sources.

In the receiver cabin, the L-band 19-beam receiver is mounted on a Stewart manipulator which acts as a stabilizer depressing the vibration caused by flexible cables (Jiang et al. 2019). In the limited range of a few mm, the receiver can be finely adjusted to the desired position and tilted to a designed angle within only a few seconds. Considering this very fine feature which is enough for adjusting telescope pointing for several arcminutes, we designed the snapshot observation mode (see Fig. 4) in four steps: (1) first a normal pointing is made to a desired position in the sky, working as pointing No.1, and then tracking observation is carried out for some time, e.g. 5 minutes for the GPPS survey. All data from the 19-beam receiver can be recorded; (2) second, the central beam (certainly also other beams) is offset by $3'$ to the right, working as pointing No.2, and then tracking observations and data-recording can be made in the same mode; (3) then it is offset by $3'$ to the lower-right and tracking, working as pointing No.3; and (4) finally offset by $3'$ to the left and tracking, working as pointing No.4. With these four points, a *cover* of the sky patch of about 0.1575 square degrees can be surveyed. An example for the trajectory of the central beam in the sky plane during observations of a cover is displayed in Figure 5. The beam-switching between these pointings can be realized within a few seconds. To ensure the accuracy of upcoming tracking, 20 seconds are given for each beam-switching. The GPPS observations for a cover therefore cost only 21 minutes, including the four tracking observations each with an integration time of 5 minutes plus the three beam-switches each lasting 20 seconds. The snapshot observation mode enables high efficiency for the usage of telescope time. From the real observation data, we found that the stability of FAST pointings is better than $4''$.

For the snapshot survey of the Galactic plane, the L-band 19-beam receiver is rotated to be parallel with the Galactic plane, i.e., beams No.08, No.02, No.01, No.05 and No.14 (see Fig. 4) are aligned with the Galactic plane, so that beams observed in different covers can be easily connected continuously.

The telescope control parameters and the position of the phase-center of the central beam receiver are recorded in an xlsx file, with proper time stamps, forming part of the metadata of FAST operations. Combining these metadata data and the original fits data files recorded by the digital backends (see below), one can make a proper fits file for each beam of every pointing.

In the open risk-share observation session of FAST in 2019, we successfully designed and tested the snapshot observation mode in March 2019.

### 2.3 The Digital Backends and Data Storage

The radio signals from two orthogonal linear polarizations $X$ and $Y$, from each beam of the L-band 19-beam receiver, are amplified and filtered, and then transferred to the data-recording room via optical fibers connected with an optical transmitter and an optical receiver (see Fig. 1). The voltage signals are filtered against interference and aliasing, and then sampled and channelized by using a pulsar digital-backend developed on Re-configurable Open Architecture Computing Hardware-2 (ROACH2). After self-correlation and cross-correlation and also accumulation in the field-programmable gate array (FPGA) board, the power data of the four polarization channels of $XX$, $X^*Y$, $XY^*$ and $YY$ are produced. These data can be recorded with selected channel numbers, such as 4096, 2048, 1024 or even 512 channels, with accumulation times of 98.304 μs, 49.152 μs, 24.563 μs and 12.281 μs for four polarization channels or just two polarization channels (i.e., $XX$ and $YY$).

Specifically, for the GPPS survey observations, the digital backends work for recording data from 19 beams. The accumulation time, i.e., the sampling time of each channel, is taken as being $\tau_{\rm sampling} = 49.152$ μs. The $XX$ and $YY$ data are recorded for 2048 channels by default, though the data from 4096 channels with four polarizations were always recorded in the pilot phase of the GPPS survey before February 2020. These data are stored in fits files for each beam with proper timestamps, and each original fits file stores data for 12.885 s for four polarization channels or for 25.770 s for two polarization channels.

In addition, the amplified voltage signals $X$ and $Y$ are split and fed to a number of digital spectrometers, which can simultaneously work for spectral line observations for all 19 beams. We record the spectral data in the whole band between 1000 – 1500 MHz by using 1024 K channels and an accumulation time of 1 s as default, so that anyone who is interested in the spectral lines of the interstellar medium in the Galactic disk can have spectral data for free.

**Table 1** Relevant Parameters for the GPPS Survey

| Parameter | Value |
|---|---|
| FAST location: latitude | N 25.647° |
| FAST location: longitude | E 106.856° |
| Effective aperture diameter | 300 m |
| Beam size | $\sim 3'$ |
| Aperture efficiency | 60% |
| Beam number for a cover | $4 \times 19$ |
| $T_{\rm sys}$+$T_{\rm sky}$ | ∼25 K |
| Telescope gain | $\sim$16 K Jy$^{-1}$ |
| Sky region to obs. | $GB < 10°$ |
| Zenith angle limit for a full gain | $< 26.4°$ |
| Covers to obs. | 16 538 |
| Obs. freq. range | 1.0–1.5 GHz |
| Freq. channel number | 2048 |
| Freq. resolution | 0.24414 MHz |
| Effective useful bandwidth | 450 MHz |
| Polarization channels | $XX$+$YY$ |
| Sampling time $\tau_{\rm sampling}$ | 49.152 μs |
| Survey integration time $t_{\rm survey\ obs}$ | 300 s |
| Verification integration time $t_{\rm verify\ obs}$ | 900 s |

### 2.4 The Strategy for FAST GPPS Survey

By referencing the parameters for the GPPS survey listed in Table 1 we can calculate the sensitivity for detection of pulsars with an assumed pulse-width of 10% of pulsar periods, as plotted in Figure 6. This is the most sensitive pulsar survey up to now, the first down to a level of μJy.

FAST is located at the latitude of N 25.647°, the longitude of E 106.856°, and can observe the sky area in the declination range of $-0.9° <$Dec$< 52.2°$ with full gain in the zenith angle of $< 26.4°$. The Galactic plane between the Galactic longitude of about $GL = 30°$ to 90° in the inner Galaxy and between about $GL = 145°$ to 215° in the outer disk are visible by FAST (see Fig. 7). We currently plan to survey the Galactic disk within the Galactic latitude of $\pm 10°$ from the Galactic plane, 76 beams per cover and 16 538 covers in the first stage. The highest priority is given to 4024 covers in the area for Galactic longitude of $\pm 5°$ in the inner Galactic disk (see Fig. 8).

After the survey for the area accessible within the zenith angle of 26.4° is finished, the survey will extend to the area observable within the zenith angle of $\pm 40°$, because the control system will become more sophisticated and the spillover radiation is better screened in near future.

## 3 OBSERVATIONS AND DATA PROCESSING

### 3.1 The GPPS Survey Observations

After initial tests for the snapshot observation mode and data file storage in March 2019, we successfully carried out a pilot project in the FAST shared-risk open session

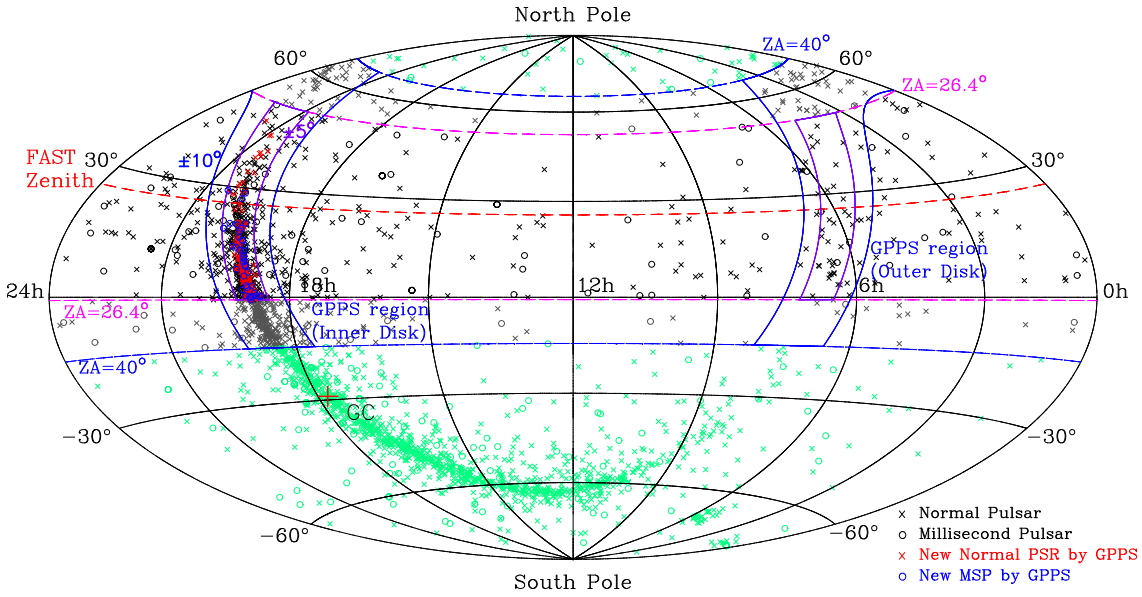


**Fig. 7** The sky area in the Galactic latitude of $\pm 10^\circ$ of the Galactic disk accessible by FAST is planned for the GPPS survey as outlined by the blue lines. High priority is given to the area of the Galactic latitude of $\pm 5^\circ$ in the inner disk. Observations within the zenith angle ZA$< 26.4^\circ$ are now carried out with the full gain of FAST.

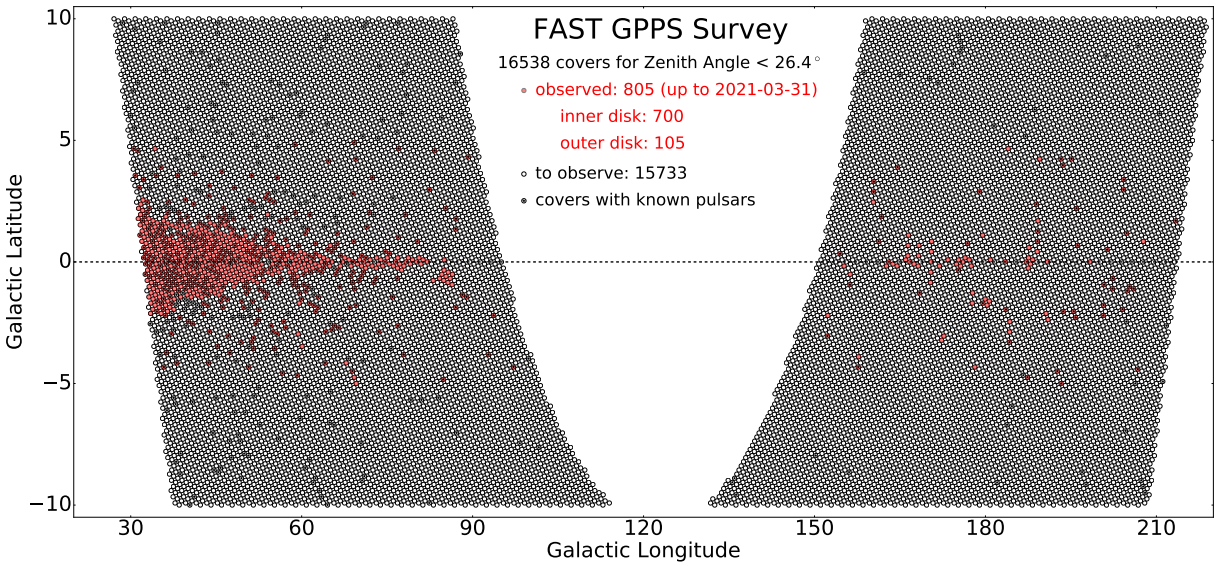


**Fig. 8** The distribution of covers for the GPPS survey with the full gain of FAST, i.e., observable within the zenith angle ZA $< 26.4^\circ$. Each small circle is a cover for 76 beams. Observed covers are marked in red, and covers with any known pulsars are marked with a black star inside.

in 2019 targeting the outer Galactic disk. Observations in 2019 have data recorded in "the standard format" for 4096 channels, 19 beams and four polarization channels ($XX$, $X^*Y$, $XY^*$, $YY$) for signals in the radio band from 1000 – 1500 MHz. To save disk space, since February 2020, only two polarization channels ($XX$ and $YY$) have been recorded for 2048 channels for the frequency range. A cover is named by the pointing position in Galactic coordinates of the central beam and observation date, such as G184.19–3.30_20190422. See Figure 8 for the distribution of covers and observation status, which are updated often on the GPPS webpage[8].

To scale the flux of discovered pulsars, at the beginning and end of each observation session lasting about 2 to 3 hours, data are recorded for 2 minutes with calibration signals on-off (1 second each) on the pointing position. The cal-signals and the receiver gain are found to be very stable in general.

[8] http://zmtt.bao.ac.cn/GPPS/

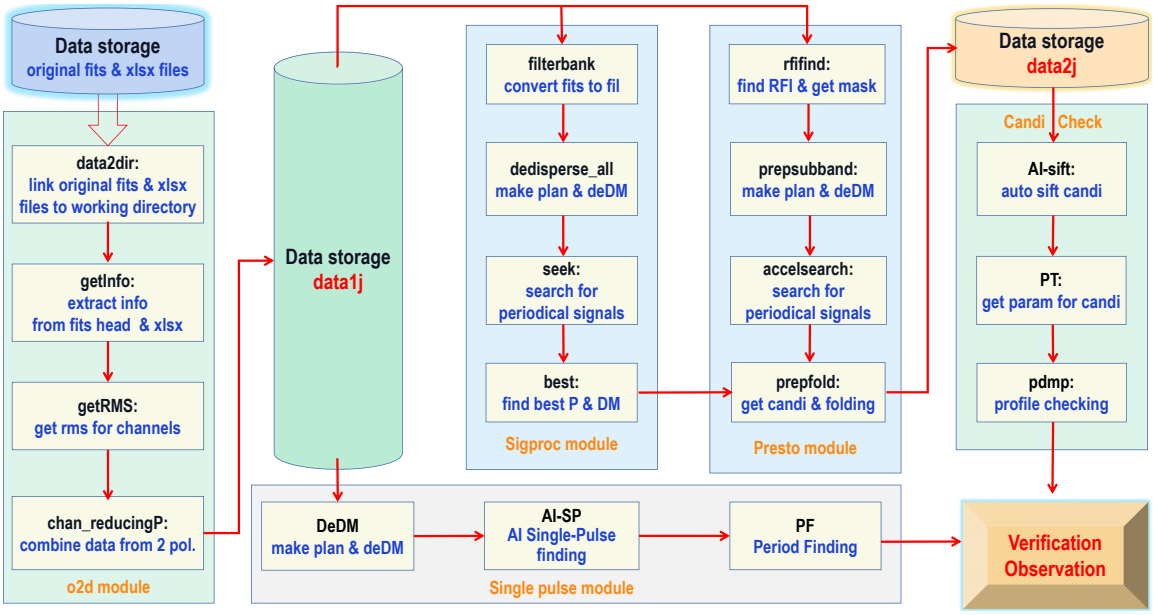


**Fig. 9** The flowchart for data processing.

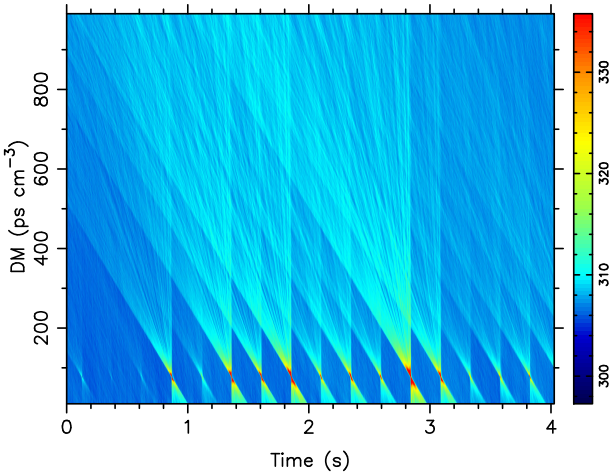


**Fig. 10** An example of DM-time plots of a strong pulsar, which show a large number of peaks as fake pulsar candidates in a very wide range of DM values. This example is taken from data of beam No.08 at pointing No.2 of the GPPS survey cover of G184.19–3.30_20190422, where a strong pulsar, PSR J0543+2329 with DM=77.7 cm$^{-3}$pc, is in the beam.

### 3.2 Data Processing

For pulsar search, there are three major steps involved in processing the data: (1) data preparing; (2) pulsar search; (3) results evaluation. See Figure 9 for a flow-chart of data processing.

#### *3.2.1 Data preparing*

A series of original fits files with a given size are recorded for each beam and stored in the repository with proper timestamps. As mentioned above, for each observation of a source, there is also an xlsx file that archives the control parameters and the focus cabin's position. It is necessary to combine these metadata with fits files for pulsar search.

We first make a directory for the cover and link all original recovered data files in the repository for the snapshot observations including the fits file and the xlsx file, or tracking observations for verification, into a sub-directory called *ori*. The calibration files will be linked into a sub-directory called *cal*. The relevant information from fits files is extracted in the order of being time-stamped with Modified Julian Date (MJD), as is the position information on the feed of the central beam from the xlsx file. These metadata are matched in MJD so that the coordinates of the telescope pointings of snapshot observations can be calculated (see Fig. 5). Based on such a list of coordinates, we can split sub-integration data of different original fits files for different pointings of every beam in a cover.

The next step is to add the data from $XX$ and $YY$ to form the total power data series for pulsar searches. High-resolution data are good for short-period pulsars so that 2048 channels and the default time resolution of 49.152 μs are taken as defaults. The so-combined fits data are stored in the repository *data1j* for various searches in the following steps.

When combining data from two polarization channels of $XX$ and $YY$, their different band-passes, different signal to noise ratios (S/Ns), and also the RFI in different channels have to be considered. In order to save computer disk space, we also cut off the 256 channels at both sides of the band, which always have a very degraded

**Table 2** A List of Pulsars Discovered by the GPPS Survey (See *http://zmtt.bao.ac.cn/GPPS/* for Updates)

| Name* | gpps No. | Period (s) | DM ($cm^{-3}pc$) | RA(2000) (hh:mm:ss) | Dec(2000) (±dd:mm) | GL (°) | GB (°) | $S_{1.25GHz}$ (μJy) | $D_{NE2001}$ (kpc) | $D_{YMW16}$ (kpc) |
|---|---|---|---|---|---|---|---|---|---|---|
| J1901+0659g | gpps0001 | 0.07573 | 126.2 | 19:01:24.8 | +06:59 | 40.2854 | +0.9763 | 51.8 | 3.7 | 3.8 |
| J1924+1923g | gpps0002 | 0.68924 | 386.7 | 19:24:20.5 | +19:23 | 53.8632 | +1.7939 | 54.7 | 12.0 | 9.8 |
| J1904+0823g | gpps0003 | 1.50773 | 60.4 | 19:04:43.8 | +08:23 | 41.9112 | +0.8895 | 22.0 | 2.8 | 1.8 |
| J1928+1915g | gpps0004 | 0.97435 | 201.0 | 19:28:59.6 | +19:15 | 54.2628 | +0.7624 | 5.1 | 6.6 | 4.6 |
| J1838+0044g | gpps0005 | 2.20317 | 229.6 | 18:38:10.8 | +00:44 | 32.0861 | +3.2910 | 72.9 | 5.6 | 6.9 |
| J1924+1932g | gpps0006 | 0.38886 | 280.3 | 19:24:49.0 | +19:32 | 54.0482 | +1.7661 | 20.8 | 8.9 | 6.6 |
| J1925+1629g | gpps0007 | 0.00411 | 214.1 | 19:25:10.1 | +16:29 | 51.4006 | +0.2470 | 87.8 | 6.7 | 5.1 |
| J1905+0656g | gpps0008 | 2.51165 | 23.0 | 19:05:45.3 | +06:56 | 40.7393 | −0.0019 | 27.6 | 1.6 | 1.0 |
| J1904+0852g | gpps0009 | 0.00619 | 195.1 | 19:04:55.0 | +08:52 | 42.3646 | +1.0716 | 36.0 | 5.3 | 5.9 |
| J1857+0214g | gpps0010 | 0.33389 | 986.3 | 18:57:08.2 | +02:14 | 35.5819 | −0.2422 | 56.2 | 14.8 | 7.8 |
| J1947+2011g | gpps0011 | 0.00817 | 127.4 | 19:47:47.0 | +20:11 | 57.2512 | −2.6299 | 9.8 | 5.1 | 4.3 |
| J1917+1259g | gpps0012 | 0.00563 | 117.0 | 19:17:29.0 | +12:59 | 47.4303 | +0.2353 | 36.1 | 4.3 | 3.6 |
| J1930+1403g | gpps0013 | 0.00321 | 150.5 | 19:30:17.9 | +14:03 | 49.8431 | −2.0053 | 94.1 | 5.4 | 4.7 |
| J1852+0056g | gpps0014 | 1.17779 | 905.7 | 18:52:14.0 | +00:56 | 33.8644 | +0.2543 | 37.9 | 11.7 | 7.2 |
| J1859+0430g | gpps0015 | 0.33629 | 783.8 | 18:59:10.4 | +04:30 | 37.8266 | +0.3389 | 28.0 | 11.9 | 8.9 |
| J1900+0405g | gpps0016 | 0.07238 | 634.4 | 19:00:39.6 | +04:05 | 37.6202 | −0.1839 | 32.5 | 9.4 | 6.7 |
| J1906+0822g | gpps0017 | 0.43344 | 367.9 | 19:06:37.7 | +08:22 | 42.1147 | +0.4661 | 9.5 | 7.6 | 7.1 |
| J1850−0020g | gpps0018 | 1.57459 | 605.4 | 18:50:05.9 | −00:20 | 32.4771 | +0.1433 | 44.2 | 8.1 | 5.7 |
| J2052+4421g | gpps0019 | 0.37531 | 547.0 | 20:52:53.2 | +44:21 | 84.8417 | −0.1616 | 280.3 | 50.0 | 25.0 |
| J1854+0012g | gpps0020 | 0.00271 | 204.1 | 18:54:18.4 | +00:12 | 33.4516 | −0.5396 | 11.8 | 5.3 | 4.1 |
| J1912+1105g | gpps0021 | 0.67071 | 150.4 | 19:12:25.6 | +11:05 | 45.1765 | +0.4480 | 17.7 | 4.4 | 4.4 |
| J1854−0033g | gpps0022 | 0.36147 | 617.5 | 18:54:29.6 | −00:33 | 32.7882 | −0.9319 | 17.7 | 9.6 | 8.3 |
| J1917+1411g | gpps0023 | 0.44646 | 123.4 | 19:17:25.5 | +14:11 | 48.4969 | +0.8145 | 12.5 | 4.6 | 4.0 |
| J1905+0450g | gpps0024 | 0.78330 | 442.3 | 19:05:59.3 | +04:50 | 38.9029 | −1.0168 | 8.1 | 8.3 | 9.8 |
| J1926+1857g | gpps0025 | 0.27873 | 424.2 | 19:26:58.9 | +18:57 | 53.7730 | +1.0372 | 30.4 | 12.3 | 9.6 |
| J1855+0139g | gpps0026 | 0.44414 | 405.6 | 18:55:13.6 | +01:39 | 34.8429 | −0.0849 | 36.8 | 7.0 | 5.2 |
| J1849−0014g | gpps0027 | 0.49171 | 346.6 | 18:49:30.6 | −00:14 | 32.4943 | +0.3174 | 107.3 | 6.3 | 4.9 |
| J1901+0712g | gpps0028 | 1.03771 | 332.4 | 19:01:29.8 | +07:12 | 40.4908 | +1.0586 | 43.1 | 6.6 | 8.9 |
| J1859+0434g | gpps0029 | 0.45834 | 320.1 | 18:59:41.1 | +04:34 | 37.9367 | +0.2522 | 15.2 | 6.4 | 5.3 |
| J1853+0013g | gpps0030 | 0.92853 | 312.4 | 18:53:52.9 | +00:13 | 33.4145 | −0.4392 | 17.0 | 6.2 | 4.7 |
| J1908+0811g | gpps0031 | 0.18164 | 300.1 | 19:08:43.6 | +08:11 | 42.1800 | −0.0847 | 19.1 | 6.6 | 5.6 |
| J1924+1343g | gpps0032 | 0.00572 | 98.5 | 19:24:20.0 | +13:43 | 48.8687 | −0.8864 | 32.2 | 4.1 | 3.0 |
| J1904+0358g | gpps0033 | 0.75154 | 532.0 | 19:04:22.5 | +03:58 | 37.9509 | −1.0557 | 14.2 | 9.3 | 12.1 |
| J1914+1029g | gpps0034 | 2.48499 | 59.7 | 19:14:22.9 | +10:29 | 44.8706 | −0.2541 | 11.8 | 2.8 | 1.9 |
| J1848+0127g | gpps0035 | 0.53402 | 77.0 | 18:48:19.1 | +01:27 | 33.8770 | +1.3601 | 36.9 | 2.7 | 2.5 |
| J1904+0535g | gpps0036 | 0.60376 | 78.4 | 19:04:51.8 | +05:35 | 39.4407 | −0.4236 | 45.4 | 3.1 | 2.4 |
| J1904+0519g | gpps0037 | 1.68053 | 80.8 | 19:04:07.6 | +05:19 | 39.1228 | −0.3814 | 77.4 | 3.1 | 2.5 |
| J1858−0024g | gpps0038 | 0.40060 | 190.0 | 18:58:46.5 | −00:24 | 33.3996 | −1.8214 | 25.8 | 5.2 | 4.7 |
| J1904+0553g | gpps0039 | 0.00491 | 164.2 | 19:04:16.9 | +05:53 | 39.6443 | −0.1556 | 825.6 | 4.5 | 4.0 |
| J1912+0934g | gpps0040 | 0.89747 | 143.8 | 19:12:41.2 | +09:34 | 43.8581 | −0.3134 | 30.3 | 2.6 | 4.0 |
| J1933+2038g | gpps0041 | 0.04075 | 302.9 | 19:33:42.5 | +20:38 | 56.0116 | +0.4585 | 22.9 | 9.1 | 8.5 |
| J1852−0024g | gpps0042 | 0.35545 | 290.0 | 18:52:13.7 | −00:24 | 32.6549 | −0.3640 | 35.2 | 5.9 | 4.5 |
| J1905+0758g | gpps0043 | 1.19276 | 200.7 | 19:05:47.8 | +07:58 | 41.6666 | +0.4660 | 14.7 | 5.2 | 4.8 |
| J2017+2819g | gpps0044 | 1.83246 | 66.0 | 20:17:19.9 | +28:19 | 67.7232 | −4.0410 | 46.2 | 3.7 | 4.9 |
| J2009+3122g | gpps0045 | 0.07654 | 144.1 | 20:09:40.1 | +31:22 | 69.3534 | −0.9742 | 17.1 | 5.8 | 6.5 |
| J1956+2826g | gpps0046 | 0.07179 | 112.0 | 19:56:47.4 | +28:26 | 65.3854 | −0.1721 | 13.2 | 4.8 | 6.5 |
| J1924+1510g | gpps0047 | 0.49863 | 115.6 | 19:24:01.8 | +15:10 | 50.1028 | −0.1402 | 9.6 | 4.5 | 3.5 |
| J1903+0845g | gpps0048 | 0.15314 | 129.1 | 19:03:36.0 | +08:45 | 42.1036 | +1.3030 | 18.1 | 4.2 | 4.3 |
| J1910+1054g | gpps0049 | 0.00387 | 139.4 | 19:10:01.4 | +10:54 | 44.7481 | +0.8898 | 15.5 | 4.0 | 4.4 |
| J1930+1357g | gpps0050 | 0.32354 | 186.6 | 19:30:12.0 | +13:57 | 49.7499 | −2.0289 | 27.9 | 6.3 | 5.6 |
| J1837+0033g | gpps0051 | 0.41814 | 186.9 | 18:37:41.1 | +00:33 | 31.8669 | +3.3179 | 10.1 | 4.7 | 5.5 |
| J1847+0133g | gpps0052 | 2.84691 | 193.8 | 18:47:00.9 | +01:33 | 33.8153 | +1.6945 | 10.1 | 5.3 | 4.9 |
| J1926+1631g | gpps0053 | 0.67839 | 195.1 | 19:26:24.2 | +16:31 | 51.5693 | +0.0016 | 46.4 | 6.2 | 4.8 |
| J1952+2702g | gpps0054 | 0.00414 | 213.1 | 19:52:18.4 | +27:02 | 63.6790 | −0.0424 | 14.0 | 7.4 | 7.8 |
| J1911+0751g | gpps0055 | 0.79691 | 220.7 | 19:11:43.2 | +07:51 | 42.2258 | −0.8963 | 51.9 | 5.7 | 5.6 |
| J1915+0832g | gpps0056 | 2.71009 | 36.2 | 19:15:05.8 | +08:32 | 43.2318 | −1.3131 | 15.9 | 2.2 | 1.4 |
| J1910+1117g | gpps0057 | 1.32152 | 296.5 | 19:10:27.2 | +11:17 | 45.1394 | +0.9745 | 17.5 | 7.0 | 7.9 |
| J1926+1452g | gpps0058 | 0.30451 | 298.1 | 19:26:54.6 | +14:52 | 50.1780 | −0.8897 | 5.5 | 8.6 | 6.5 |
| J1924+1509g | gpps0059 | 0.23995 | 296.6 | 19:24:33.5 | +15:09 | 50.1512 | −0.2590 | 14.1 | 8.3 | 6.4 |
| J1917+1121g | gpps0060 | 0.51031 | 303.5 | 19:17:26.8 | +11:21 | 45.9926 | −0.5138 | 9.2 | 7.6 | 7.1 |
| J1855+0511g | gpps0061 | 1.42147 | 307.5 | 18:55:11.6 | +05:11 | 37.9847 | +1.5342 | 29.9 | 6.7 | 9.1 |
| J1929+1615g | gpps0062 | 0.04460 | 308.7 | 19:29:36.4 | +16:15 | 51.6945 | −0.8048 | 11.7 | 9.1 | 6.1 |
| J1900+0213g | gpps0063 | 0.03209 | 310.5 | 19:00:12.5 | +02:13 | 35.9189 | −0.9318 | 24.7 | 6.2 | 5.7 |
| J1952+2836g | gpps0064 | 0.01802 | 313.0 | 19:52:47.7 | +28:36 | 65.0826 | +0.6701 | 95.4 | 9.7 | 10.5 |
| J1936+1952g | gpps0065 | 0.00972 | 325.0 | 19:36:00.1 | +19:52 | 55.6078 | −0.3812 | 29.3 | 9.4 | 8.6 |
| J1859+0026g | gpps0066 | 0.00857 | 334.1 | 18:59:58.0 | +00:26 | 34.3029 | −1.6933 | 29.1 | 7.2 | 6.5 |
| J1856+0615g | gpps0067 | 0.32697 | 333.1 | 18:56:39.1 | +06:15 | 39.0950 | +1.6947 | 38.8 | 7.6 | 11.6 |

"g" indicates the temporary nature, due to position uncertainty of about 1.5′.

**Table 2** *–Continued.*

| Name* | gpps No. | Period (s) | DM ($cm^{-3}pc$) | RA(2000) (hh:mm:ss) | Dec(2000) (±dd:mm) | GL (°) | GB (°) | $S_{1.25GHz}$ (μJy) | $D_{NE2001}$ (kpc) | $D_{YMW16}$ (kpc) |
|---|---|---|---|---|---|---|---|---|---|---|
| J1853+0312g | gpps0068 | 0.43809 | 345.0 | 18:53:14.9 | +03:12 | 35.9921 | +1.0592 | 12.0 | 7.0 | 6.7 |
| J1855+0455g | gpps0069 | 0.10101 | 372.9 | 18:55:15.4 | +04:55 | 37.7532 | +1.3980 | 40.3 | 7.5 | 10.3 |
| J1858+0609g | gpps0070 | 0.48435 | 381.5 | 18:58:09.5 | +06:09 | 39.1719 | +1.3133 | 14.0 | 7.9 | 11.6 |
| J1914+0805g | gpps0071 | 0.45555 | 339.2 | 19:14:05.4 | +08:05 | 42.7106 | −1.3051 | 17.4 | 8.0 | 10.5 |
| J1857+0224g | gpps0072 | 0.87595 | 401.0 | 18:57:08.1 | +02:24 | 35.7231 | −0.1693 | 13.1 | 7.0 | 5.3 |
| J1903+0534g | gpps0073 | 0.35765 | 407.7 | 19:03:29.3 | +05:34 | 39.2697 | −0.1269 | 41.1 | 7.2 | 5.9 |
| J1928+1809g | gpps0074 | 0.29446 | 431.1 | 19:28:06.0 | +18:09 | 53.1982 | +0.4240 | 29.9 | 11.8 | 9.3 |
| J1856+0011g | gpps0075 | 0.92847 | 455.8 | 18:56:47.5 | +00:11 | 33.7176 | −1.1013 | 8.6 | 8.1 | 6.9 |
| J2022+3845g | gpps0076 | 1.00890 | 487.5 | 20:22:11.4 | +38:45 | 76.9110 | +1.0169 | 54.7 | 50.0 | 17.2 |
| J2005+3411g | gpps0077 | 0.65105 | 489.0 | 20:05:45.0 | +34:11 | 71.2811 | +1.2438 | 81.9 | 50.0 | 17.3 |
| J1921+1505g | gpps0078 | 0.61190 | 519.9 | 19:21:24.7 | +15:05 | 49.7378 | +0.3812 | 14.5 | 13.6 | 10.6 |
| J1904+0415g | gpps0079 | 0.23145 | 521.0 | 19:04:05.7 | +04:15 | 38.1707 | −0.8637 | 53.0 | 8.8 | 9.5 |
| J1859+0126g | gpps0080 | 0.95770 | 531.7 | 18:59:15.4 | +01:26 | 35.1076 | −1.0810 | 35.9 | 9.0 | 9.6 |
| J1918+1340g | gpps0081 | 0.23299 | 575.9 | 19:18:53.9 | +13:40 | 48.2019 | +0.2541 | 43.7 | 14.3 | 11.9 |
| J1911+0939g | gpps0082 | 0.36547 | 597.3 | 19:11:38.3 | +09:39 | 43.8189 | −0.0423 | 25.8 | 8.1 | 10.6 |
| J1852+0158g | gpps0083 | 0.18573 | 607.5 | 18:52:43.8 | +01:58 | 34.8424 | +0.6159 | 35.8 | 9.2 | 7.6 |
| J1849+0037g | gpps0084 | 0.39649 | 611.5 | 18:49:28.0 | +00:37 | 33.2692 | +0.7265 | 65.8 | 9.0 | 8.0 |
| J2051+4434g | gpps0085 | 1.30316 | 616.0 | 20:51:28.6 | +44:34 | 84.8479 | +0.1706 | 341.8 | 50.0 | 25.0 |
| J1920+1515g | gpps0086 | 1.60276 | 655.5 | 19:20:22.4 | +15:15 | 49.7623 | +0.6780 | 19.0 | 50.0 | 15.7 |
| J2021+4024g | gpps0087 | 0.37054 | 680.5 | 20:21:12.9 | +40:24 | 78.1680 | +2.1153 | 88.1 | 50.0 | 25.0 |
| J1921+1340g | gpps0088 | 4.60294 | 754.9 | 19:21:29.7 | +13:40 | 48.4946 | −0.3047 | 30.8 | 50.0 | 25.0 |
| J1853+0023g | gpps0089 | 0.57686 | 203.3 | 18:53:09.5 | +00:23 | 33.4769 | −0.2041 | 45.3 | 5.3 | 4.0 |
| J1903+0433g | gpps0090 | 14.0499 | 202.6 | 19:03:19.0 | +04:33 | 38.3396 | −0.5584 | 14.3 | 4.9 | 4.4 |
| J1859+0239g | gpps0091 | 0.05611 | 250.9 | 18:59:18.4 | +02:39 | 36.1937 | −0.5373 | 10.1 | 5.8 | 4.7 |
| J1906+0646g | gpps0092 | 0.35552 | 290.5 | 19:06:15.1 | +06:46 | 40.6461 | −0.1889 | 48.4 | 6.1 | 5.3 |
| J1849+0001g | gpps0093 | 0.52560 | 189.4 | 18:49:23.2 | +00:01 | 32.7166 | +0.4659 | 12.7 | 5.1 | 4.0 |
| J1858+0026g | gpps0094 | 4.71467 | 415.3 | 18:58:04.9 | +00:26 | 34.0801 | −1.2779 | 41.9 | 7.9 | 6.8 |
| J1850+0011g | gpps0095 | 0.16754 | 506.5 | 18:50:03.9 | +00:11 | 32.9428 | +0.3912 | 30.5 | 7.6 | 5.7 |
| J1849+0009g | gpps0096 | 1.31855 | 501.5 | 18:49:42.0 | +00:09 | 32.8816 | +0.4624 | 14.1 | 7.6 | 5.8 |
| J1850−0002g | gpps0097 | 0.89336 | 543.9 | 18:50:00.0 | −00:02 | 32.7376 | +0.3044 | 30.3 | 7.8 | 5.7 |
| J1852−0002g | gpps0098 | 0.24510 | 558.1 | 18:52:10.3 | −00:02 | 32.9763 | −0.1834 | 41.5 | 7.9 | 5.6 |
| J1921+1259g | gpps0099 | 0.57316 | 366.3 | 19:21:18.1 | +12:59 | 47.8792 | −0.5795 | 14.6 | 9.3 | 8.2 |
| J1903+0839g | gpps0100 | 0.00462 | 166.5 | 19:03:52.3 | +08:39 | 42.0470 | +1.1983 | 181.1 | 4.9 | 5.3 |
| J1903+0851g | gpps0101 | 1.23197 | 78.9 | 19:03:04.3 | +08:51 | 42.1353 | +1.4661 | 14.8 | 3.2 | 2.5 |
| J1906+0757g | gpps0102 | 0.05719 | 79.0 | 19:06:39.8 | +07:57 | 41.7447 | +0.2648 | 14.5 | 3.2 | 2.5 |
| J1852+0018g | gpps0103 | 0.31876 | 452.0 | 18:52:29.5 | +00:18 | 33.3272 | −0.0935 | 29.0 | 7.1 | 5.2 |
| J1904+0836g | gpps0104 | 0.00444 | 90.5 | 19:04:35.4 | +08:36 | 42.0824 | +1.0168 | 17.3 | 3.5 | 2.9 |
| J1900+0715g | gpps0105 | 0.97044 | 266.1 | 19:00:22.4 | +07:15 | 40.4103 | +1.3306 | 60.5 | 6.1 | 8.7 |
| J2139+4738g | gpps0106 | 0.55704 | 138.9 | 21:39:57.7 | +47:38 | 92.8848 | −3.7423 | 12.2 | 5.0 | 4.1 |
| J1838+0022g | gpps0107 | 0.00509 | 122.6 | 18:38:24.4 | +00:22 | 31.7733 | +3.0672 | 32.3 | 3.4 | 4.1 |
| J1848+0150g | gpps0108 | 3.29015 | 500.8 | 18:48:43.4 | +01:50 | 34.2558 | +1.4403 | 12.4 | 9.7 | 10.0 |
| J1844+0028g | gpps0109 | 0.00357 | 181.2 | 18:44:35.5 | +00:28 | 32.5683 | +1.7368 | 53.8 | 5.0 | 4.6 |
| J1853−0003g | gpps0110 | 0.17152 | 667.2 | 18:53:24.1 | −00:03 | 33.1063 | −0.4623 | 7.1 | 9.1 | 6.3 |
| J1949+2516g | gpps0111 | 0.41034 | 425.7 | 19:49:36.6 | +25:16 | 61.8501 | −0.4234 | 5.3 | 13.0 | 15.1 |
| J1845−0028g | gpps0112 | 0.08450 | 301.0 | 18:45:39.7 | −00:28 | 31.8488 | +1.0676 | 10.2 | 6.2 | 5.3 |
| J1901+0020g | gpps0113 | 0.21481 | 237.6 | 19:01:17.2 | +00:20 | 34.3569 | −2.0365 | 41.6 | 5.8 | 5.6 |
| J1908+1035g | gpps0114 | 0.01069 | 10.9 | 19:08:23.2 | +10:35 | 44.2835 | +1.1015 | 11.6 | 0.6 | 0.7 |
| J1925+1532g | gpps0115 | 1.65510 | 145.9 | 19:25:00.3 | +15:32 | 50.5449 | −0.1694 | 20.6 | 5.1 | 4.2 |
| J1849+0225g | gpps0116 | 1.47452 | 259.9 | 18:49:13.1 | +02:25 | 34.8363 | +1.5983 | 13.8 | 6.2 | 5.8 |
| J1854+0131g | gpps0117 | 2.04385 | 474.9 | 18:54:34.0 | +01:31 | 34.6470 | +0.0001 | 312.9 | 7.5 | 5.5 |
| J2030+3944g | gpps0118 | 0.30618 | 937.4 | 20:30:21.5 | +39:44 | 78.6299 | +0.2988 | 218.4 | 50.0 | 25.0 |
| J1849−0019g | gpps0119 | 0.91137 | 513.2 | 18:49:15.2 | −00:19 | 32.3966 | +0.3394 | 8.9 | 7.6 | 5.6 |
| J1907+0709g | gpps0120 | 0.34410 | 278.1 | 19:07:56.7 | +07:09 | 41.1741 | −0.3886 | 83.8 | 6.1 | 5.4 |
| J1928+1816g | gpps0121 | 0.01054 | 346.3 | 19:28:10.0 | +18:16 | 53.3088 | +0.4661 | 26.2 | 9.7 | 7.2 |
| J1914+1228g | gpps0122 | 2.27755 | 312.0 | 19:14:55.1 | +12:28 | 46.6871 | +0.5509 | 22.9 | 7.9 | 7.3 |
| J1955+2912g | gpps0123 | 0.27951 | 193.0 | 19:55:23.1 | +29:12 | 65.8853 | +0.4914 | 5.5 | 7.0 | 7.4 |
| J1838+0027g | gpps0124 | 0.05413 | 205.9 | 18:38:12.7 | +00:27 | 31.8265 | +3.1492 | 7.5 | 5.0 | 5.8 |
| J1858+0244g | gpps0125 | 0.00261 | 282.6 | 18:58:01.2 | +02:44 | 36.1246 | −0.2117 | 73.0 | 6.1 | 4.7 |
| J1847+0110g | gpps0126 | 0.00653 | 183.4 | 18:47:23.1 | +01:10 | 33.5218 | +1.4405 | 37.4 | 5.1 | 4.6 |
| J1907+0658g | gpps0127 | 0.21834 | 523.0 | 19:07:34.0 | +06:58 | 40.9807 | −0.3831 | 54.1 | 9.0 | 7.7 |
| J1908+0949g | gpps0128 | 0.00905 | 220.3 | 19:08:07.8 | +09:49 | 43.5742 | +0.8048 | 19.4 | 5.7 | 6.0 |
| J1923+1521g | gpps0129 | 1.04876 | 346.0 | 19:23:12.0 | +15:21 | 50.1781 | +0.1273 | 15.5 | 9.5 | 7.0 |
| J1919+1527g | gpps0130 | 1.37146 | 697.5 | 19:19:50.2 | +15:27 | 49.8846 | +0.8895 | 7.1 | 50.0 | 16.9 |
| J1859+0313g | gpps0131 | 0.00161 | 107.7 | 18:59:35.5 | +03:13 | 36.7345 | −0.3395 | 60.3 | 3.4 | 3.1 |
| J1858+0310g | gpps0132 | 0.37275 | 699.5 | 18:58:05.1 | +03:10 | 36.5152 | −0.0293 | 119.0 | 9.9 | 6.7 |
| J1856+0243g | gpps0133 | 0.54660 | 178.3 | 18:56:01.4 | +02:43 | 35.8826 | +0.2246 | 114.5 | 5.1 | 4.0 |
| J1909+0657g | gpps0134 | 1.24589 | 59.9 | 19:09:13.8 | +06:57 | 41.1462 | −0.7623 | 87.2 | 2.8 | 1.8 |
| J1855+0339g | gpps0135 | 1.76134 | 416.2 | 18:55:42.5 | +03:39 | 36.6771 | +0.7203 | 12.3 | 7.5 | 6.9 |

**Table 2** *–Continued.*

| Name* | gpps No. | Period (s) | DM ($cm^{-3}pc$) | RA(2000) (hh:mm:ss) | Dec(2000) (±dd:mm) | GL (°) | GB (°) | $S_{1.25GHz}$ (μJy) | $D_{NE2001}$ (kpc) | $D_{YMW16}$ (kpc) |
|---|---|---|---|---|---|---|---|---|---|---|
| J2011+3006g | gpps0136 | 2.50566 | 14.0 | 20:11:12.1 | +30:06 | 68.4718 | −1.9414 | 312.3 | 1.2 | 0.9 |
| J1904+0207g | gpps0137 | 0.00504 | 229.9 | 19:04:44.4 | +02:07 | 36.3346 | −1.9911 | 17.9 | 4.2 | 6.0 |
| J1924+2027g | gpps0138 | 0.00195 | 211.7 | 19:24:33.5 | +20:27 | 54.8223 | +2.2501 | 82.5 | 7.3 | 5.3 |
| J1855+0228g | gpps0139 | 0.25317 | 530.0 | 18:55:45.0 | +02:28 | 35.6253 | +0.1694 | 37.4 | 8.1 | 5.9 |
| J1909+1132g | gpps0140 | 0.00680 | 276.1 | 19:09:36.7 | +11:32 | 45.2621 | +1.2707 | 14.8 | 6.9 | 8.1 |
| J1914+1054g | gpps0141 | 0.13887 | 418.7 | 19:14:06.8 | +10:54 | 45.2132 | −0.0000 | 33.0 | 8.8 | 7.8 |
| J1913+1054g | gpps0142 | 0.45062 | 338.0 | 19:13:07.0 | +10:54 | 45.0905 | +0.2120 | 24.1 | 7.6 | 7.1 |
| J1928+1852g | gpps0143 | 0.79281 | 291.6 | 19:28:04.7 | +18:52 | 53.8248 | +0.7703 | 20.0 | 8.8 | 5.8 |
| J1918+1540g | gpps0144 | 0.00428 | 271.2 | 19:18:19.1 | +15:40 | 49.9066 | +1.3149 | 15.9 | 8.2 | 6.5 |
| J1918+1536g | gpps0145 | 0.10995 | 123.7 | 19:18:23.4 | +15:36 | 49.8602 | +1.2709 | 10.0 | 4.7 | 3.8 |
| J1840+0012g | gpps0146 | 0.00534 | 100.9 | 18:40:49.4 | +00:12 | 31.9078 | +2.4571 | 164.9 | 2.9 | 3.5 |
| J1916+1030Bg | gpps0147 | 0.34938 | 519.7 | 19:16:46.1 | +10:30 | 45.1641 | −0.7626 | 11.4 | 11.4 | 11.3 |
| J1855+0235g | gpps0148 | 0.98303 | 103.3 | 18:55:48.9 | +02:35 | 35.7442 | +0.2121 | 21.8 | 3.3 | 3.0 |
| J1913+1037g | gpps0149 | 0.43421 | 437.0 | 19:13:52.6 | +10:37 | 44.9266 | −0.0846 | 8.1 | 9.0 | 7.9 |
| J1939+2352g | gpps0150 | 2.14534 | 415.5 | 19:39:48.6 | +23:52 | 59.5212 | +0.8047 | 7.5 | 12.7 | 12.3 |
| J1855+0424g | gpps0151 | 2.22025 | 678.5 | 18:55:00.4 | +04:24 | 37.2690 | +1.2201 | 11.7 | 12.8 | 17.4 |
| J2030+3929g | gpps0152 | 1.71842 | 491.9 | 20:30:47.2 | +39:29 | 78.4765 | +0.0848 | 35.2 | 50.0 | 25.0 |
| J1905+0936g | gpps0153 | 1.63451 | 414.0 | 19:05:24.7 | +09:36 | 43.0608 | +1.2934 | 46.8 | 9.2 | 12.3 |
| J1950+2352g | gpps0154 | 0.31976 | 342.5 | 19:50:56.1 | +23:52 | 60.7928 | −1.3979 | 32.4 | 10.9 | 13.3 |
| J1923+2022g | gpps0155 | 0.03799 | 175.3 | 19:23:55.9 | +20:22 | 54.6782 | +2.3395 | 8.4 | 6.2 | 4.6 |
| J1923+1143g | gpps0156 | 0.37121 | 260.6 | 19:23:38.0 | +11:43 | 47.0176 | −1.6852 | 9.2 | 7.6 | 7.8 |
| J1917+1046g | gpps0157 | 0.08773 | 163.1 | 19:17:55.3 | +10:46 | 45.5310 | −0.8894 | 14.1 | 5.1 | 4.9 |
| J1856+0211g | gpps0158 | 9.89012 | 113.9 | 18:56:53.1 | +02:11 | 35.5031 | −0.2120 | 10.7 | 3.4 | 3.1 |
| J1933+1923g | gpps0159 | 0.37173 | 97.7 | 19:33:58.1 | +19:23 | 54.9486 | −0.1999 | 16.3 | 4.1 | 3.1 |
| J1918+1547g | gpps0160 | 0.00376 | 64.6 | 19:18:34.0 | +15:47 | 50.0313 | +1.3133 | 16.5 | 3.3 | 2.2 |
| J1854+0704g | gpps0161 | 0.45090 | 10.8 | 18:54:31.0 | +07:04 | 39.5878 | +2.5417 | 34.6 | 1.0 | 0.6 |
| J1859+0658g | gpps0162 | 0.00511 | 290.4 | 18:59:04.7 | +06:58 | 40.0033 | +1.4828 | 35.6 | 6.8 | 9.4 |
| J1928+1902g | gpps0163 | 0.00580 | 28.9 | 19:28:05.0 | +19:02 | 53.9692 | +0.8474 | 7.1 | 2.3 | 1.5 |
| J1851+0056g | gpps0164 | 0.29110 | 332.3 | 18:51:27.0 | +00:56 | 33.7751 | +0.4286 | 13.4 | 6.4 | 5.0 |
| J1847+0614g | gpps0165 | 1.66302 | 270.5 | 18:47:33.7 | +06:14 | 38.0557 | +3.7011 | 50.5 | 8.0 | 16.7 |
| J1916+0741g | gpps0166 | 0.01122 | 220.1 | 19:16:17.4 | +07:41 | 42.6135 | −1.9711 | 29.8 | 6.2 | 8.4 |
| J1917+0743g | gpps0167 | 0.81347 | 199.5 | 19:17:26.3 | +07:43 | 42.7679 | −2.2114 | 22.7 | 5.9 | 8.2 |
| J1904+0603g | gpps0168 | 1.97493 | 413.2 | 19:04:52.4 | +06:03 | 39.8565 | −0.2117 | 23.5 | 7.4 | 6.1 |
| J1912+1417g | gpps0169 | 0.00317 | 66.6 | 19:12:31.9 | +14:17 | 48.0257 | +1.9063 | 39.8 | 3.4 | 2.2 |
| J1950+2556g | gpps0170 | 2.03864 | 420.4 | 19:50:03.7 | +25:56 | 62.4808 | −0.1695 | 20.1 | 12.7 | 14.5 |
| J1852+0309g | gpps0171 | 0.00558 | 358.0 | 18:52:10.9 | +03:09 | 35.8211 | +1.2707 | 89.7 | 7.3 | 7.1 |
| J1852+0857g | gpps0172 | 3.77214 | 85.9 | 18:52:37.4 | +08:57 | 41.0548 | +3.8125 | 21.5 | 3.4 | 3.4 |
| J1852−0033g | gpps0173 | 1.36903 | 320.7 | 18:52:25.9 | −00:33 | 32.5466 | −0.4766 | 18.9 | 6.2 | 4.7 |
| J1852−0044g | gpps0174 | 0.00241 | 272.9 | 18:52:27.4 | −00:44 | 32.3907 | −0.5634 | 556.1 | 5.8 | 4.5 |
| J1916+0748g | gpps0175 | 0.86791 | 153.1 | 19:16:59.9 | +07:48 | 42.7917 | −2.0758 | 14.3 | 4.9 | 6.4 |
| J1929+1937g | gpps0176 | 0.56373 | 458.1 | 19:29:10.0 | +19:37 | 54.6040 | +0.9018 | 17.0 | 13.4 | 10.0 |
| J1852−0039g | gpps0177 | 0.80291 | 361.7 | 18:52:10.6 | −00:39 | 32.4255 | −0.4670 | 85.5 | 6.5 | 4.9 |
| J1909+0905g | gpps0178 | 1.49488 | 250.6 | 19:09:39.3 | +09:05 | 43.0852 | +0.1271 | 12.0 | 5.9 | 5.4 |
| J1928+1839g | gpps0179 | 2.26091 | 70.0 | 19:28:38.5 | +18:39 | 53.7001 | +0.5507 | 8.2 | 3.4 | 2.5 |
| J1855+0327g | gpps0180 | 0.78282 | 298.6 | 18:55:45.1 | +03:27 | 36.5008 | +0.6178 | 13.7 | 6.3 | 5.3 |
| J1911+1252g | gpps0181 | 0.02724 | 68.8 | 19:11:28.4 | +12:52 | 46.6561 | +1.4829 | 26.5 | 3.3 | 2.2 |
| J1905+0920g | gpps0182 | 0.17047 | 396.6 | 19:05:08.7 | +09:20 | 42.7949 | +1.2302 | 9.6 | 8.8 | 11.6 |
| J1927+1430g | gpps0183 | 0.20288 | 207.2 | 19:27:39.6 | +14:30 | 49.9334 | −1.2284 | 12.8 | 6.6 | 5.6 |
| J1849+0339g | gpps0184 | 1.66672 | 349.5 | 18:49:54.7 | +03:39 | 36.0225 | +2.0100 | 55.2 | 7.6 | 10.0 |
| J1902+0809g | gpps0185 | 0.19023 | 436.9 | 19:02:19.7 | +08:09 | 41.4253 | +1.3075 | 10.0 | 9.2 | 13.9 |
| J2013+3100g | gpps0186 | 0.36855 | 158.4 | 20:13:56.6 | +31:00 | 69.5489 | −1.9394 | 26.9 | 6.2 | 6.8 |
| J2030+3818g | gpps0187 | 0.13372 | 596.7 | 20:30:08.5 | +38:18 | 77.4491 | −0.5085 | 17.3 | 50.0 | 25.0 |
| J1853+0237g | gpps0188 | 0.42739 | 725.5 | 18:53:57.3 | +02:37 | 35.5518 | +0.6355 | 38.1 | 10.8 | 10.0 |
| J2018+3418g | gpps0189 | 2.19160 | 317.1 | 20:18:15.0 | +34:18 | 72.8022 | −0.8473 | 4.9 | 10.4 | 10.4 |
| J1953+1844g | gpps0190 | 0.00444 | 113.1 | 19:53:44.0 | +18:44 | 56.7087 | −4.5750 | 121.8 | 4.8 | 4.4 |
| J2008+2755g | gpps0191 | 1.51926 | 155.1 | 20:08:16.6 | +27:55 | 66.2982 | −2.5868 | 110.5 | 6.3 | 7.4 |
| J1924+2037g | gpps0192 | 0.68480 | 82.3 | 19:24:33.5 | +20:37 | 54.9718 | +2.3301 | 3.3 | 3.8 | 2.9 |
| J1853−0008g | gpps0193 | 0.00282 | 285.3 | 18:53:12.3 | −00:08 | 33.0086 | −0.4571 | 13.8 | 5.9 | 4.6 |
| J1929+1731g | gpps0194 | 3.99540 | 431.1 | 19:29:04.2 | +17:31 | 52.7463 | −0.0848 | 13.4 | 11.6 | 9.2 |
| J1909+0930g | gpps0195 | 2.02078 | 479.6 | 19:09:46.6 | +09:30 | 43.4764 | +0.2967 | 16.0 | 8.5 | 8.4 |
| J1925+1636g | gpps0196 | 0.04971 | 33.1 | 19:25:47.6 | +16:36 | 51.5723 | +0.1693 | 11.2 | 2.3 | 1.5 |
| J1936+2036g | gpps0197 | 0.03292 | 198.8 | 19:36:41.0 | +20:36 | 56.3160 | −0.1689 | 28.6 | 6.7 | 5.0 |
| J1849+0016g | gpps0198 | 0.00181 | 271.4 | 18:49:58.2 | +00:16 | 33.008 | +0.4511 | 53.8 | 5.8 | 4.6 |
| J1852−0055g | gpps0199 | 0.16403 | 211.7 | 18:52:22.7 | −00:55 | 32.2216 | −0.6281 | 51.9 | 5.3 | 4.1 |
| J1901+0315g | gpps0200 | 0.81982 | 410.5 | 19:01:33.7 | +03:15 | 36.9871 | −0.7625 | 26.9 | 7.5 | 6.5 |
| J2023+2853g | gpps0201 | 0.01133 | 22.8 | 20:23:15.6 | +28:52 | 68.9127 | −4.8032 | 161.1 | 2.0 | 1.6 |

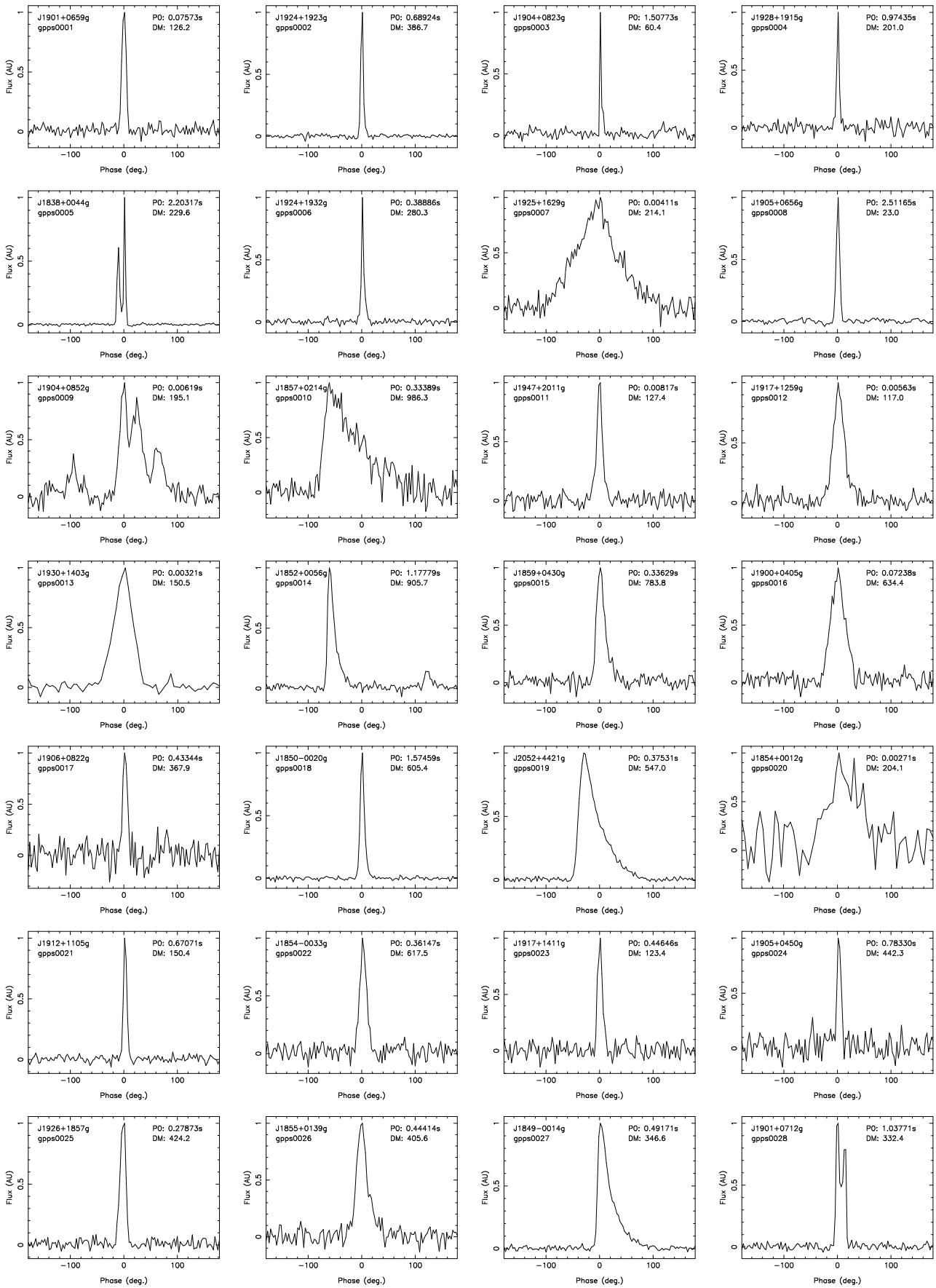


**Fig. 11** Integrated profiles of newly discovered pulsars, scaled to the peak and plotted in rotation phase of 360° for a full period. The pulsar name, gpps number, period and DM are noted in each panel.

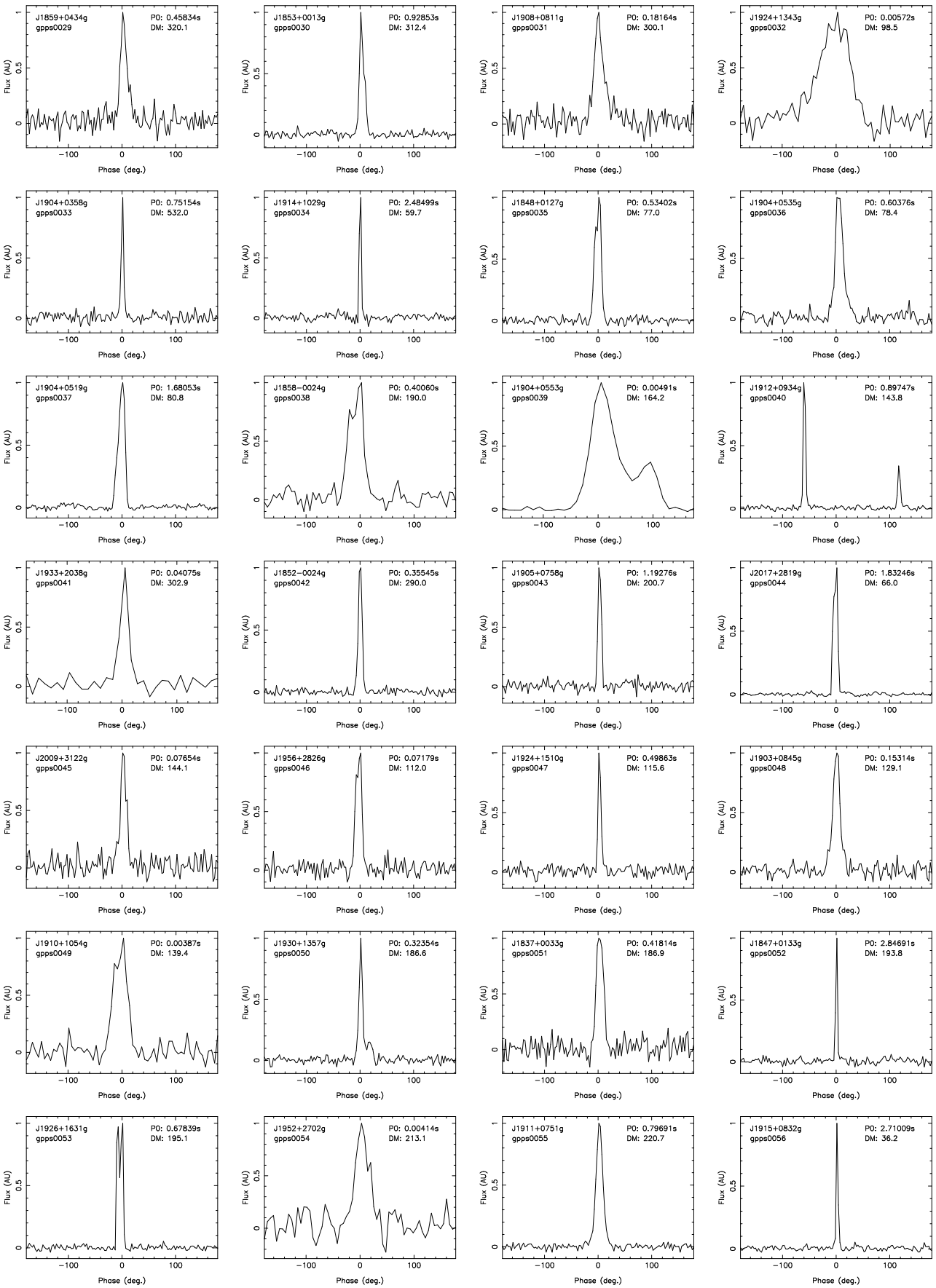


**Fig. 11** – *Continued*.

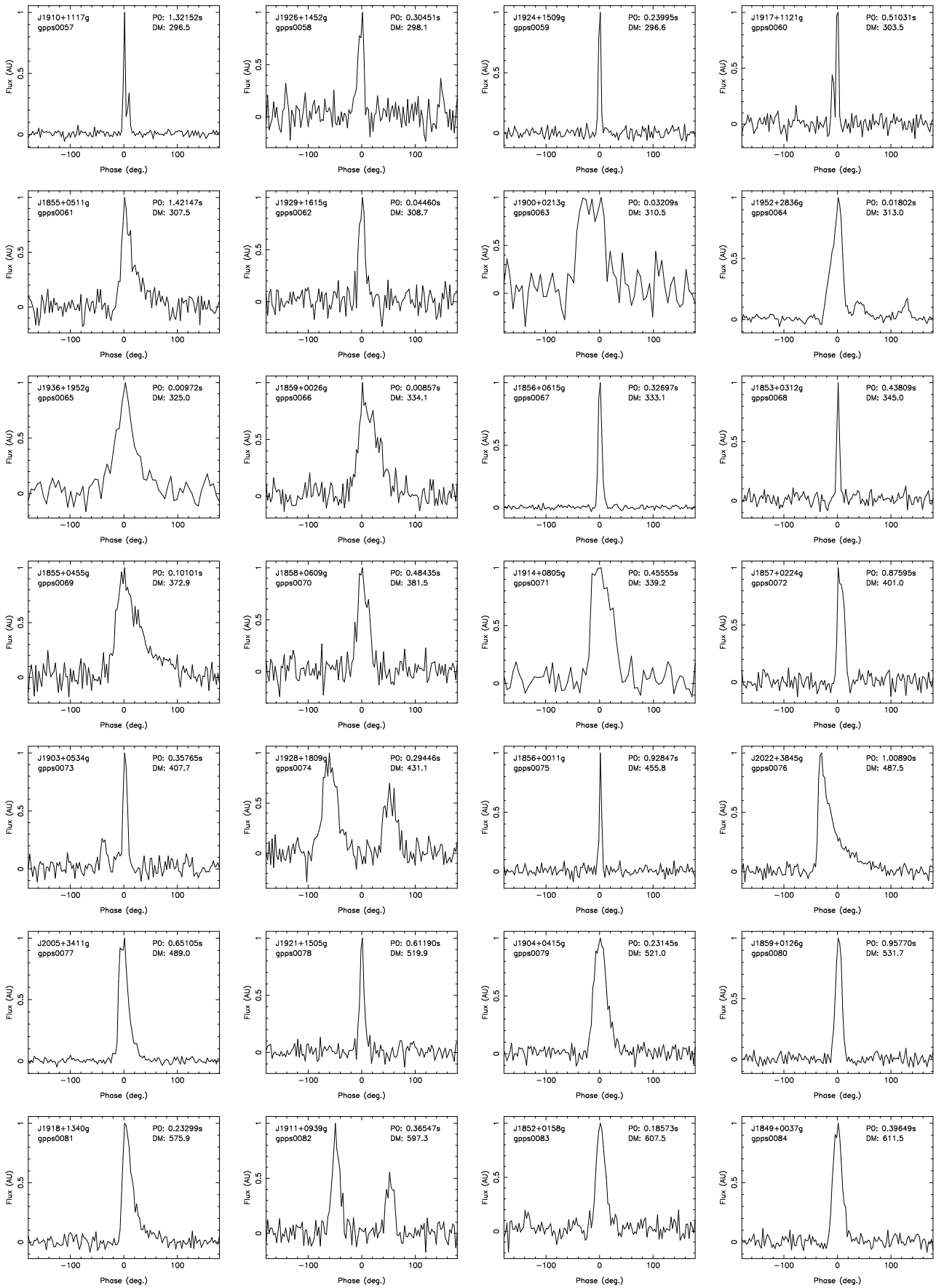


**Fig. 11** – *Continued*.

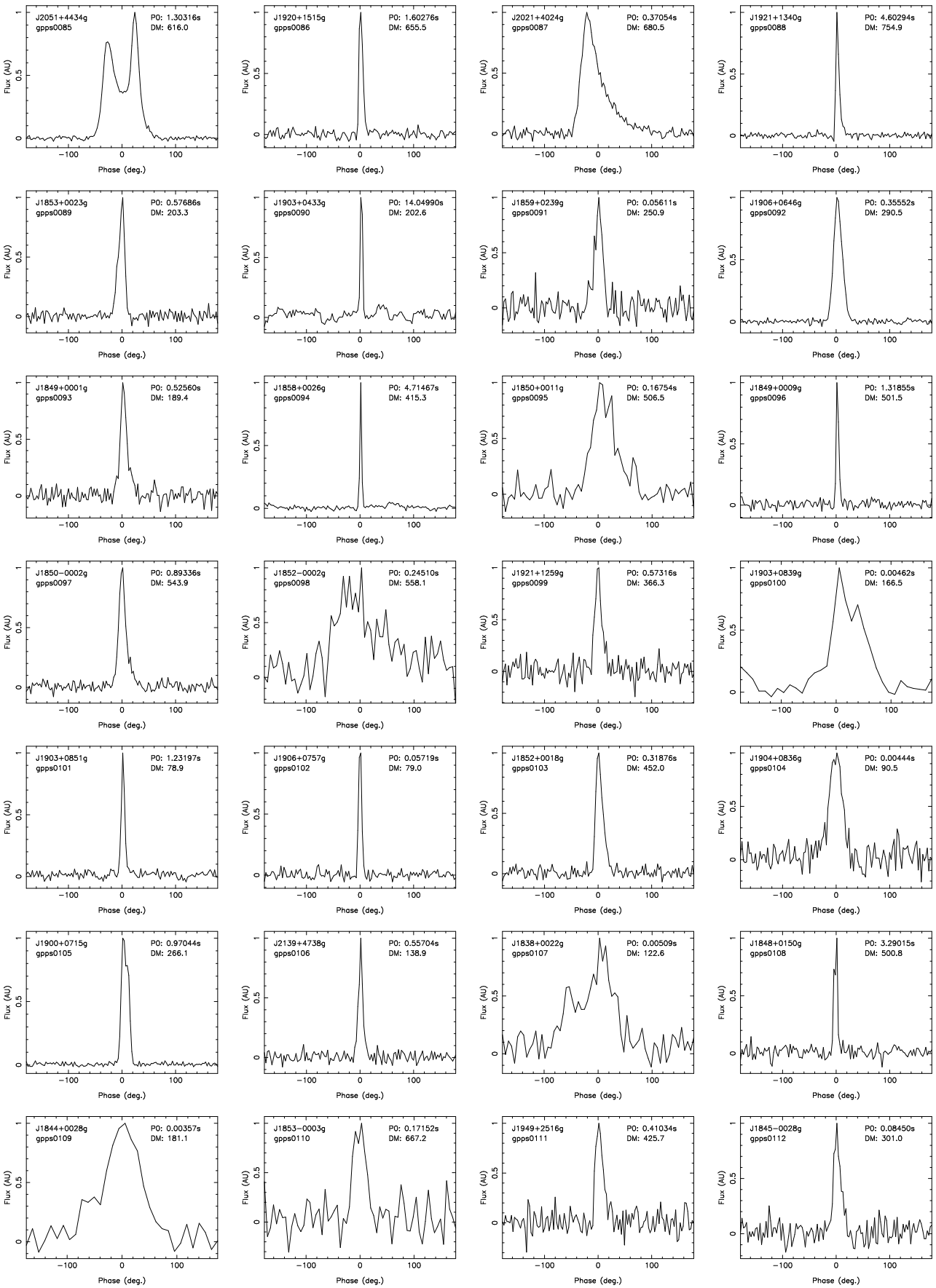


**Fig. 11** – *Continued*.

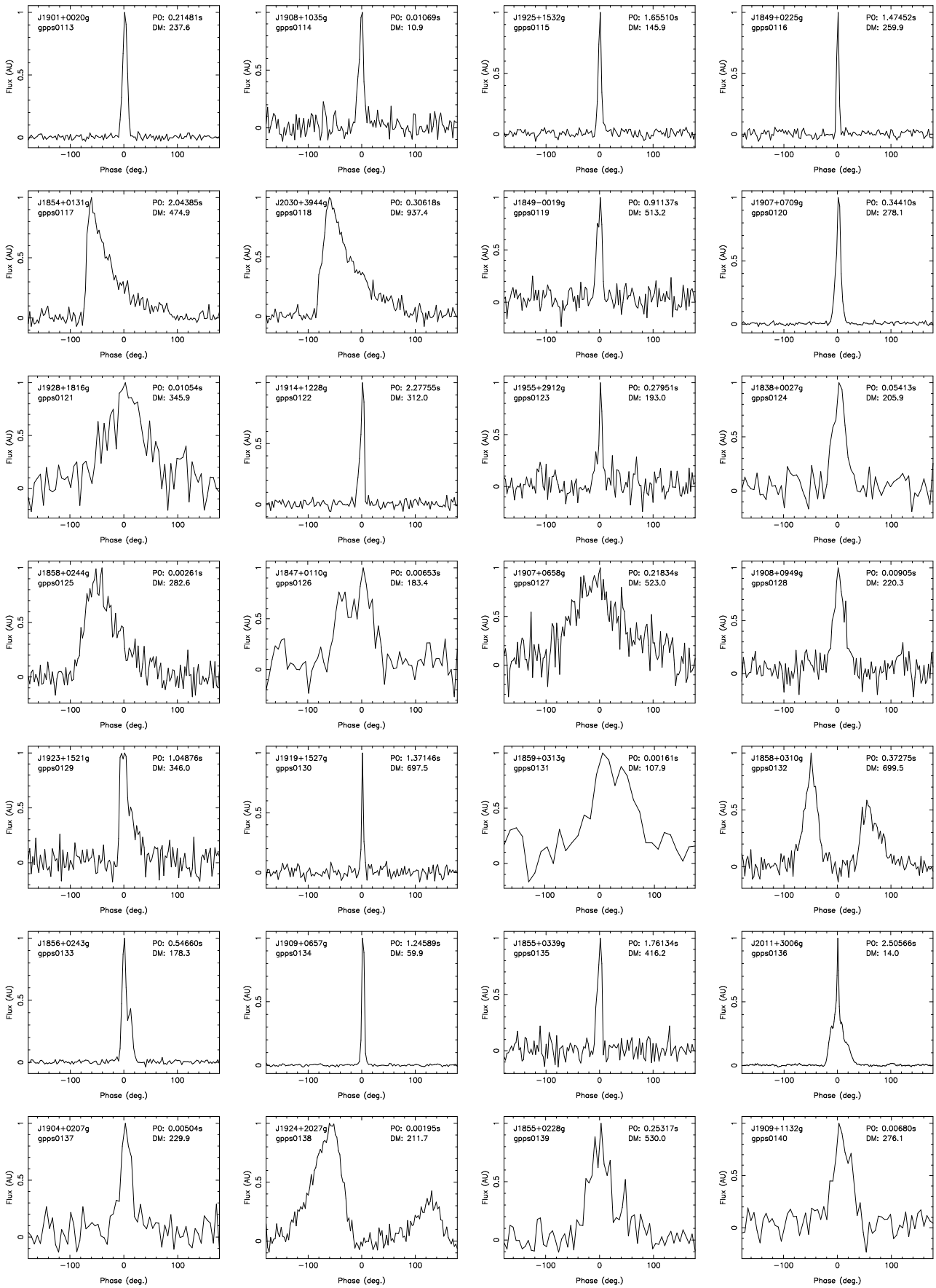


**Fig. 11** – *Continued*.

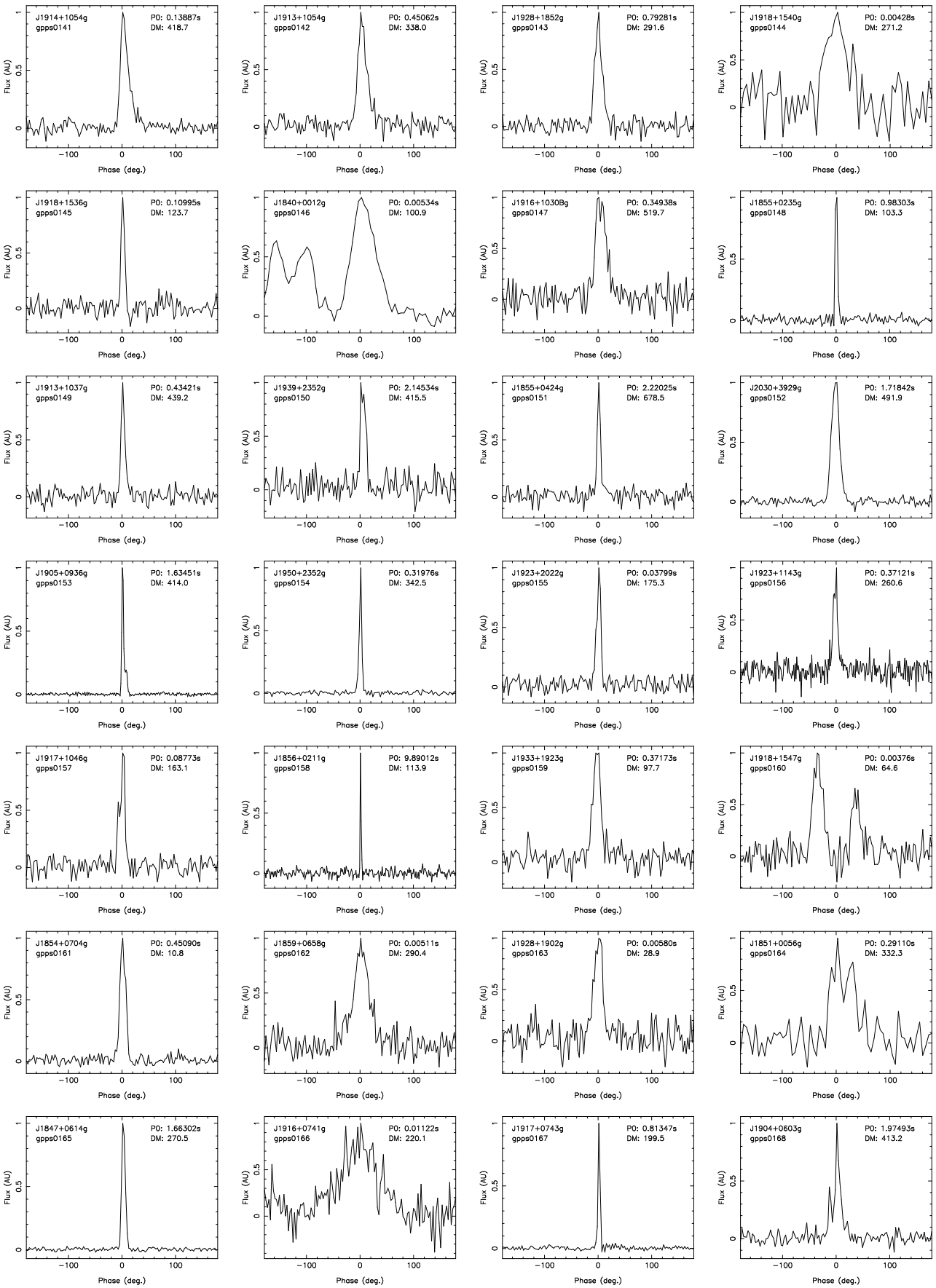


**Fig. 11** – *Continued*.

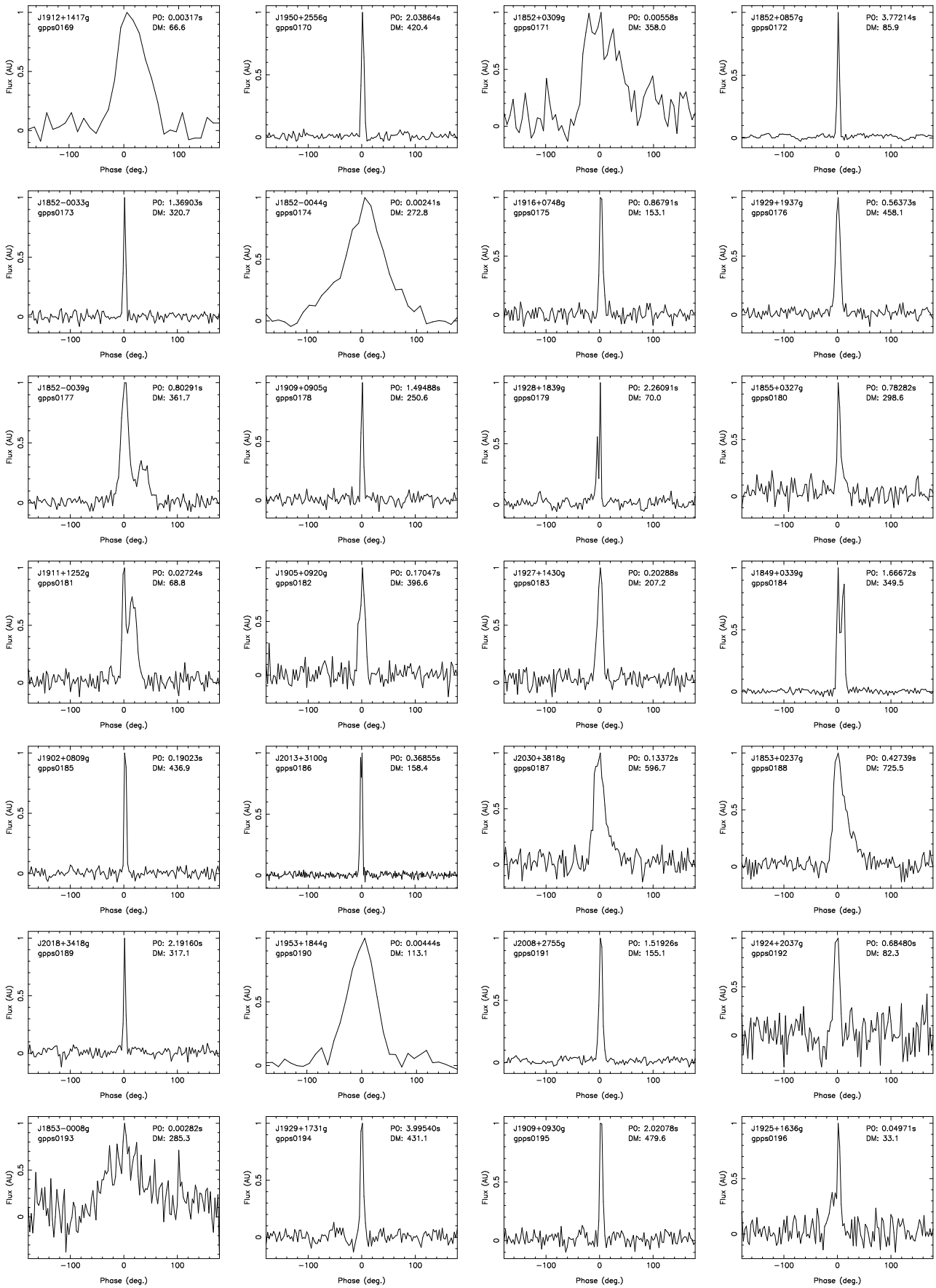


**Fig. 11** – *Continued*.

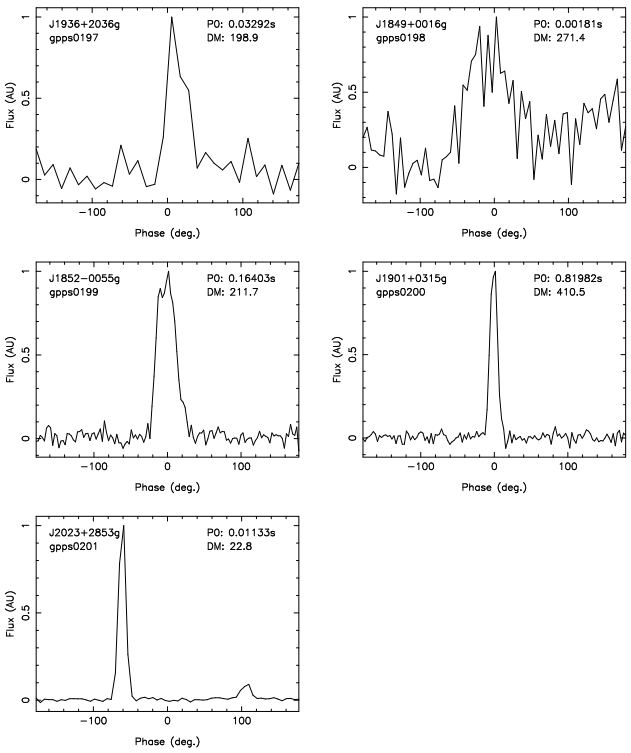


**Fig. 11** *– end.*

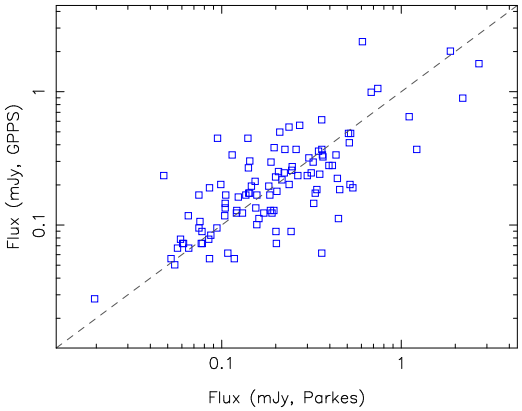


**Fig. 12** The estimated flux densities for Parkes pulsars detected in the GPPS survey are compared to the values in the ATNF pulsar catalog, which exhibits a remarkable consistence.

gain, so that there are only 1792 channels in the actual fits files in *data1j*. All relevant parameters, such as the channel frequency resolution, sampling time, MJD, etc., are accordingly stored in the head of fits files.

### *3.2.2 Searching for pulsars and pulses*

Three main approaches have been realized to search for pulsars and individual pulses: PRESTO (Ransom 2011), SIGPROC (Lorimer 2011) and our single pulse detection module developed in-house. Most of the data processing is carried out via multi-jobs (Tange 2020). Currently, the PRESTO module and the single pulse module have been applied to searching for all covers, and the SIGPROC module has been tested and will be applied for re-searching for all GPPS survey data by utilizing a new computer cluster that will be available in March 2021.

In the PRESTO module (Ransom 2011), a pipeline has been constructed to perform the pulsar search with a few steps:
(1) read the fits file, and check the RFI and make RFI masks, by using the *rfifind*;
(2) make the de-dispersion plan and de-disperse data by using *prepsubband*;
(3) search for periodical signals by using *accelsearch*;
(4) sift through the detected signals to find candidates and then fold data by using *prepfold*.
Through this processing, a number of candidates have been found, and the *.pfd* and *.bestprof* files and also corresponding plots are stored in the repository *data2j*.

In the SIGPROC module (Lorimer 2011), the fits data file is converted to filter-bank format first by utilizing the command *filterbank*, then de-dispersion is done by running the command *dedisperse_all* and then periodical signals are searched by using *seek*, and finally the results are combined and sorted to find the best $P$ and $DM$ for pulsar candidates by utilizing *best*. These candidates can be folded from the fits data by using *prepfold* in the PRESTO module, and the results are also stored in the repository *data2j*.

We have developed a single pulse module, which has three steps: de-dispersion, finding a single pulse from the image of data-array of DM-time with speedy artificial intelligence (AI) recognition in GPU clusters and the period finding for the picked pulses.

In addition, the pulsar acceleration search has been tested for a few beams for binary candidates, and will be carried out for all GPPS survey data when the new computer clusters are available.

### *3.2.3 Evaluation of searching results*

After pulsar searching has been completed, a large number of pulsar candidates have been found. Each candidate has a *.pfd*, *.bestprof* and *.ps* file in the repository *data2j*. In fact, not only pulsar signals but also some RFI which mimics pulsar signal features can be selected by pulsar searching software. Therefore, evaluation of searching results is desired.

We found that the AI code developed by Zhu et al. (2014) is very efficient for discriminating a pulsar signal from RFI. A new AI module has been developed and tested, and is applied in parallel. After this AI-sifting of candidates, only a small number of false candidates

have to be discarded during manual checking of pulsar candidates. The relevant parameters can be extracted from *.bestprof* and tabulated. These candidates from each survey observation are cross-matched with known pulsars, and certainly only real candidates for new pulsars will be further manually examined and undergo folding by *pdmp*. If the result is good, the candidate will be observed again for verification.

One side effect of high S/N pulses, which is seen more often with the highly sensitivity FAST, is that there are too many candidates in a wide range of cross-modulated period and DM values, as illuminated by the peaks in Figure 10 caused by a strong pulsar. The searching software can pick up these fake candidates, which have to be carefully discarded by using a naive analysis above a high threshold.

### 3.3 Verification Observations and Processing

Thanks to the excellent pointing accuracy of FAST, the position of any good candidate detected from one beam can be determined with an accuracy better than $1.5'$ in radius. For strong pulsars detected in a few nearby beams in the snapshot observations, more accurate coordinates can be determined according to their beam center positions in the sky and the S/N of a pulsar detected from these beams.

Once the position of a good candidate is determined, follow-up tracking observation is carried out for 15 min, with the central beam of the L-band 19-beam receiver pointed to the position. To investigate the properties of the pulsar, data of four polarization channels ($XX$, $YY$, $X^*Y$, $XY^*$) from the verification observations are always recorded. Before the beginning and after the end of the observation session, the calibration signals are switched on and off, for 1 second each, and the data are recorded for two minutes and will be utilized for calibrations. In order to maximize the FAST time efficiency for pulsar detection, data on the other 18 beams, in addition to the central beam, are also recorded for a deeper pulsar search.

Data processing for the verification observations follows the same searching procedure. In general, a new pulsar is detected with a better S/N. In addition, the data are folded by running *pdmp*. The times of arrival (TOAs) of these observations will be used to derive the period $P$ of a pulsar at a given epoch and the period derivative $\dot{P}$ when several measurements are available.

## 4 DISCOVERIES OF NEW PULSARS

The available GPPS survey data have been processed for only the first round. About 330 previously known pulsars have been detected, some of which will be discussed in the next section for updated parameters. Here we report 201 newly discovered pulsars, including several pulsars with

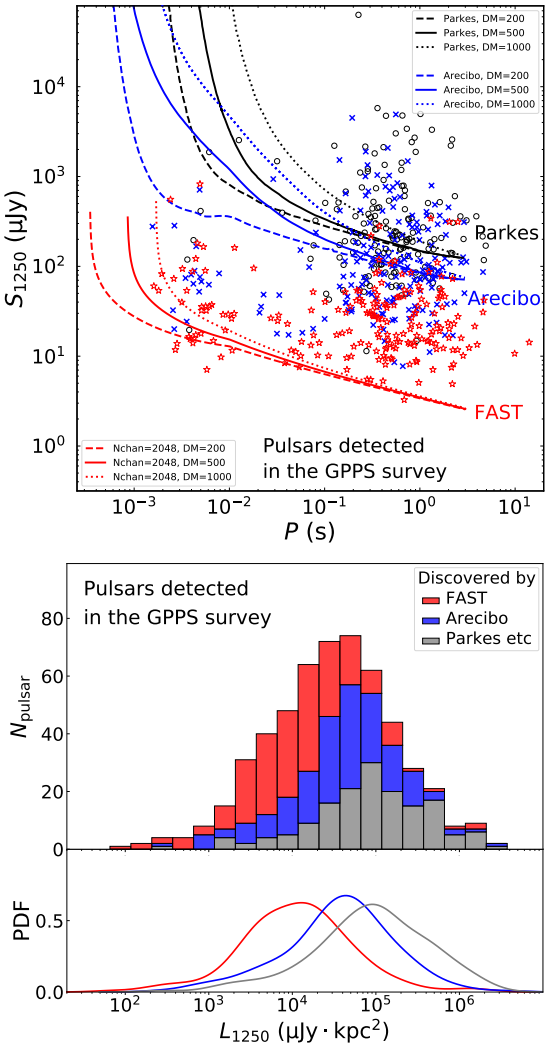


**Fig. 13** *Top*: the GPPS pulsars (201) always have a smaller flux, as indicated by red stars, compared to the pulsars discovered by, e.g., Arecibo (180), Parkes, etc. (156) radio telescopes. All pulsars featured here are detected in the GPPS survey. Some pulsars below the sensitivity curves are nulling pulsars, or pulsars with a narrower pulse than the assumed 5% of the period, or pulsars first detected by verification observations. *Bottom*: comparison of the luminosity distribution of the GPPS pulsars with those of other surveys, in terms of the number distribution (the *upper panel*) and the probability density function (PDF, the *lower panel*).

polarization measurements and an RRAT found through the single pulse module. The integrated profiles of newly discovered pulsars are featured in Figure 11. In Table 2, we list the basic parameters for new discoveries, including a temporary name with a suffix "g", period (in seconds), DM, coordinates in RA (J2000) and Dec (J2000) which have an uncertainty of less than $1.5'$, and the Galactic coordinates GL and GB, an averaged flux density at 1.25 GHz, two values of derived distances by using the electron density models of NE2001 (Cordes & Lazio 2001)

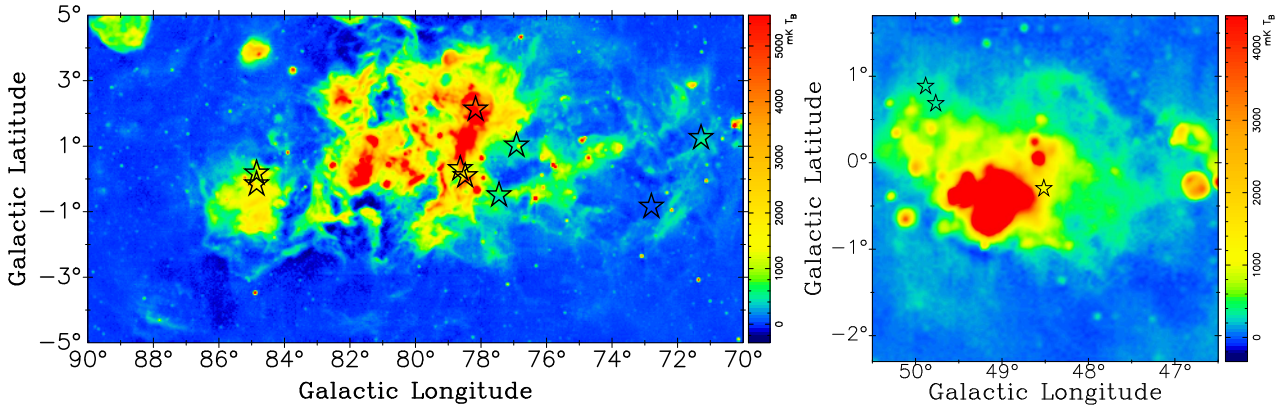


**Fig. 14** These pulsars have a large DM, marked as stars on the 11 cm radio map (Reich et al. 1990; Furst et al. 1990), probably because they are located just in the tangential directions of the Local Arm (*the left panel*) and the Sagittarius arm (*the right panel*), where HII regions obviously contribute significant DMs.

and YMW16 (Yao et al. 2017). Often the periods found in the search process are harmonics, so that a correct period has to be found (e.g. 2×, 3×, 5×, 7×, 11×, 13× and 17× the harmonic period). For a bright pulsar detected in several beams, its position is determined from a weighted average of the center positions of these beams; here the S/Ns of profiles from these beams are taken as the weighting factor. So-determined position has an accuracy of better than $1'$. For a weak pulsar detected in just one beam, the beam center is simply taken as the position, so that the position uncertainty is about the beam size that is about $1.5'$ in radius. It is possible that a pulsar is very offset from the center of a beam, so that it is stronger but looks like a weaker pulsar due to the reduced gain of the beam.

Pulsar flux densities are estimated from the integrated pulse energy over the off-pulse deviations which are related to $T_{\rm sys} + T_{\rm sky}$. We extract their values for the flux density estimations since $T_{\rm sys}$ depends on the zenith angle (Jiang et al. 2020) and $T_{\rm sky}$ varies with the Galactic longitude and latitude (Reich et al. 1990; Furst et al. 1990). The so-estimated flux densities of Parkes pulsars are compared to the values in the ATNF Pulsar Catalogue, and we found excellent consistence (see Fig. 12).

Follow-up observations are going on for many newly discovered pulsars, especially binaries. On the website for the FAST GPPS survey[9] are releases of new discoveries and updates of survey status and pulsar parameters.

In the following, we highlight some interesting pulsars, and the first are μJy weak pulsars.

### 4.1 Discovery of Faintest Pulsars

As shown in Figure 13 and also flux values in Table 2, the GPPS survey can detect weak pulsars. There are 23 pulsars with a flux density less than 10 μJy at 1.25 GHz, much weaker than those previously detected by Parkes pulsar surveys or Arecibo pulsar surveys. Up to now, the weakest known pulsar was discovered in the GPPS survey, that is PSR J1924+2037g (gpps0192, $S_{1250\rm MHz}$ = 3.3 μJy), a very nulling pulsar discovered first via the single-pulse module and later sorted by the PRESTO module. A number of weakest pulsars around 5 μJy are PSR J2018+3418g (gpps0189, 4.9 μJy), PSR J1928+1915g (gpps0004, 5.1 μJy), PSR J1949+2516g (gpps0111, 5.3 μJy), PSR J1926+1452g (gpps0058, 5.5 μJy) and PSR J1955+2912g (gpps0123, 5.5 μJy).

On the other hand, the intrinsically faintest pulsars should have both flux density and distance considered. Currently, three very nearby pulsars, PSR J1908+1035g (gpps0114, 11.6 μJy, DM = 10.9 $\rm cm^{-3}pc$, $\rm Dist_{YMW16}$ = 0.7 kpc, L = 5.7 μJy $\rm kpc^2$), PSR J1854+0704g (gpps0161, 34.6 μJy, DM = 10.8 $\rm cm^{-3}pc$, $\rm Dist_{YMW16}$ = 0.6 kpc, L = 12.5 μJy $\rm kpc^2$) and PSR J1928+1902g (gpps0163, 7.1 μJy, DM = 29.8 $\rm cm^{-3}pc$, $\rm Dist_{YMW16}$ = 1.5 kpc, L = 16.0 μJy $\rm kpc^2$) have a luminosity of less than 20 μJy $\rm kpc^2$, which are the faintest known pulsars discovered by the GPPS survey. The luminosity distribution given in the lower panel of Figure 13 clearly affirms that the GPPS survey has significantly improved the determination of the faint end of the pulsar luminosity function, which has to be included in many relevant simulations (Lorimer et al. 2019; Huang & Wang 2020).

### 4.2 Discovery of Pulsars with Excess DMs Not Modeled

By looking at Table 2, one may notice that some pulsars have large DMs, and hence their distances estimated based on the electron distribution models (Cordes & Lazio 2001; Yao et al. 2017) are very large, i.e., $>$ 25 kpc in the YMW16 model (Yao et al. 2017) or $>$ 50 kpc in the NE2001 model (Cordes & Lazio 2001), see Figure 15,

[9] http://zmtt.bao.ac.cn/GPPS/

**Table 3** Distant Pulsars with Excess DMs Challenging the Currently Widely Used Models

| PSR name | gpps No. | GL (°) | GB (°) | DM ($cm^{-3}$ pc) | $D_{NE2001}$ (kpc) | $D_{YMW16}$ (kpc) | $DM^{max}_{NE2001}$ ($cm^{-3}$ pc) | $DM^{max}_{YMW16}$ ($cm^{-3}$ pc) |
|---|---|---|---|---|---|---|---|---|
| J2052+4421g | gpps0019 | 84.8417 | −0.1616 | 547.0 | 50.0 | 25.0 | 365.6 | 428.5 |
| J2051+4434g | gpps0085 | 84.8479 | +0.1706 | 616.0 | 50.0 | 25.0 | 365.5 | 443.2 |
| J2030+3944g | gpps0118 | 78.6299 | +0.2988 | 937.4 | 50.0 | 25.0 | 398.1 | 466.3 |
| J2030+3929g | gpps0152 | 78.4765 | +0.0848 | 491.9 | 50.0 | 25.0 | 400.4 | 456.8 |
| J2021+4024g | gpps0087 | 78.1680 | +2.1153 | 680.5 | 50.0 | 25.0 | 349.2 | 500.2 |
| J2030+3818g | gpps0187 | 77.4492 | −0.5085 | 596.7 | 50.0 | 25.0 | 401.9 | 427.3 |
| J2022+3845g | gpps0076 | 76.9110 | +1.0169 | 487.5 | 50.0 | 17.2 | 392.9 | 495.1 |
| J2005+3411g | gpps0077 | 71.2811 | +1.2438 | 489.0 | 50.0 | 17.3 | 415.6 | 501.8 |
| J1919+1527g | gpps0130 | 49.8846 | +0.8895 | 697.5 | 50.0 | 16.9 | 612.7 | 771.5 |
| J1920+1515g | gpps0086 | 49.7623 | +0.6780 | 655.5 | 50.0 | 15.7 | 630.7 | 777.6 |
| J1921+1340g | gpps0088 | 48.4946 | −0.3047 | 754.9 | 50.0 | 25.0 | 674.9 | 754.3 |

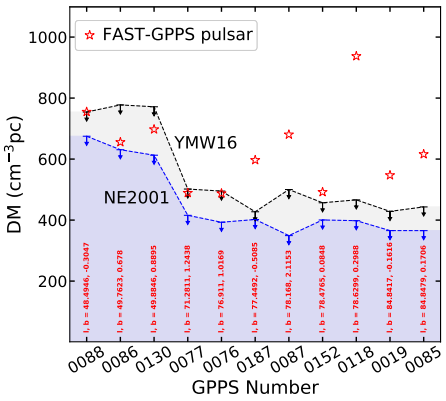


**Fig. 15** DMs of the newly discovered GPPS pulsars in Table 3 are larger than the maximum given by YMW16 model (Yao et al. 2017) and/or NE2001 model (Cordes & Lazio 2001).

which are an indication of their possible locations outside the Milky Way. We extract their relevant parameters and put them in Table 3. Notice that these pulsars are in the direction of the Local Arm (Xu et al. 2016) or the tangential direction of spiral arms (Hou & Han 2014), therefore the large DMs are not surprising at these low Galactic latitudes since lines of sight will intersect spiral arms that are wider than those in the models. HII regions in the lines of sight as shown in Figure 14 should contribute a large amount of thermal electrons.

How much DM can an HII region contribute to a pulsar? A quick answer comes from the DMs of pulsars in the outer Galaxy ($90° < GL < 270°$) where mostly HII regions in the Perseus arm contribute. In the ATNF Pulsar Catalogue of Manchester et al. (2005), these pulsars in general have DM values of several tens, but 10 pulsars have DM between 200 to 300 $cm^{-3}$ pc. If occasionally the line of sight to a pulsar passes through three such HII regions, it is not impossible to have a DM of several hundred. The probability is very small for a pulsar with such radio flux densities located in a background galaxy just behind these spiral arms. We therefore suspect that these pulsars in Table 3 are located in or just behind the spiral arms and that these HII regions in these spiral arms are responsible for the observed large DMs. In other words, the electron density from HII regions in these spiral arms is probably underestimated and should be updated in the electron density distribution models. In Table 3, the asymptotic maximum DM values provided by the two models are also listed, which shows that the observed DMs have exceeded the maximum DM in the model. The largest DM excess is given by PSR J2030+3944g (gpps0118, DM=937.4 $cm^{-3}$ pc), while the modeled DM is around 400 – 500 $cm^{-3}$ pc. Obviously, a better model is desired to account for the excess DMs.

### 4.3 Discovery of Pulsars in Supernova Remnants?

Among the newly discovered pulsars, several are coincident with known supernova remnants (SNRs, see a catalog by Green 2019), as seen in Figure 16 and listed in Table 4. Then the question arises: are they physically associated?

To ensure the association, a simple criterion must be satisfied that a young pulsar must be inside the remnant in three-dimensional space. In addition to coincidence on the sky, as displayed in Figure 16, accurate measurements for the distance to the pulsar and the remnant are desired, which are in general difficult to achieve. As seen in Table 4, the distance estimate for SNR G65.1+0.6 is in the range of 8.7−10.1 kpc (Tian & Leahy 2006), and that for G78.2+2.1 is 1.9 kpc (Lin et al. 2013; Shan et al. 2018). The distance of pulsars can be estimated from DMs. Given large uncertainties in the estimated distances, other supplementary arguments for the association could be that the pulsar is young, which has to be determined by the period derivatives deduced from more TOA data which are being measured now.

On the top-right of G33.2−0.6 (see Fig. 16), we discovered a pulsar PSR J1853−0003g (gpps0110) with a period of $P$ = 0.17152 s and DM = 667.2 $cm^{-3}$ pc, very nearby but different from a known pulsar PSR J1853−0004 discovered by the Parkes multibeam survey (Hobbs et al. 2004) with a period of $P$ = 0.101436 s and DM = 437.5 $cm^{-3}$ pc at a distance of 5.3 kpc estimated by the YMW16 model (Yao et al. 2017).

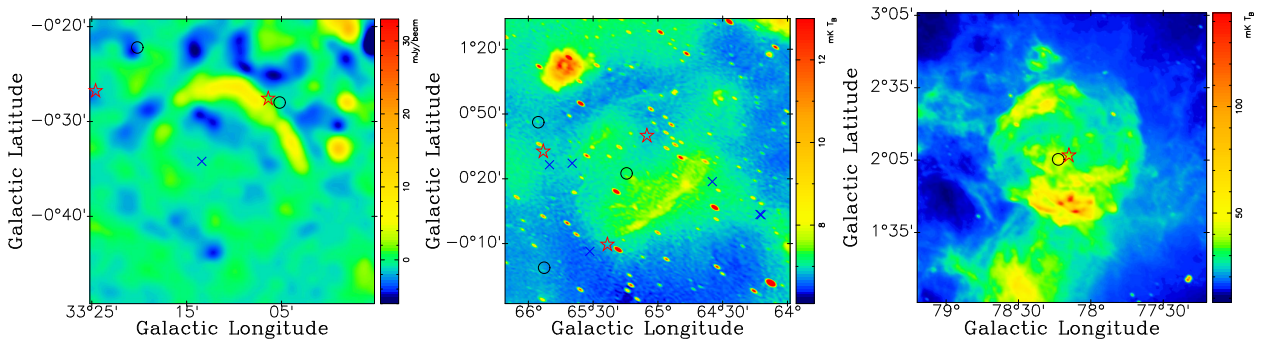


**Fig. 16** Newly discovered pulsars coincident with supernova remnants, signified as stars in these plots. Previously known pulsars are marked as crosses or circles (ref. Fig. 13). The background radio images are extracted from the NRAO VLA Sky Survey (Condon et al. 1998) for SNR G33.2−0.6 and from the Canadian Galactic Plane Survey (English et al. 1998; Taylor et al. 2003) for the others.

**Table 4** Pulsars Coincident with Supernova Remnants

| SNR | RA(2000) (hh:mm:ss) | Dec(2000) (dd:mm) | Size (′) | $D_{SNR}$ (kps) | gpps No. | RA(2000) (hh:mm:ss) | Dec (2000) (dd:mm) | offset (′) | P (s) | DM ($cm^{-3}$ pc) | $D_{YMW16}$ (kpc) | $D_{NE2001}$ (kpc) |
|---|---|---|---|---|---|---|---|---|---|---|---|---|
| G33.2−0.6 | 18:53:50 | −00:02 | 18 | | gpps0110 | 18:53:24 | −00:03 | 6.6′ | 0.1715 | 667.2 | 9.1 | 6.3 |
| G65.1+0.6 | 19:54:40 | +28:35 | 90×50 | 8.7–10.1 | gpps0046 | 19:56:48 | +28:26 | 29.4′ | 0.0718 | 112.0 | 4.8 | 6.5 |
| | | | | | gpps0064 | 19:52:48 | +28:36 | 24.5′ | 0.0180 | 313.0 | 9.7 | 10.5 |
| | | | | | gpps0123 | 19:55:11 | +29:12 | 39.7′ | 0.2795 | 193.0 | 7.0 | 7.4 |
| G78.2+2.1 | 20:20:50 | +40:26 | 60 | 1.9 | gpps0087 | 20:21:13 | +40:24 | 4.3′ | 0.3705 | 680.5 | 25.0 | 50.0 |

By looking at the period and estimated distances of these pulsars in the field of SNR G65.1+0.6, one might guess that PSR J1956+2826g (gpps0046) has a period similar to the values of young pulsars, but the distance of PSR J1952+2836g (gpps0064) is closer to that of SNR G65.1+0.6. Tian & Leahy (2006) argued previously that PSR J1957+2831 ($P$ = 0.307683 s, DM = 139.0 $cm^{-3}$ ps, GL = 65.5240°, GB = −0.2249°) is associated with the remnant, which in fact is further away from the remnant than PSR J1956+2826g. Another new pulsar, PSR J1955+2912g (gpps0123), is also further away and probably not associated with the SNR.

Near the center of adiabatically expanding shell-type SNR G78.2+2.1, a radio quiet X-ray and gamma-ray pulsar, PSR J2021+4026, was located and has been claimed to be associated with the SNR (Lin et al. 2013). The X-ray and gamma-ray timings show that it is a young pulsar with a period of $P$ = 0.265318 s (Hui et al. 2015), $\dot{P}$ =5.48 × $10^{-14}$ s $s^{-1}$ and hence a spin-down age of ∼77 kyr (Abdo et al. 2009). The newly discovered pulsar from the GPPS survey, PSR J2020+4024g (gpps0087), which has a larger period of 0.37054 s (about 7/5 period of PSR J2021+4026) and is also located at the very center of G78.2+2.1. We suspected PSR J2020+4024g is the radio counterpart of PSR J2021+4026. However, we cannot get the folded profile around the period of PSR J2021+4026. Considering that 1) the newly discovered pulsar has a very different period; 2) it has a very large DM (680.5 $cm^{-3}$ ps) and hence a much greater distance (though probably overestimated as mentioned above) than the estimated distance of less than 2 kpc for the remnant (Shan et al. 2018); 3) its profile has an obviously scattered tail, we therefore conclude the new pulsar PSR J2020+4024g is distant and just coincident with the remnant in the direction of the Local Arm.

In summary, no physical association for any newly discovered pulsars with these supernova remnants can be concluded from available data.

**Table 5** Binary Pulsars Discovered in the GPPS Survey (Sorted by Pulsar Period)

| PSR Name | P (ms) | MJD | DM ($cm^{-3}$ pc) | Acc* ($ms^{-2}$) |
|---|---|---|---|---|
| J1859+0313g | 1.6133516 | 58770.464631 | 107.7 | 9.0 |
| J1852−0044g | 2.4117532 | 59281.036276 | 272.9 | 16.0 |
| J1912+1417g | 3.1661676 | 59270.015017 | 66.6 | −8.7 |
| J1930+1403g | 3.2092399 | 58885.155530 | 150.5 | 0.1 |
| J1844+0028g | 3.5705885 | 59126.433750 | 181.2 | 2.0 |
| J1953+1844g | 4.4441330 | 59293.074883 | 113.1 | −1.9 |
| J1903+0839g | 4.6213782 | 59084.555017 | 166.5 | −5.6 |
| J1904+0553g | 4.9073156 | 58940.003865 | 164.3 | 0.9 |
| J1840+0012g | 5.3394411 | 59215.208372 | 100.8 | 5.2 |
| J1917+1259g | 5.6378496 | 58887.175359 | 117.0 | 0.8 |
| J1928+1816g | 10.543555 | 58999.880554 | 346.3 | −73.0 |
| J2023+2853g | 11.331753 | 59080.693995 | 22.8 | −9.6 |
| J1952+2836g | 18.023112 | 59135.498861 | 313.4 | 1.5 |
| J1936+2036g | 32.923094 | 59091.606022 | 198.8 | −7.5 |
| J1933+2038g | 40.706716 | 59004.760866 | 302.8 | −18.0 |
| J1913+1037g | 434.21498 | 59214.259211 | 437.0 | −4.0 |

*Acceleration parameter obtained from *pdmp*.

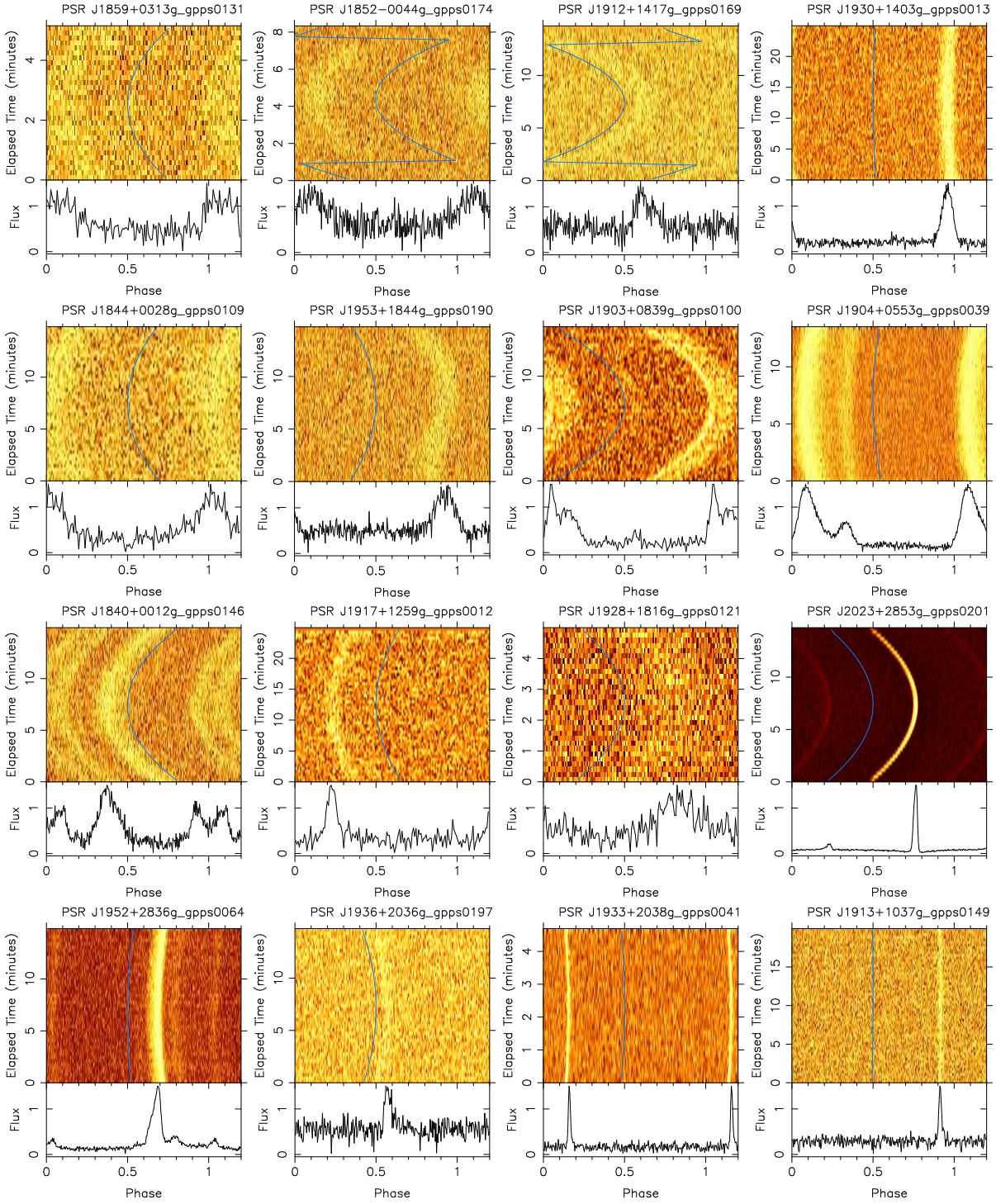


**Fig. 17** Phase changes of pulses during a session of observations of a few newly discovered pulsars in the GPPS survey indicating their nature in a binary system. For each pulsar, the upper panel is the phase-time waterfall plot, with the phase defined in the unit of the spin period of a pulsar; the lower panel is the integrated profile after the phase shifts are corrected.

### 4.4 Discovery of Millisecond Pulsars and Binary Pulsars

In Table 2, there are 40 pulsars with a period less than 30 ms, which can be regarded as MSPs according to the $P - \dot{P}$ diagram for previously known pulsars, though the $\dot{P}$ values of newly discovered pulsars are not available yet. The current young pulsars all have a period greater than 30 ms. Among these MSPs, 14 pulsars manifest their obvious pulse shift (coming early or delayed from the best phase bin, as shown in Fig. 17) in

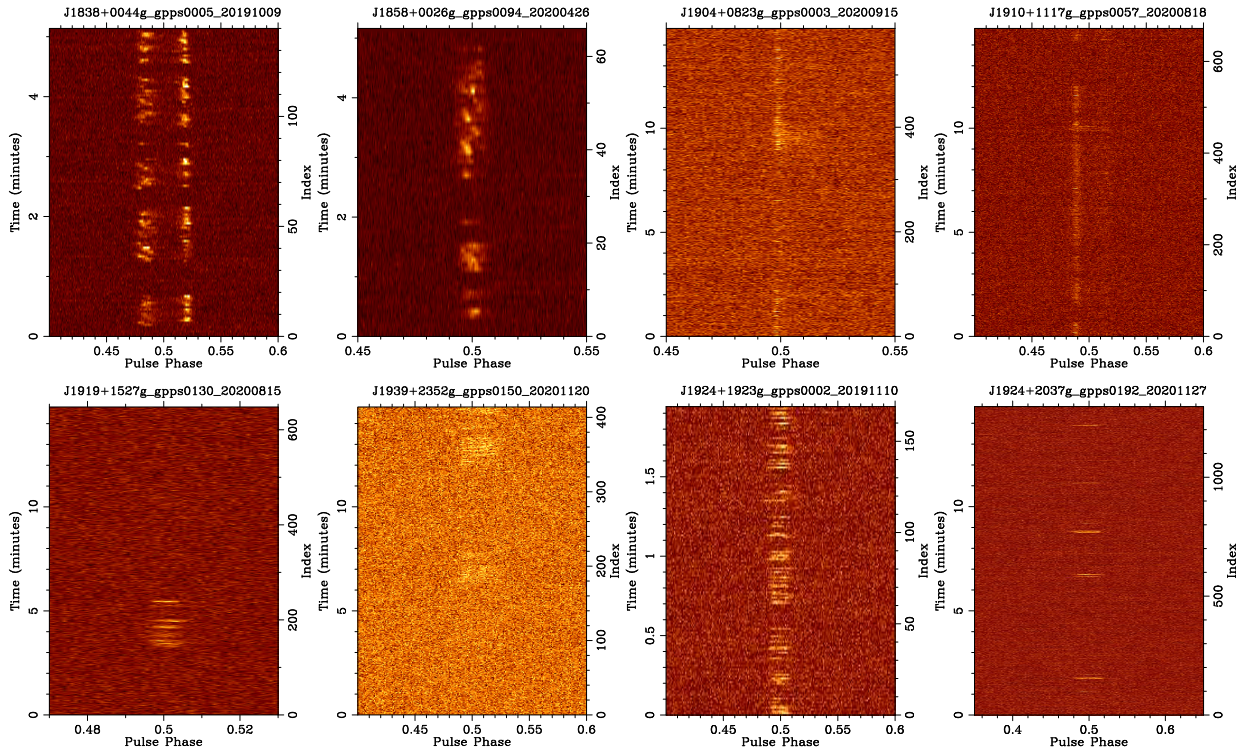


**Fig. 18** Phase-time plots exhibit nulling phenomena for eight newly discovered pulsars in the GPPS survey.

a short observation session, which indicates their binary nature, as listed in Table 5, as do two longer period pulsars J1933+2038g (gpps0041, $P$ = 40.7 ms) and PSR J1913+1037g (gpps0149, $P$ = 434.2 ms).

Two interesting binaries are remarkable. The binary pulsar, J1953+1844g (see Fig. 17) was discovered in a snapshot survey with $P$ = 4.44 ms and DM = 113.1 cm$^{-3}$ pc, and is probably located in the global cluster M71, because it is only 2.5′ away from M71A/PSR J1953+1846 (DM = 117.0 cm$^{-3}$ pc, Hessels et al. 2007) and has a similar but smaller DM than the four previously known pulsars in M71[10]. The binary pulsar J2023+2853g (gpps0201,$P$ = 11.33 ms, DM = 22.8 cm$^{-3}$ pc) was found in the vicinity of a bright known pulsar, J2022+2854 ($P$ = 343.402 ms, DM = 24.6 cm$^{-3}$ pc). Its signals were easily misinterpreted as a harmonic of the known pulsar because they have similar but slightly different DM values.

Parameters of all these millisecond and binary pulsars have to be determined in more follow-up observations, which are going on by the survey team members. Careful observations and detailed analyses of these binary systems may reveal a number of relativistic effects and lead to excellent tests of some fundamental properties of gravity.

[10] https://fast.bao.ac.cn/cms/article/65/

### 4.5 Discovery of Nulling and Mode-Changing Pulsars

By viewing the phase-time plots of newly discovered pulsars, we noticed that several pulsars display the mode-changing or nulling phenomenon (see examples in Fig. 18) in the duration of observations, i.e., they switch their emission modes or even cease their emission for some periods. More interesting are subpulses of PSR J1838+0046g, which drift and modulate both in the leading and trailing profile components, in addition to the nullings around pulses, e.g., Nos. 20, 60, 90 and 120. PSR J1858+0028g undergoes nulling and subpulse-drifting. PSRs J1904+0823g and J1910+1117g occasionally have a bright pulse, even during a long nulling session (e.g., PSR J1904+0823g at the period index No.260) similar to that for PSR B0826−34 reported by Esamdin et al. (2012). Mode-changing and nulling are obvious for PSR J1910+1117g. Very nulling pulsars, PSR J1919+1527g (gpps0130), J1939+2352g (gpps0150) and PSR J1924+2037g (gpps0192), have a short duration for emission but a longer duration for nulling (see Fig. 18). They were first detected as a few individual pulses via a self-developed single pulse module, and later the period emission was found from a track observation for 15 minutes via the PRESTO search module.

Since the duration of the GPPS survey is only 300 s and that for follow-up verification observations is only 15 minutes, it is hard to get the nulling fraction or study the details of mode-changes or get statistical properties

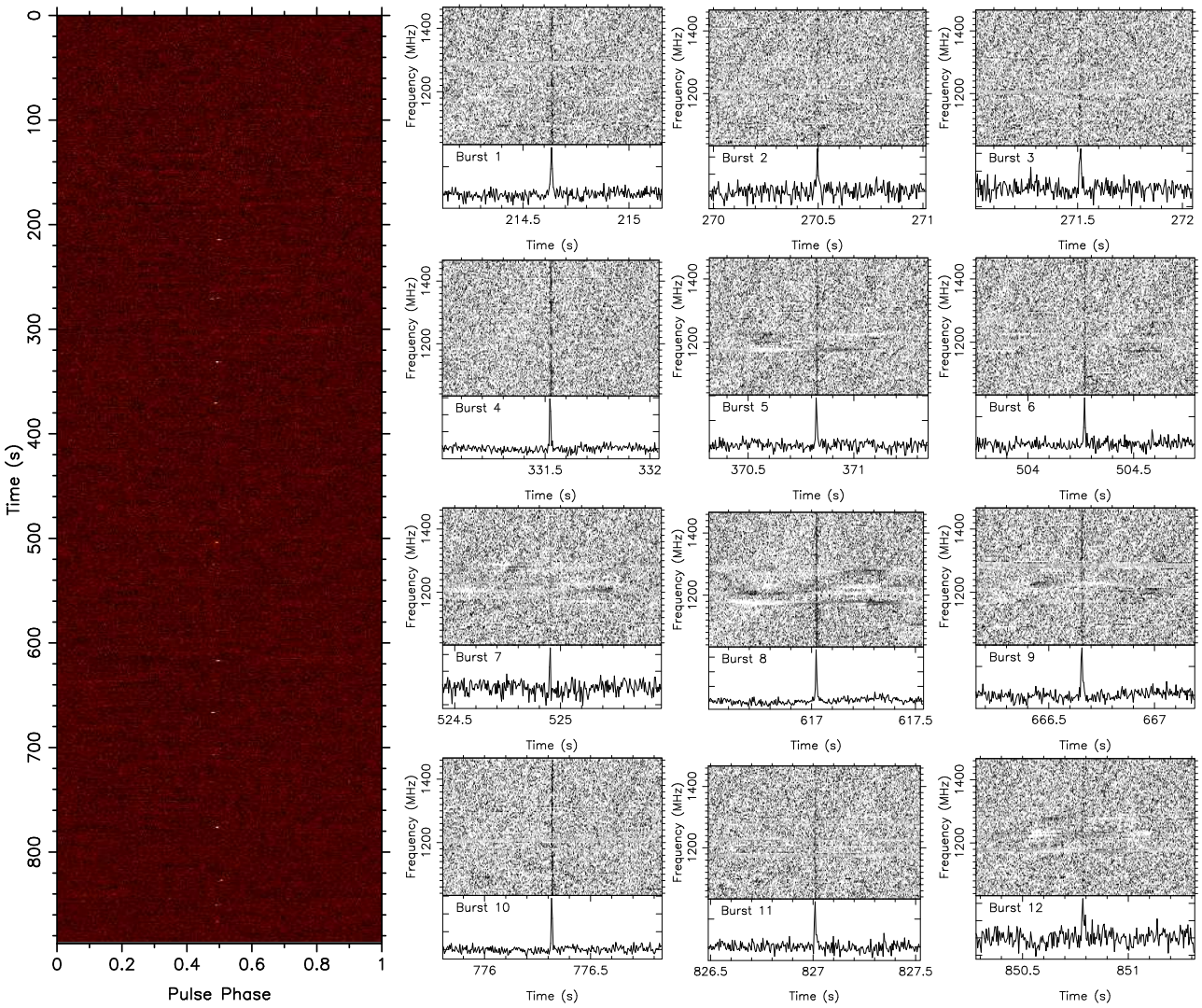


**Fig. 19** Discovery of RRAT J1905+0849 in the GPPS survey, which has a period of $1.0343 \pm 0.0052$ s and a DM of $257.8 \pm 2.3$ cm$^{-3}$ pc. In the *left long panel*, the 12 bright pulses were detected in the verification observations on 2020 Nov. 21, and aligned with the folding period. On the *right panels*, the de-dispersed waterfall plots for the intensity on the frequency against time are depicted for 12 pulses, and with an integrated profile in the bottom panel for each pulse.

of these nullings from available observation sessions, though we do see the nulling or mode-changing of these pulsars from available data. Longer observations with high sensitivity are desired for this purpose (e.g. Wang et al. 2020b). Presented here are just the first results from short GPPS survey observations. More results on newly detected nulling, mode-changing and subpulse-drifting phenomena for previously known pulsars and also the newly discovered pulsars in the GPPS survey will be reported by Yan et al. (in preparation).

### 4.6 Discovery of Long Period Pulsars

The GPPS survey discovered a few pulsars with very long periods. For example, PSR J1903+0433g (gpps0090) has a period of 14.05 s, which is the second longest period known, and PSR J1856+0211g (gpps0158) has a period of $P$ = 9.89012 s. Currently in the ATNF Pulsar Catalogue (Manchester et al. 2005) the longest period is $P$ = 23.535378 s for PSR J0250+5854, which was discovered by LOFAR (Tan et al. 2018).

PSR J1903+0433g (gpps0090) was discovered in the 15th harmonic ($P$ =0.93671 s) from a snapshot survey on 2020 Mar. 30 with a very good S/N = 21.2. It was rediscovered in the 17th harmonic ($P$ =0.82684 s) in an another survey cover on 2020 Apr. 22. Within the uncertainty they have a similar DM value. In the verification observations on 2020 Aug. 29, the 6th harmonic of $P$ =2.3417 s was detected, and on 2020 Sep. 11 the 5th harmonic of $P$ =2.8099 s. From these harmonics, the right period was found to be $P$ =14.0508 s and the pulse width is 123.5 ms.

**Table 6** Parameters of RRAT J1905+0849

| Parameter (unit) | Value |
|---|---|
| First discovery date / MJD | 20190917 / 58743 |
| Confirmed date / MJD | 20201121 / 59174 |
| Burst period, $P$ (s) | 1.034 |
| Dispersion measure, DM (pc cm$^3$) | 257.8 (23) |
| Distance (kpc, YMW2016) | 7.73 |
| Right ascension (J2000, hh:mm:ss) | 19:05:03 |
| Declination (J2000, dd:mm) | 08:49 |
| Galactic longitude (deg.) | 42.327 |
| Galactic latitude (deg.) | 1.017 |
| Max burst rate (n hr$^{-1}$) | 48 |
| Mean width (ms) of pulses | 3.74 |
| $S_{mean}$ (mJy) of pulses at 1.25 GHz | 14.67 |
| RM (rad m$^{-2}$) | 493.9(14) |

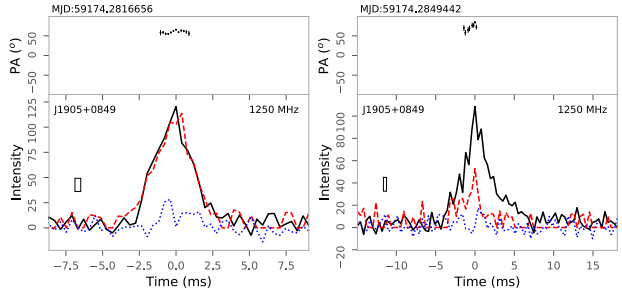


**Fig. 20** Polarization profiles of two pulses of RRAT J1905+0849, No.4 and No.8. The polarization angle variations are plotted in the upper panels, and the total intensity (*thick line*), linear (*dashed line*) and circular (*dotted line*) polarization ($> 0$ for the left-hand sense) are featured in the bottom panels.

Discovery of PSR J1856+0211g (gpps0158) has a different story. Its single pulses were first detected via the single pulse module with marginal significance in a snapshot survey for the cover of G35.58+0.00_20201003. In the follow-up observations that lasted for 15 minutes on 2021 Jan. 13, the pulsar was detected in its 8th harmonic ($P$ = 1.23627 s). In further verification observations on 2021 Jan. 26, the pulsar was detected by its 4th harmonic ($P$ = 2.47253 s). The procedure for harmonic-checking led to the discovery of the proper period of $P$ = 9.89012 s. This pulsar also has a relatively very narrow pulse, with a pulse width of about 38 ms.

### 4.7 Discovery of RRAT J1905+0849

In addition to pulsars listed in Table 2, the single pulse search of the GPPS survey data using the newly developed single pulse module detected some RRATs. Here is the first case, RRAT J1905+0849, featured in Figure 19. Four pulses around DM of 257.8 $\pm$ 2.3 cm$^{-3}$ pc of this RRAT were first detected from a cover of the GPPS survey G42.38+0.93_20190917, on the beam of M06-P1. During the verification observation on 2020 Nov. 21, twelve pulses were discovered, with the polarization signals recorded. Further analyses of TOAs of 12 pulses (see the method of Keane et al. 2010) yield a period of 1.0343 $\pm$ 0.0052 s. Basic parameters of this RRAT are listed in Table 6. The DM is obtained by maximizing S/N for pulses, and $S_{mean}$ is the mean of the averaged flux densities in the duration of detected pulses (not an average over a period or even the whole session). Polarization profiles of two pulses are plotted in Figure 20. The first is pulse No.4, which is almost 100% polarized with a flat polarization angle curve from which the rotation measure (RM) is derived (see Table 6). The other is for No.8, which is mildly polarized with a sweep-up polarization angle curve. The pulses of this RRAT have a diverse polarization feature.

More RRATs discovered in the GPPS survey will be presented by Zhou et al. (2021, in preparation).

**Table 7** Polarization Parameters of Eight Newly Discovered Pulsars

| PSR | $W_{50}$ (°) | $L/I$ (%) | $V/I$ (%) | $\|V\|/I$ (%) | RM (rad m$^{-2}$) |
|---|---|---|---|---|---|
| J1848+0127g | 7.0 | 49.2 | 2.5 | 8.2 | −50.1(15) |
| J1849−0014g | 26.7 | 22.8 | −1.6 | 3.4 | −110.3(16) |
| J1852−0023g | 8.4 | 27.2 | 1.2 | 9.1 | 93.8(20) |
| J1852+0056g | 16.9 | 58.7 | −29.6 | 30.1 | −93.6(16) |
| J1856+0211g | 1.4 | 58.3 | 30.0 | 37.2 | −180.7(27) |
| J1903+0433g | 3.8 | 16.6 | -8.3 | 16.9 | 213.2(31) |
| J1926+1857g | 16.9 | 78.7 | 13.6 | 15.2 | 262.3(13) |
| J2052+4421g | 40.8 | 62.4 | 9.5 | 9.8 | −276.7(5) |

### 4.8 Follow-up Observations for Polarization Profiles of Newly Discovered Pulsars

The L-band 19-beam receiver mounted on FAST has excellent stable performance in terms of polarization (Luo et al. 2020). During the verification observation, the polarization data were recorded, which are very useful to get the polarization profiles when a candidate is verified, without further costs of valuable FAST observation time. For this purpose, as mentioned above, the calibration signal was on-off and the signals for four polarization channels were recorded for 2 minutes before and after each verification session.

The polarization data and observation parameters in each fits file are carefully checked, and then data are calibrated and processed by using the package PSRCHIVE (Hotan et al. 2004). We obtained the polarization profiles (see Fig. 21) and also the Faraday RMs (see examples in Table 7). The RMs have been corrected for the ionosphere contribution. To verify the results, FAST data on two pulsars, PSR B0355+54 and PSR B1237+25, were processed with the same procedures, and results are consistent with polarization profiles at L-band previously published in Gould & Lyne (1998), Stinebring et al. (1984) and Johnston et al. (2005). For newly discovered pulsars in the GPPS survey, the polarization profiles of only a few pulsars are presented here. More results will be presented by Wang P.F. et al. (2021, in preparation).

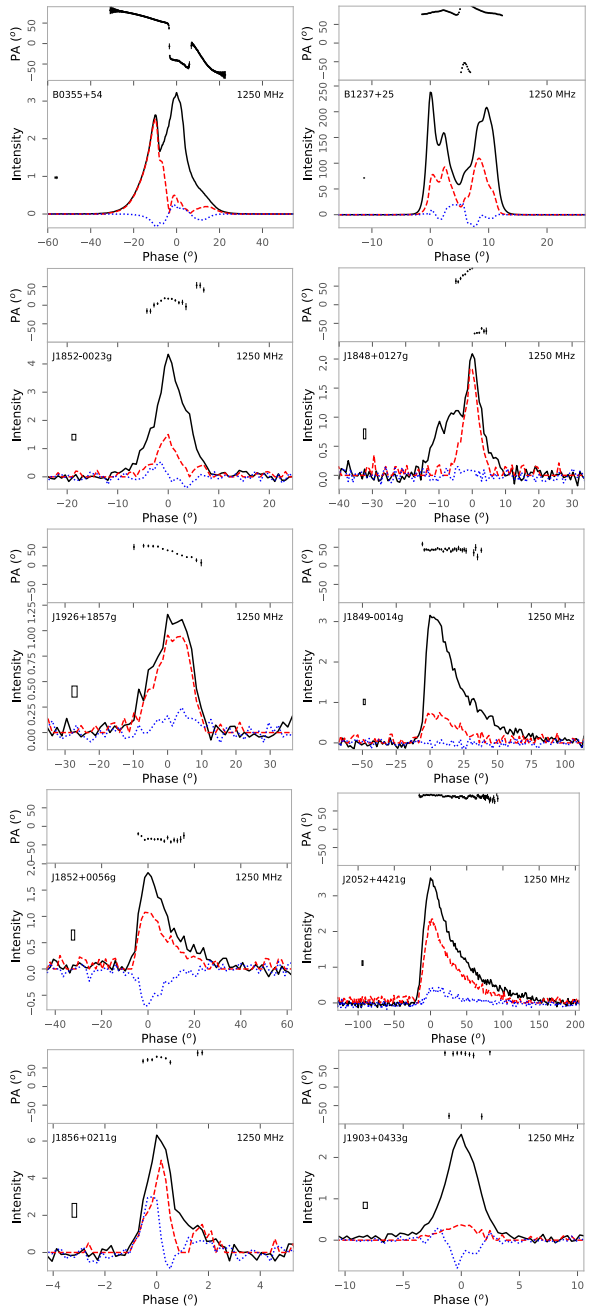


**Fig. 21** Integrated polarization profiles of eight newly discovered pulsars by FAST. PSRs B0355+54 and B1237+25 are taken as tests for the data processing pipeline. For each pulsar, the upper panel is polarization angles, and the bottom panel includes total intensity (*thick line*), linear (*dashed line*) and circular (*dotted line*) polarization with the positive values for the left-hand sense. The phase is defined as 0°–360° for a period, starting at the peak of the pulse.

The polarization profiles of PSR J1852−0023g (gpps0042) presented here look like a typical unresolved cone-core pulsar (Rankin 1993), with a sense reversal of circular polarization at the profile center. PSR J1848+0127g (gpps0035) has a highly polarized trailing component (i.e. the second class in Wang & Han 2016) and a very steep polarization angle sweep in the leading unpolarized component, much like a partial cone discussed by Lyne & Manchester (1988). PSR J1926+1857g (gpps0025) is highly polarized with a linearly declining polarization angle and a steep trailing edge of mean pulse, which indicates its cone nature of the emission. Three other pulsars, PSRs J1849-0014g (gpps0027), J1852+0056g (gpps0014) and J2052+4421g (gpps0019), obviously show long tails for scattered emission, in which scattering reduces the linear polarization and results in a flat polarization angle curve. Such a scattering effect on polarization profiles was first outlined by Li & Han (2003) and later confirmed by Kramer & Johnston (2008).

Polarization profiles of two long period pulsars mentioned in Sect. 4.6 are also presented in Figure 21. PSR J1856+0211g (gpps0158) is highly polarized with a strong left-hand circular polarization in the leading edge. PSR J1903+0433g (gpps0090, with the second longest period) is mildly polarized.

## 5 IMPROVED PARAMETERS FOR KNOWN PULSARS

In addition to the new discoveries, the GPPS survey detected more than 330 previously known pulsars, and most of them have a very good S/N. A full list of these pulsars and detailed studies will be published elsewhere. Here we present the integrated profiles with the phase-frequency plots (see Fig. 22) for only 64 pulsars whose parameters are significantly improved by the GPPS survey (see Table 8). The RFI affected channels have been removed, as displayed in the phase-frequency plots which in fact reflects the RFI situation at the FAST site. For pulsars observed at nighttime, the RFI occupies very few channels and we cannot see the related influences. Nevertheless, RFI in daytime could occasionally affect about 20% of channels or more. The lower DM pulsars are more easily affected so that the baseline of the profiles cannot be flattened even after pulses are averaged over all frequency channels.

For many pulsars in Table 8, their positions available in literature or on webpages have large uncertainties, even as low as 1°. The snapshot observations that rely on the FAST L-band 19-beam receiver can detect a known strong pulsar in several beams, so that the position can be determined with an accuracy of better than 1′ according to the positions of beam centers and signal-to-noise ratios of obtained profiles. See the updated positions for 45 pulsars in Table 8.

Sensitive observations of two pulsars (PSRs J1851+0242 and J1853+0029) acquired by FAST confirm that their previously available periods are just harmonics. The corrected periods are expressed in Table 8.

**Table 8** Some Parameters are Updated for 64 Known Pulsars

| PSR name | Ref. | $P$ in Ref. (s) | DM | RA(2000) hh:mm:ss.s | Dec(2000) dd:mm:ss | Updated items | $P$ ($\sigma$) (s) | Epoach for $P$ (MJD) | DM ($\sigma$) | RA(2000) hh:mm:ss.s | Dec(2000) dd:mm |
|---|---|---|---|---|---|---|---|---|---|---|---|
| (1) | (2) | (3) | (4) | (5) | (6) | (7) | (8) | (9) | (10) | (11) | (12) |
| J0611+1436 | [1] | 0.270329 | 45.7 | 06:11:18.65 | +14:36:52 | DM | 0.27032969(38) | 58847.665398 | 43.7(2) | 06:11:17 | +14:37 |
| J0658+0022 | [2] | 0.563295 | 122.0 | 06:58:15.21 | +00:22:35.3 | DM | 0.5632972(16) | 58839.756478 | 115.6(5) | 06:58:14 | +00:23 |
| J1832+0029 | [3] | 0.533917 | 28.3 | 18:32:50.7 | +00:29:27 | DM | 0.5339170(16) | 58765.445867 | 32.7(4) | 18:32:48 | +00:30 |
| J1843+01 | [8] | 1.26702 | 248.0 | 18:43 | +01 | Posi | 1.266990(12) | 59198.252593 | 251.9(16) | 18:43:28 | +01:19 |
| J1847+01 | [4] | 0.00346 | 20.0 | 18:47 | +01 | Posi | 0.0034630711(1) | 59093.545385 | 20.100(5) | 18:47:05 | +01:13 |
| J1848-0023 | [5] | 0.537624 | 30.6 | 18:48:37.89 | −00:23:17 | DM | 0.53762431(52) | 59077.578982 | 34.6(4) | 18:48:40 | −00:24 |
| J1849+01 | [4] | 1.832 | 213.6 | 18:49 | +01 | Posi | 1.832250(18) | 58909.025657 | 217.2(15) | 18:49:56 | +01:06 |
| J1849+0409 | [3] | 0.761194 | 56.1 | 18:49:3.47 | +04:09:42.3 | DM | 0.7612033(32) | 58720.600254 | 64.1(6) | 18:49:03 | +04:09 |
| J1849+04 | [4] | 0.42111 | 191.8 | 18:49 | +04 | Posi | 0.4211266(11) | 58720.585427 | 188.2(4) | 18:49:40 | +04:30 |
| J1849-0040 | [5] | 0.672481 | 1234.9 | 18:49:10.25 | −00:40:20 | DM | 0.672479(8) | 59244.140909 | 1267.6(18) | 18:49:11 | −00:40 |
| J1850-0006 | [6] | 2.191498 | 570.0 | 18:50:47.93 | −00:06:26.1 | DM | 2.1915070(88) | 59082.572228 | 655.0(18) | 18:50:47 | −00:07 |
| J1851+00 | [4] | 0.02283 | 107.4 | 18:51 | +00 | Posi | 0.0228466631(27) | 58902.066301 | 107.60(2) | 18:51:02 | +00:10 |
| J1851+0242 | [4] | 1.49714 | 534.1 | 18:51:22 | +02:42:37 | P | 4.4912(2) | 58997.792192 | 519.3(71) | 18:51:19 | +02:42 |
| J1852+00 | [4] | 1.92066 | 590.4 | 18:52 | +00 | Posi | 1.920653(21) | 58923.007492 | 590.0(15) | 18:52:39 | +00:00 |
| J1853+0009 | [4] | 0.03341 | 192.0 | 18:53 | +00:09 | Posi | 0.033395062(2) | 58939.971197 | 192.40(3) | 18:53:39 | +00:08 |
| J1853+0029 | [4] | 0.93832 | 230.0 | 18:53 | +00:29 | Posi,P | 1.8767568(63) | 59112.477816 | 227.1(15) | 18:53:18 | +00:29 |
| J1853+03 | [7] | 0.58553 | 290.2 | 18:53 | +03:00 | Posi | 0.5855545(32) | 58977.860290 | 295.8(8) | 18:53:12 | +03:00 |
| J1853+04 | [8] | 1.32065 | 549.3 | 18:53 | +04 | Posi | 1.320623(13) | 59004.780117 | 548.9(13) | 18:53:46 | +04:27 |
| J1854+00 | [7] | 0.76733 | 532.9 | 18:54 | +00:00 | Posi | 0.767278(1) | 58940.968884 | 525.0(6) | 18:54:43 | +00:50 |
| J1854+0317 | [9] | 1.36645 | 404.0 | 18:54:29.06 | +03:17:31 | DM | 1.366465(11) | 58991.813118 | 390.0(11) | 18:54:29 | +03:17 |
| J1855+0422 | [10] | 1.678106 | 438.0 | 18:55:41.37 | +04:22:47 | DM | 1.678105(15) | 59187.292726 | 455.6(13) | 18:55:41 | +04:22 |
| J1858+02 | [7] | 0.19765 | 492.1 | 18:58 | +02:00 | Posi | 0.19764740(24) | 58900.051935 | 492.8(2) | 18:58:23 | +02:41 |
| J1853+0853 | [3] | 3.914658 | 214.0 | 18:53:22.07 | +08:53:17 | DM | 3.914696(79) | 59253.091997 | 236.6(31) | 18:53:20 | +08:54 |
| J1859+00 | [11],[5] | 0.559634 | 420.0 | 18:59:46 | +00:35 | Posi | 0.5596363(18) | 58982.867548 | 424.0(4) | 18:59:47 | +00:38 |
| J1859+03 | [4] | 1.51171 | 555.1 | 18:59 | +03 | Posi | 1.511506(28) | 58867.217455 | 558.7(26) | 18:59:10 | +03:46 |
| J1901+00 | [11],[5] | 0.777662 | 345.5 | 19:01:32 | +00:26 | Posi | 0.7776620(32) | 58977.880799 | 340.3(6) | 19:01:32 | +00:32 |
| J1901+0435 | [3] | 0.690576 | 1042.6 | 19:01:32.2 | +04:35:23 | DM | 0.690605(11) | 58565.032593 | 920.0(25) | 19:01:31 | +04:35 |
| J1902+02 | [7] | 0.41532 | 281.2 | 19:02 | +02:00 | Posi | 0.4153927(11) | 59233.161342 | 280.4(4) | 19:02:31 | +02:35 |
| J1903+0415 | [7] | 1.15139 | 473.5 | 19:03 | +04:15 | Posi | 1.151411(11) | 58902.108022 | 481.9(14) | 19:03:30 | +04:15 |
| J1903+09 | [4] | 0.16631 | 362.9 | 19:03 | +09 | Posi | 0.16631690(28) | 59164.332493 | 362.9(3) | 19:03:39 | +09:12 |
| J1905+10 | [4] | 1.72688 | 165.7 | 19:05 | +10 | Posi | 1.726813(17) | 58852.191366 | 163.7(14) | 19:05:19 | +10:34 |
| J1906+0725 | [7] | 1.53651 | 480.4 | 19:06 | +07:25 | Posi | 1.536442(14) | 58770.485688 | 476.4(12) | 19:06:23 | +07:25 |
| J1907+05 | [7] | 0.16868 | 456.7 | 19:07 | +05:00 | Posi | 0.16867706(35) | 58982.878143 | 457.1(3) | 19:08:02 | +05:59 |
| J1909+12 | [4] | 1.229338 | 292.5 | 19:09:57.7 | +12:04:55.3 | DM | 1.229319(8) | 59189.269571 | 302.5(10) | 19:09:51 | +12:06 |
| J1910+1027 | [7] | 0.53147 | 705.7 | 19:10 | +10:27 | Posi | 0.5315526(26) | 59093.531512 | 715.3(7) | 19:10:48 | +10:27 |
| J1910+07 | [4] | 0.53869 | 256.5 | 19:10 | +07 | Posi | 0.5386463(54) | 58911.070131 | 255.3(15) | 19:10:06 | +07:11 |
| J1911+09 | [7] | 0.27371 | 334.7 | 19:11 | +09:00 | Posi | 0.27370588(47) | 59067.582251 | 340.7(8) | 19:11:47 | +09:22 |
| J1911+10 | [7] | 0.19089 | 446.2 | 19:11 | +10:00 | Posi | 0.19087553(57) | 59155.408562 | 445.0(5) | 19:11:43 | +10:52 |
| J1913+05 | [4] | 0.662 | 330.1 | 19:13 | +05 | Posi | 0.6619994(40) | 59185.290377 | 335.9(9) | 19:13:22 | +05:24 |
| J1914+08 | [12] | 0.440048 | 285.0 | 19:14:18 | +08:45 | Posi | 0.44003996(35) | 59090.587469 | 290.6(4) | 19:14:25 | +08:39 |
| J1916+1023 | [5] | 1.618339 | 329.8 | 19:16:36.91 | +10:23:03 | DM | 1.618330(14) | 58909.104157 | 341.8(13) | 19:16:37 | +10:23 |
| J1918+1541 | [13] | 0.370883 | 13.0 | 19:18:7.7 | +15:41:15.2 | DM | 0.37088498(71) | 59198.231761 | 11.4(3) | 19:18:10 | +15:42 |
| J1920+1110 | [10] | 0.509886 | 182.0 | 19:20:13.31 | +11:10:59 | DM | 0.5098862(16) | 58977.910791 | 188.4(4) | 19:20:14 | +11:11 |
| J1924+1628 | [7] | 0.37509 | 542.9 | 19:24 | +16:28 | Posi | 0.37508191(88) | 58808.402942 | 541.7(3) | 19:24:45 | +16:29 |
| J1924+17 | [7] | 0.75843 | 527.4 | 19:24 | +17:00 | Posi | 0.7584369(11) | 59069.686122 | 540.9(7) | 19:24:32 | +17:14 |
| J1924+2040 | [14],[15] | 0.23779 | 213.0 | 19:24:40 | +20:40:03 | DM | 0.2377930(3) | 58843.315936 | 226.6(2) | 19:24:35 | +20:40 |
| J1926+1613 | [7] | 0.3083 | 32.9 | 19:26 | +16:13 | DM,Posi | 0.308304(1) | 58936.061255 | 24.5(5) | 19:26:51 | +16:14 |
| J1927+1852 | [16] | 0.482766 | 254.0 | 19:27:10.42 | +18:52:8.5 | DM | 0.48276601(42) | 58940.066550 | 264.5(4) | 19:27:07 | +18:51 |
| J1929+1905 | [17] | 0.339243 | 553.9 | 19:29:31.7 | +19:05:43.4 | DM | 0.33921584(21) | 59174.390702 | 528.4(3) | 19:29:14 | +19:10 |
| J1930+14 | [7] | 0.42571 | 209.2 | 19:30 | +14:00 | Posi | 0.4257200(22) | 58808.383858 | 214.8(7) | 19:30:19 | +14:09 |
| J1930+17 | [18] | 1.60969 | 201.0 | 19:30:44 | +17:25 | Posi | 1.609723(13) | 59157.422738 | 197.4(13) | 19:30:31 | +17:23 |
| J1934+19 | [7] | 0.23099 | 97.6 | 19:34 | +19:00 | Posi | 0.23098462(95) | 58995.887279 | 98.4(5) | 19:34:18 | +19:26 |
| J1936+18 | [4] | 0.05835 | 125.5 | 19:36 | +18 | Posi | 0.05834513(18) | 58997.893701 | 125.9(4) | 19:36:03 | +18:05 |
| J1936+20 | [7] | 1.39088 | 205.1 | 19:36 | +20:00 | DM,Posi | 1.3907326(35) | 59102.591721 | 195.9(11) | 19:36:29 | +20:41 |
| J1936+21 | [18] | 0.642932 | 264.0 | 19:36:29 | +21:12 | Posi | 0.6429599(22) | 58944.052936 | 262.4(5) | 19:36:11 | +21:09 |
| J1936+21a | [4] | 0.0316 | 73.9 | 19:36 | +21 | Posi | 0.03158187(3) | 59155.467443 | 75.0(2) | 19:37:00 | +21:43 |
| J1938+14 | [19] | 2.90251 | 74.2 | 19:38:19 | +14:42 | Posi | 2.902504(51) | 59209.202485 | 75.4(23) | 19:38:07 | +15:06 |
| J1939+26 | [4] | 0.46593∗ | 48.1 | 19:39 | +26 | Posi | 0.4669615(11) | 59253.183278 | 47.5(4) | 19:39:42 | +26:09 |
| J1940+26 | [4] | 0.00481 | 171.6 | 19:40 | +26 | Posi | 0.0048135292(14) | 59253.175813 | 171.61(4) | 19:40:13 | +26:01 |
| J1955+29 | [4] | 1.07377 | 206.0 | 19:55 | +29 | Posi | 1.0738820(62) | 58735.618100 | 212.4(9) | 19:55:07 | +29:31 |
| J2000+29 | [8] | 3.0737 | 132.5 | 20:00 | +29 | Posi | 3.073809(58) | 58901.180519 | 131.3(25) | 20:00:14 | +29:21 |
| J2003+29 | [4] | 1.00987 | 208.7 | 20:03 | +29 | Posi | 1.0098800(56) | 58943.068686 | 209.5(8) | 20:03:02 | +29:16 |
| J2010+31 | [4] | 1.55147 | 251.0 | 20:10 | +31 | Posi | 1.551535(24) | 58910.171365 | 251.8(23) | 20:10:35 | +31:50 |
| J2138+4911 | [20] | 0.696 | 168.0 | 21:38 | +49:11 | Posi | 0.696171(3) | 58941.118314 | 168.0(6) | 21:38:15 | +49:12 |

(1) Reference in Column (2): [1]: Lyne et al. (2017); [2]: Burgay et al. (2013); [3]: Lorimer et al. (2006b); [4]: http://www.naic.edu/~palfa/newpulsars/; [5]: Hobbs et al. (2004); [6]: Keith et al. (2009); [7]: Lazarus et al. (2015); [8]: Patel et al. (2018); [9]: Eatough et al. (2013b); [10]: Morris et al. (2002); [11]: Camilo et al. (1996) [12]: Keane et al. (2018); [13]: Camilo & Nice (1995); [14]: Weisberg et al. (1981); [15]: Vivekanand et al. (1983); [16]: Lorimer et al. (2002); [17]: http://astro.phys.wvu.edu/dmb/; [18]: Lorimer et al. (2013); [19]: Deneva et al. (2016); [20]: Hessels et al. (2008).
(2) Columns (3)–(6) are paraemeters in the reference, and Cols. (7), (9), (10) and (11) are paraemters obtained in the GPPS survey;
DM has the unit of cm$^{-3}$ pc. Newly measured $P$ and DM have an uncertainty in brackets. ∗: mistyping in the reference.

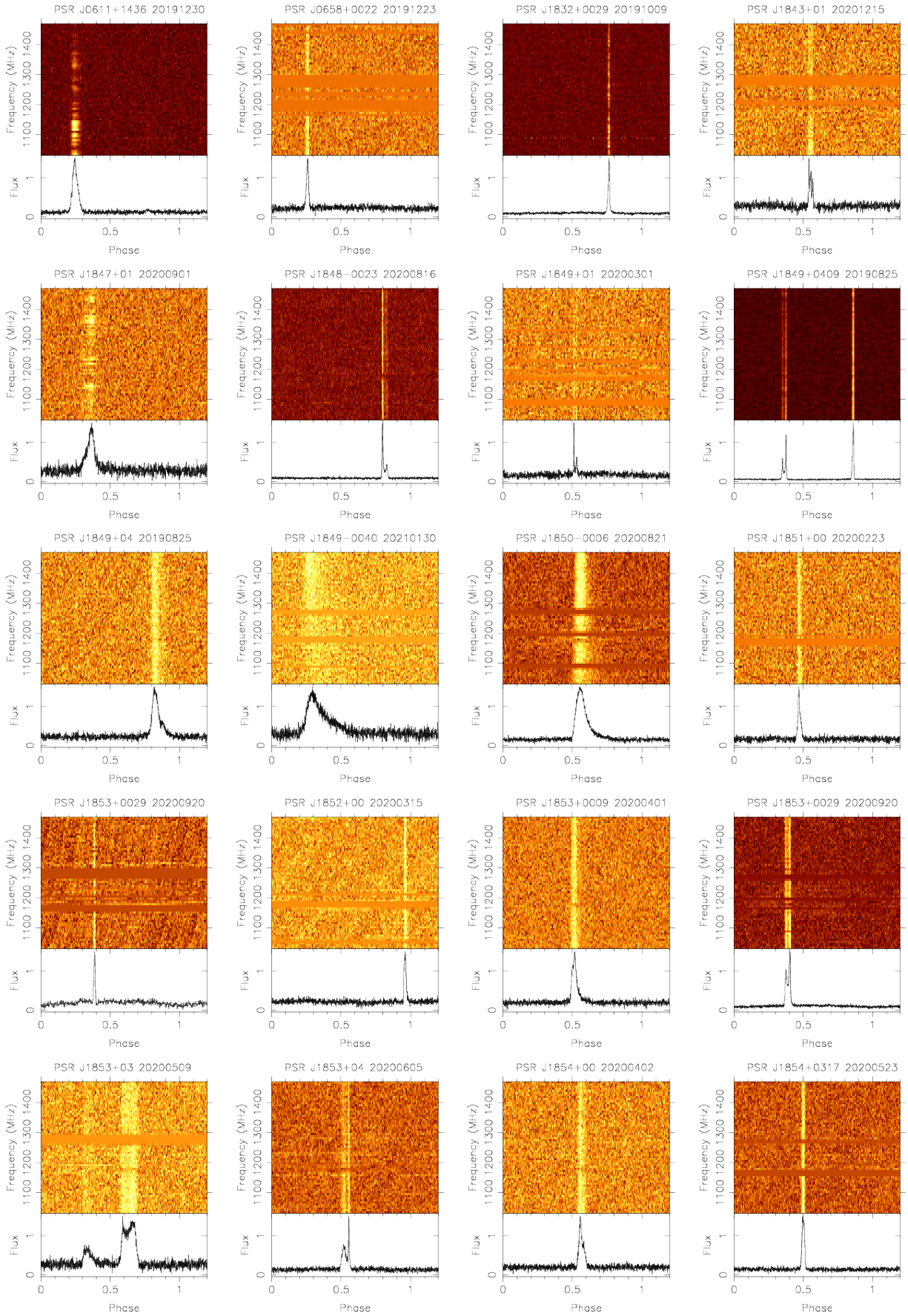


**Fig. 22** The phase-frequency plot and the integrated profile for 64 previously known pulsars for which the GPPS survey gives updated parameters. Channels with RFI are cleaned or suppressed.

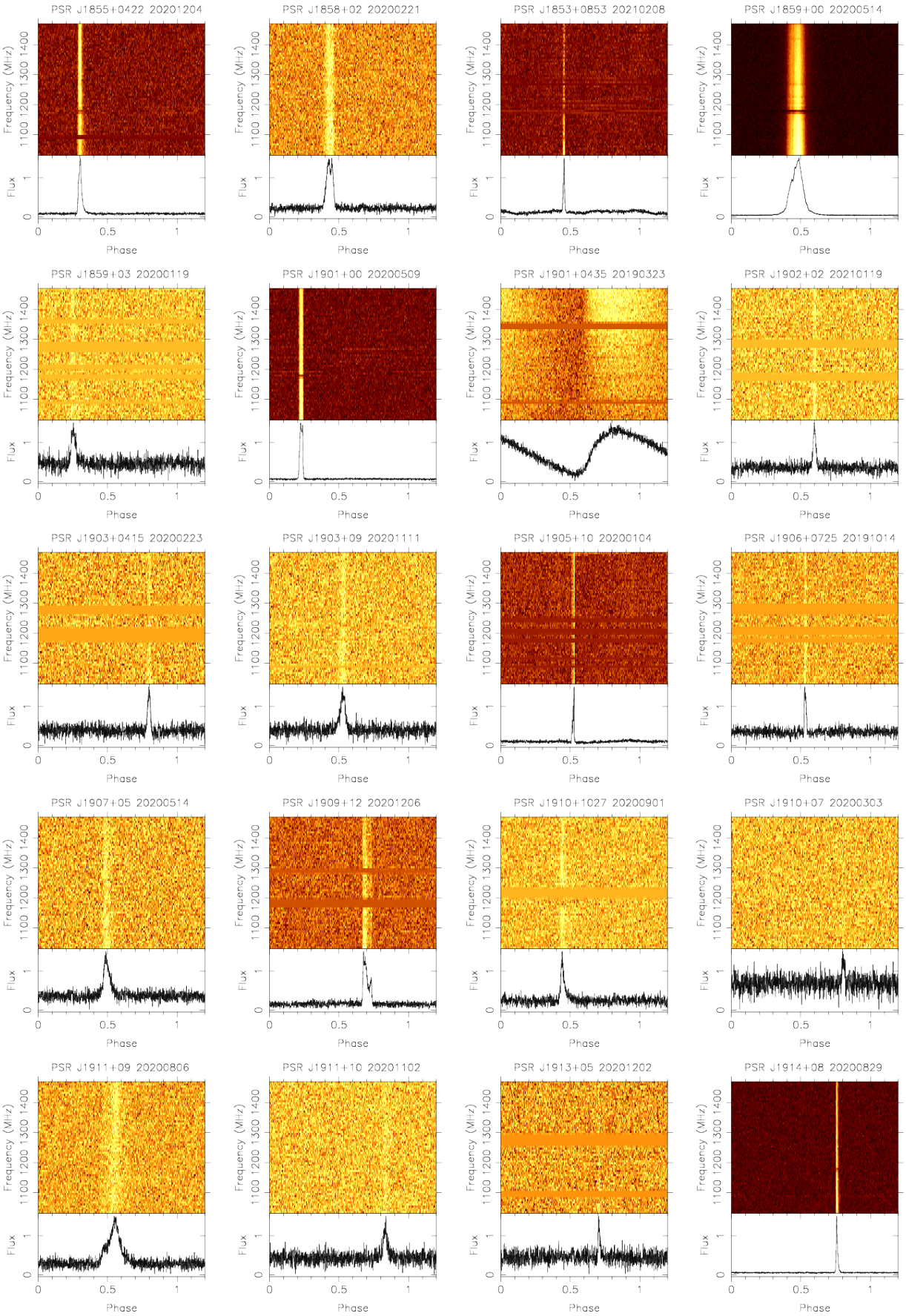


**Fig. 22** – *Continued.*

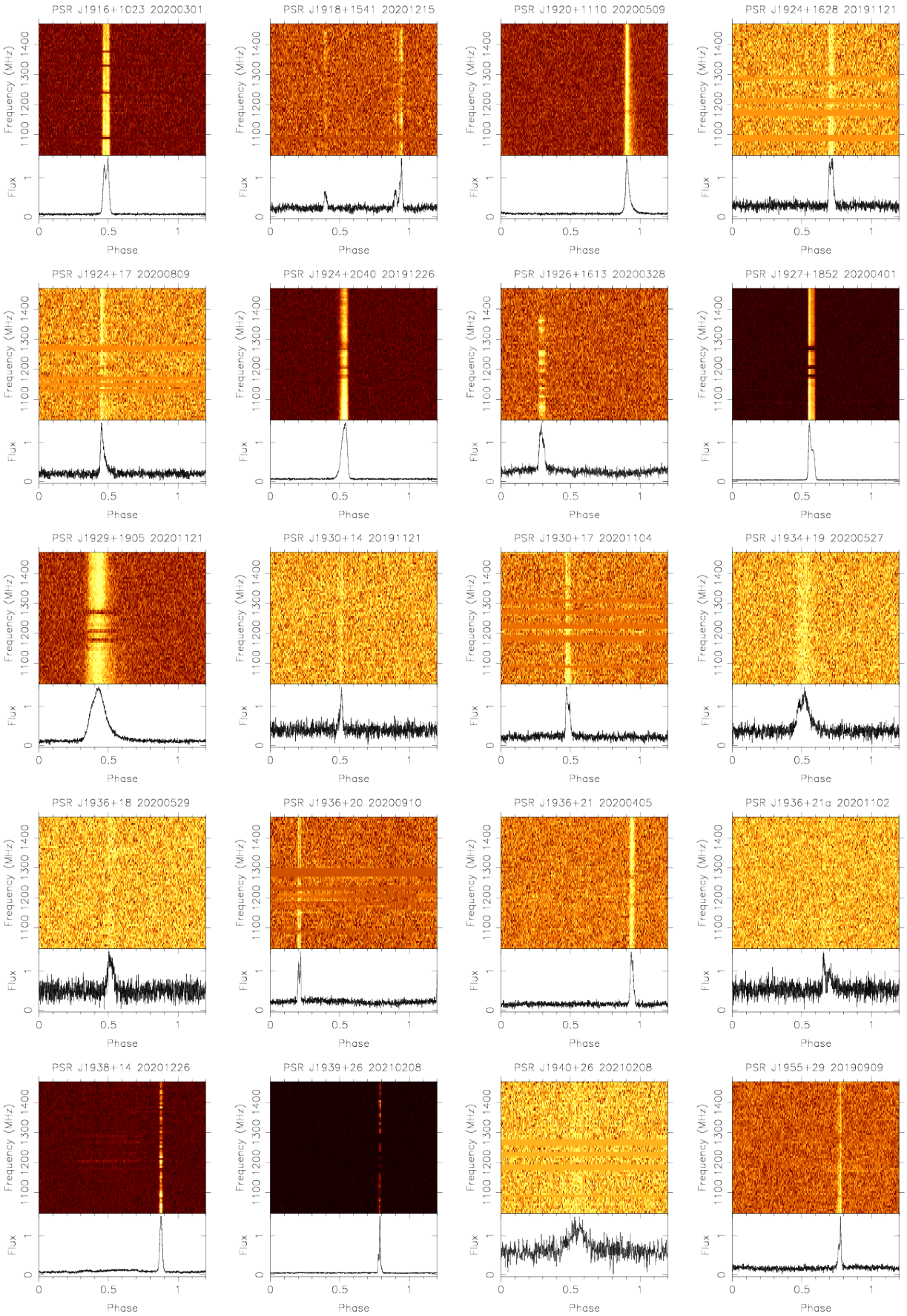


**Fig. 22** – *Continued*.

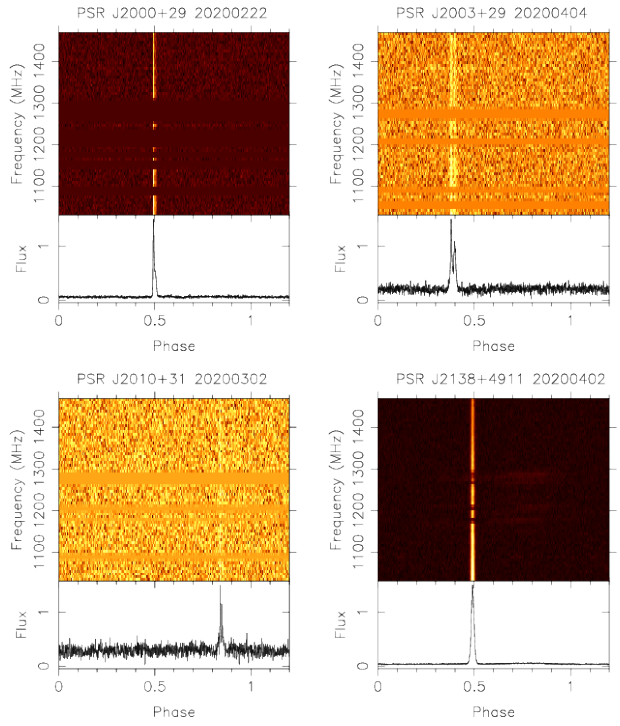


**Fig. 22** – *end.*

An accurate DM can be determined by a higher S/N of profiles. The GPPS survey improved the DM values for 20 pulsars, as given in Table 8.

In addition to these improved parameters, some remarkable features are noticed as follows.

(1) Eight low-DM pulsars: PSRs J0611+1436 (DM = 43.7 $\mathrm{cm^{-3}\,pc}$), J1832+0029 (DM = 32.7 $\mathrm{cm^{-3}\,pc}$), J1847+01 (DM = 20.1 $\mathrm{cm^{-3}\,pc}$), J1910+1256 (DM = 38.1 $\mathrm{cm^{-3}\,pc}$), J1918+1541 (DM = 13.0 $\mathrm{cm^{-3}\,pc}$), J1926+1613 (DM = 24.5 $\mathrm{cm^{-3}\,pc}$), J1938+14 (DM = 75.4 $\mathrm{cm^{-3}\,pc}$) and J1939+26 (DM = 47.5 $\mathrm{cm^{-3}\,pc}$), manifest obvious scintillation features in their phase-frequency plots.

(2) Five high DM pulsars: PSRs J1849−0040 (DM = 1267.6 $\mathrm{cm^{-3}\,pc}$), J1850−0006 (DM = 655.0 $\mathrm{cm^{-3}\,pc}$), J1855+0422 (DM = 455.6 $\mathrm{cm^{-3}\,pc}$), J1920+1110 (DM = 188.4 $\mathrm{cm^{-3}\,pc}$) and J1929+1905 (DM = 528.4 $\mathrm{cm^{-3}\,pc}$), exhibit scattering features, i.e. emission seen in a wider phase range towards the lower frequency end.

(3) PSR J1901+0435 has a very large DM (920.0 ± 2.5 $\mathrm{cm^{-3}\,pc}$) and very wide profile, which was discovered in the Parkes multi-beam survey (Lorimer et al. 2006a) and is located behind the Scutum spiral arm of the Milky Way. The much stronger pulses are seen in the high frequency end of the band, and much weaker emission in the lower end, effectively looking like an inverted steep spectrum, which is simply caused by the scattering effect rather than the intrinsic emission feature. The scattering caused by ionized gas clouds in the spiral arms redistribute much more emission at lower frequencies to other directions, so that the sources or the pulses look weaker and pulsed emission is much more delayed at lower frequencies, even not appearing as pulsed emission. In such a case, caution should be taken for the DM determination due to such scattering. Simple alignment of pulsed emission peaks in a wide range of frequency would cause an overestimated DM. In fact, any Galactic pulsars (Kijak et al. 2011; Basu et al. 2018) or extragalactic radio sources with such an inverted spectrum at lower frequencies (Guerra et al. 2002; Gopal-Krishna et al. 2014; Mhaskey et al. 2019a,b) can be so explained by the scattering effect caused by very cloudy ionized gas in front of or in the environment of a strong emission source. The flux densities and polarization properties may vary if the source and the intervening clouds are moving relatively in any transverse direction.

## 6 PERSPECTIVES

In the Milky Way, over 10 000 pulsars can potentially be found by upcoming surveys (Lorimer et al. 2019), and currently only about 3000 pulsars are known. FAST, as the most sensitive radio telescope currently in the world, can survey a limited part of the Milky Way and should be able to discover about 1000 pulsars, depending on available observation time (Smits et al. 2009). The GPPS survey is so-far the deepest survey for the FAST-accessible Galactic plane, and the results presented here are the first of many expected from this highly sensitive system. Among the list of newly discovered pulsars, about 20% are MSPs. The most interesting are binaries awaiting for timing observations and are valuable for excellent science on tests on theories of gravity. The long-term timing of more MSPs discovered by the GPPS survey could enlarge the chance for possible detection of ultra-low-frequency gravitational waves by the Chinese Pulsar Timing Array.

The GPPS survey provides sensitive observations of newly discovered and previously known pulsars, and can obtain their polarization profiles and spectra with excellent quality, which can act as a fundamental database for pulsar astrophysics, such as exploring the emission process, emission region and emission mechanisms. For example, as clearly revealed by FAST observations for pulsars with a strong scattering effect, their inverted spectrum can be interpreted due to missing flux densities at lower frequencies caused by the scattering. Therefore, the results presented in this paper are only the tip of the iceberg for FAST pulsar observations.

**Acknowledgements** We thank Prof. R.T. Gangadhara and the referees, Prof. R.N. Manchester and Prof. Jim Cordes, for helpful comments. This project, as one of five key projects, is being carried out by using FAST, a Chinese national mega-science facility built and operated by the

National Astronomical Observatories, Chinese Academy of Sciences. J.L. Han is supported by the National Natural Science Foundation of China (NSFC, Nos. 11988101 and 11833009) and the Key Research Program of the Chinese Academy of Sciences (Grant No. QYZDJ-SSW-SLH021); C. Wang is partially supported by NSFC No. U1731120; X.Y. Gao is partially supported by NSFC No. U1831103; P.F. Wang is partially supported by the NSFC No. 11873058 and the National SKA program of China No. 2020SKA0120200. Jun Xu is partially supported by NSFC No. U2031115; H.G. Wang is partially supported by the National SKA program of China (No. 2020SKA0120100). R. Yuen is partly supported by Xiaofeng Yang's Xinjiang Tianchi Bairen project and CAS Pioneer Hundred Talents Program. L.G. Hou thanks the support from the Youth Innovation Promotion Association CAS.

## AUTHORS CONTRIBUTIONS

The GPPS survey is a key science project of FAST and is being carried out via teamwork. J. L. Han initially proposed the survey project by using the snapshot mode, coordinated the teamwork, then realized the pipeline for data processing, coordinated the computational resources and processed most of the data, and finally was in charge of writing this paper; Chen Wang designed the observation plan, and fed targets for each observation session and monitored the progress of observations, tested and realized the snapshot mode together with Jing-Hai Sun, verified the data integrity, and initialized the data preparing module with Tao Wang; P. F. Wang realized the initial PRESTO searching pipeline, contributed to processing the data, realized the polarization processing pipeline, obtained the relevant results for this paper and also contributed to verifying pulsar candidates; Tao Wang and D. J. Zhou realized the data preparing module, and also contributed to the candidates-checking module; Jun Xu realized the Sigproc pipeline; D. J. Zhou developed the single pulse module and later was in charge of processing data for picking up single pulses, contributed to manual verification of newly discovered pulsars and calculated pulsar flux; Yi Yan was in charge of checking the detected known pulsars, and obtained proper positions for previously known pulsars and also newly discovered pulsars from the signal-to-noise ratios from several nearby beams, and preparing the relevant results for this paper; Xue Chen was in charge of checking the RFI of data; Wei-Cong Jing and Wei-Qi Su were in charge of checking the results for newly discovered pulsars: Wei-Cong Jing checked the period, Wei-Qi Su folded the pulsar profiles, and they prepared the relevant results in this paper and also the webpage; Li-Gang Hou was in charge of checking the beam pattern, and X. Y. Gao was in charge of making a log of the observations, and prepared the plots for coincidence of SNRs and pulsars; Jun Xu also contributed to analyzing the RMs of pulsars for this paper. K.J. Lee, N. Wang, P. Jiang, R. X. Xu and J. Yan jointly planned the project and coordinated the commissioning, and P. Jiang and Chun Sun coordinated FAST observations; other people jointly made the formal proposal for the project and/or ensured the proper operations of observation systems.

## DATA AVAILABILITY

All pulsar profile data presented in this paper are available on the webpage of the GPPS survey *http://zmtt.bao.ac.cn/GPPS/*.

## References

Abbott, B. P., Abbott, R., Abbott, T. D., et al. 2016, ApJL, 833, L1

Abbott, B. P., Abbott, R., Abbott, T. D., et al. 2019, Physical Review X, 9, 011001

Abbott, B. P., Abbott, R., Abbott, T. D., et al. 2020, ApJL, 892, L3

Abdo, A. A., Ackermann, M., Ajello, M., et al. 2009, ApJS, 183, 46

Abdo, A. A., Ajello, M., Allafort, A., et al. 2013, ApJS, 208, 17

Alcock, C., Farhi, E., & Olinto, A. 1986, ApJ, 310, 261

Andersen, B. C., & Ransom, S. M. 2018, ApJL, 863, L13

Antoniadis, J., Freire, P. C. C., Wex, N., et al. 2013, Science, 340, 448

Backer, D. C., Kulkarni, S. R., Heiles, C., et al. 1982, Nature, 300, 615

Basu, R., RoŻko, K., Kijak, J., & Lewandowski, W. 2018, MNRAS, 475, 1469

Bhattacharyya, B., Cooper, S., Malenta, M., et al. 2016, ApJ, 817, 130

Bhattacharyya, B., Roy, J., Stappers, B. W., et al. 2019, ApJ, 881, 59

Boyles, J., Lynch, R. S., Ransom, S. M., et al. 2013, ApJ, 763, 80

Burgay, M., D'Amico, N., Possenti, A., et al. 2003, Nature, 426, 531

Burgay, M., Joshi, B. C., D'Amico, N., et al. 2006, MNRAS, 368, 283

Burgay, M., Keith, M. J., Lorimer, D. R., et al. 2013, MNRAS, 429, 579

Cameron, A. D., Li, D., Hobbs, G., et al. 2020, MNRAS, 495, 3515

Camilo, F., & Nice, D. J. 1995, ApJ, 445, 756

Camilo, F., Nice, D. J., Shrauner, J. A., & Taylor, J. H. 1996, ApJ, 469, 819

Chattopadhyay, D., Stevenson, S., Hurley, J. R., et al. 2021, arXiv:2011.13503

Clifton, T. R., & Lyne, A. G. 1986, Nature, 320, 43
Clifton, T. R., Lyne, A. G., Jones, A. W., et al. 1992, MNRAS, 254, 177
Condon, J. J., Cotton, W. D., Greisen, E. W., et al. 1998, AJ, 115, 1693
Cordes, J. M. 1978, ApJ, 222, 1006
Cordes, J. M., & Lazio, T. J. W. 2001, ApJ, 549, 997
Cordes, J. M., & McLaughlin, M. A. 2003, ApJ, 596, 1142
Cordes, J. M., Freire, P. C. C., Lorimer, D. R., et al. 2006, ApJ, 637, 446
Crawford, F., Kaspi, V. M., Manchester, R. N., et al. 2001, ApJ, 553, 367
Cromartie, H. T., Fonseca, E., Ransom, S. M., et al. 2020, Nature Astronomy, 4, 72
Damashek, M., Backus, P. R., Taylor, J. H., & Burkhardt, R. K. 1982, ApJL, 253, L57
Damashek, M., Taylor, J. H., & Hulse, R. A. 1978, ApJL, 225, L31
Davies, J. G., Horton, P. W., Lyne, A. G., et al. 1968, Nature, 217, 910
Davies, J. G., Lyne, A. G., & Seiradakis, J. H. 1973, Nature Physical Science, 244, 84
Demorest, P. B., Pennucci, T., Ransom, S. M., et al. 2010, Nature, 467, 1081
Deneva, J. S., Stovall, K., McLaughlin, M. A., et al. 2016, ApJ, 821, 10
Eatough, R. P., Keane, E. F., & Lyne, A. G. 2009, MNRAS, 395, 410
Eatough, R. P., Kramer, M., Lyne, A. G., & Keith, M. J. 2013a, MNRAS, 431, 292
Eatough, R. P., Kramer, M., Lyne, A. G., & Keith, M. J. 2013b, MNRAS, 431, 292
English, J., Taylor, A. R., Irwin, J. A., et al. 1998, PASA, 15, 56
Esamdin, A., Abdurixit, D., Manchester, R. N., & Niu, H. B. 2012, ApJL, 759, L3
Espinoza, C. M., Lyne, A. G., Stappers, B. W., & Kramer, M. 2011, MNRAS, 414, 1679
Faucher-Giguère, C.-A., & Loeb, A. 2011, MNRAS, 415, 3951
Faulkner, A. J., Stairs, I. H., Kramer, M., et al. 2004, MNRAS, 355, 147
Freire, P. C. C., Wex, N., Esposito-Farèse, G., et al. 2012, MNRAS, 423, 3328
Furst, E., Reich, W., Reich, P., & Reif, K. 1990, A&AS, 85, 691
Gopal-Krishna, Sirothia, S. K., Mhaskey, M., et al. 2014, MNRAS, 443, 2824
Gould, D. M., & Lyne, A. G. 1998, MNRAS, 301, 235
Green, D. A. 2019, Journal of Astrophysics and Astronomy, 40, 36
Guerra, E. J., Newlander, S. M., Haarsma, D. B., & Bruce Partridge, R. 2002, New Astron. Rev., 46, 303
Han, J. L., Demorest, P. B., van Straten, W., & Lyne, A. G. 2009, ApJS, 181, 557
Han, J. L., Ferriere, K., & Manchester, R. N. 2004a, ApJ, 610, 820
Han, J. L., & Manchester, R. N. 2001, MNRAS, 320, L35
Han, J. L., Manchester, R. N., Lyne, A. G., & Qiao, G. J. 2002, ApJL, 570, L17
Han, J. L., Manchester, R. N., Lyne, A. G., & Qiao, G. J. 2004b, in Young Neutron Stars and Their Environments, eds. F. Camilo & B. M. Gaensler, 218, 135
Han, J. L., Manchester, R. N., van Straten, W., & Demorest, P. 2018, ApJS, 234, 11
Han, J. L., Manchester, R. N., Xu, R. X., & Qiao, G. J. 1998, MNRAS, 300, 373
Hessels, J. W. T., Ransom, S. M., Kaspi, V. M., et al. 2008, in American Institute of Physics Conference Series, 983, 40 Years of Pulsars: Millisecond Pulsars, Magnetars and More, eds. C. Bassa, Z. Wang, A. Cumming, & V. M. Kaspi, 613
Hessels, J. W. T., Ransom, S. M., Stairs, I. H., et al. 2006, Science, 311, 1901
Hessels, J. W. T., Ransom, S. M., Stairs, I. H., et al. 2007, ApJ, 670, 363
Hewish, A., Bell, S. J., Pilkington, J. D. H., et al. 1968, Nature, 217, 709
Hobbs, G., Faulkner, A., Stairs, I. H., et al. 2004, MNRAS, 352, 1439
Hobbs, G., Guo, L., Caballero, R. N., et al. 2020, MNRAS, 491, 5951
Hotan, A. W., van Straten, W., & Manchester, R. N. 2004, PASA, 21, 302
Hou, L. G., & Han, J. L. 2014, A&A, 569, A125
Hu, H., Kramer, M., Wex, N., et al. 2020, MNRAS, 497, 3118
Huang, W. J., & Wang, H. G. 2020, ApJ, 905, 144
Hui, C. Y., Seo, K. A., Lin, L. C. C., et al. 2015, ApJ, 799, 76
Hulse, R. A., & Taylor, J. H. 1974, ApJL, 191, L59
Hulse, R. A., & Taylor, J. H. 1975, ApJL, 195, L51
Jessner, A., Popov, M. V., Kondratiev, V. I., et al. 2010, A&A, 524, A60
Jiang, L., Li, X.-D., Dey, J., & Dey, M. 2015, ApJ, 807, 41
Jiang, P., Yue, Y., Gan, H., et al. 2019, Science China Physics, Mechanics, and Astronomy, 62, 959502
Jiang, P., Tang, N.-Y., Hou, L.-G., et al. 2020, RAA (Research in Astronomy and Astrophysics), 20, 064
Johnston, S., Hobbs, G., Vigeland, S., et al. 2005, MNRAS, 364, 1397
Johnston, S., Lyne, A. G., Manchester, R. N., et al. 1992, MNRAS, 255, 401
Kaspi, V. M., & Beloborodov, A. M. 2017, ARA&A, 55, 261
Keane, E. F., Ludovici, D. A., Eatough, R. P., et al. 2010, MNRAS, 401, 1057
Keane, E. F., Barr, E. D., Jameson, A., et al. 2018, MNRAS, 473, 116

Keith, M. J., Eatough, R. P., Lyne, A. G., et al. 2009, MNRAS, 395, 837
Keith, M. J., Jameson, A., van Straten, W., et al. 2010, MNRAS, 409, 619
Kijak, J., Lewandowski, W., Maron, O., et al. 2011, A&A, 531, A16
Komesaroff, M. M., Ables, J. G., Cooke, D. J., et al. 1973, Astrophys. Lett., 15, 169
Kramer, M., & Johnston, S. 2008, MNRAS, 390, 87
Kramer, M., Bell, J. F., Manchester, R. N., et al. 2003, MNRAS, 342, 1299
Kramer, M., Stairs, I. H., Manchester, R. N., et al. 2006, Science, 314, 97
Large, M. L., & Vaughan, A. E. 1971, MNRAS, 151, 277
Lazarus, P., Brazier, A., Hessels, J. W. T., et al. 2015, ApJ, 812, 81
Li, D., Wang, P., Qian, L., et al. 2018, IEEE Microwave Magazine, 19, 112
Li, X. H., & Han, J. L. 2003, A&A, 410, 253
Lin, L. C. C., Hui, C. Y., Hu, C. P., et al. 2013, ApJL, 770, L9
Lorimer, D. R. 2011, SIGPROC: Pulsar Signal Processing Programs
Lorimer, D. R., Bailes, M., McLaughlin, M. A., et al. 2007, Science, 318, 777
Lorimer, D. R., Camilo, F., & McLaughlin, M. A. 2013, MNRAS, 434, 347
Lorimer, D. R., Camilo, F., & Xilouris, K. M. 2002, AJ, 123, 1750
Lorimer, D. R., Faulkner, A. J., Lyne, A. G., et al. 2006a, MNRAS, 372, 777
Lorimer, D. R., Faulkner, A. J., Lyne, A. G., et al. 2006b, MNRAS, 372, 777
Lorimer, D., Pol, N., Rajwade, K., et al. 2019, BAAS, 51, 261
Luo, R., Wang, B. J., Men, Y. P., et al. 2020, Nature, 586, 693
Lyne, A. G., & Manchester, R. N. 1988, MNRAS, 234, 477
Lyne, A. G., Shemar, S. L., & Smith, F. G. 2000, MNRAS, 315, 534
Lyne, A. G., Manchester, R. N., Lorimer, D. R., et al. 1998, MNRAS, 295, 743
Lyne, A. G., Burgay, M., Kramer, M., et al. 2004, Science, 303, 1153
Lyne, A. G., Stappers, B. W., Bogdanov, S., et al. 2017, ApJ, 834, 137
Lyon, R. J., Stappers, B. W., Cooper, S., et al. 2016, MNRAS, 459, 1104
Manchester, R. N., Fan, G., Lyne, A. G., et al. 2006, ApJ, 649, 235
Manchester, R. N., & Han, J. L. 2004, ApJ, 609, 354
Manchester, R. N., Hobbs, G. B., Teoh, A., & Hobbs, M. 2005, AJ, 129, 1993
Manchester, R. N., Lyne, A. G., Taylor, J. H., et al. 1978, MNRAS, 185, 409
Manchester, R. N., Lyne, A. G., D'Amico, N., et al. 1996, MNRAS, 279, 1235
Manchester, R. N., Lyne, A. G., Camilo, F., et al. 2001, MNRAS, 328, 17
McConnell, D., McCulloch, P. M., Hamilton, P. A., et al. 1991, MNRAS, 249, 654
McKee, J. W., Stappers, B. W., Bassa, C. G., et al. 2019, MNRAS, 483, 4784
McLaughlin, M. A., Lyne, A. G., Lorimer, D. R., et al. 2006, Nature, 439, 817
Mhaskey, M., Gopal-Krishna, Dabhade, P., et al. 2019a, MNRAS, 485, 2447
Mhaskey, M., Gopal-Krishna, Paul, S., et al. 2019b, MNRAS, 489, 3506
Michilli, D., Bassa, C., Cooper, S., et al. 2020, MNRAS, 491, 725
Mitra, D., & Deshpande, A. A. 1999, A&A, 346, 906
Morris, D. J., Hobbs, G., Lyne, A. G., et al. 2002, MNRAS, 335, 275
Nan, R. 2008, in Society of Photo-Optical Instrumentation Engineers (SPIE) Conference Series, 7012, Ground-based and Airborne Telescopes II, eds. L. M. Stepp & R. Gilmozzi, 70121E
Nan, R., Li, D., Jin, C., et al. 2011, International Journal of Modern Physics D, 20, 989
Ng, C., Champion, D. J., Bailes, M., et al. 2015, MNRAS, 450, 2922
Özel, F., & Freire, P. 2016, ARA&A, 54, 401
Pan, Z., Ransom, S. M., Lorimer, D. R., et al. 2020, ApJL, 892, L6
Patel, C., Agarwal, D., Bhardwaj, M., et al. 2018, ApJ, 869, 181
Phinney, E. S. 1992, Philosophical Transactions of the Royal Society of London Series A, 341, 39
Qian, L., Pan, Z., Li, D., et al. 2019, Science China Physics, Mechanics, and Astronomy, 62, 959508
Qian, L., Yao, R., Sunt, J., et al. 2020, The Innovation, 1, 100053
Rankin, J. M. 1983, ApJ, 274, 333
Rankin, J. M. 1993, ApJ, 405, 285
Ransom, S. M. 2001, New Search Techniques for Binary Pulsars, PhD Thesis, Harvard University
Ransom, S. 2011, PRESTO: PulsaR Exploration and Search TOolkit
Ransom, S. M., Hessels, J. W. T., Stairs, I. H., et al. 2005, Science, 307, 892
Ransom, S. M., Stairs, I. H., Archibald, A. M., et al. 2014, Nature, 505, 520
Reich, W., Fuerst, E., Reich, P., & Reif, K. 1990, A&AS, 85, 633
Ridley, J. P., Crawford, F., Lorimer, D. R., et al. 2013, MNRAS, 433, 138
Robinson, B. J., Cooper, B. F. C., Gardiner, F. F., et al. 1968,

Nature, 218, 1143
Sanidas, S., Cooper, S., Bassa, C. G., et al. 2019, A&A, 626, A104
Shan, S. S., Zhu, H., Tian, W. W., et al. 2018, ApJS, 238, 35
Shao, D.-S., Tang, S.-P., Jiang, J.-L., & Fan, Y.-Z. 2020, Phys. Rev. D, 102, 063006
Shao, Y., & Li, X.-D. 2018, MNRAS, 477, L128
Smits, R., Lorimer, D. R., Kramer, M., et al. 2009, A&A, 505, 919
Spiewak, R., Flynn, C., Johnston, S., et al. 2020, MNRAS, 496, 4836
Staveley-Smith, L., Wilson, W. E., Bird, T. S., et al. 1996, PASA, 13, 243
Stinebring, D. R., Cordes, J. M., Rankin, J. M., et al. 1984, ApJS, 55, 247
Stovall, K., Lynch, R. S., Ransom, S. M., et al. 2014, ApJ, 791, 67
Stovall, K., Freire, P. C. C., Chatterjee, S., et al. 2018, ApJL, 854, L22
Surnis, M. P., Joshi, B. C., McLaughlin, M. A., et al. 2018, MNRAS, 478, 4433
Tan, C. M., Bassa, C. G., Cooper, S., et al. 2018, ApJ, 866, 54
Tange, O. 2020, GNU Parallel 20201022 ('SamuelPaty'), GNU Parallel is a General Parallelizer to Run Multiple Serial Command Line Programs in Parallel without Changing Them
Tauris, T. M., Kramer, M., Freire, P. C. C., et al. 2017, ApJ, 846, 170
Taylor, A. R., Gibson, S. J., Peracaula, M., et al. 2003, AJ, 125, 3145
Taylor, J. H., & Weisberg, J. M. 1989, ApJ, 345, 434
Thorsett, S. E. 1991, ApJ, 377, 263
Tian, W. W., & Leahy, D. A. 2006, A&A, 455, 1053
van Leeuwen, J., Mikhailov, K., Keane, E., et al. 2020, A&A, 634, A3
Vivekanand, M., Mohanty, D. K., & Salter, C. J. 1983, MNRAS, 204, 81P
Wang, B., & Liu, D. 2020, RAA (Research in Astronomy and Astrophysics), 20, 135
Wang, L., Peng, B., Stappers, B. W., et al. 2020a, ApJ, 892, 43
Wang, N., Manchester, R. N., & Johnston, S. 2007, MNRAS, 377, 1383
Wang, N., Manchester, R. N., Pace, R. T., et al. 2000, MNRAS, 317, 843
Wang, P. F., & Han, J. L. 2016, MNRAS, 462, 4416
Wang, P. F., Han, J. L., Han, L., et al. 2020b, A&A, 644, A73
Weisberg, J. M., Boriakoff, V., Ferguson, D. C., Backus, P. R., & Cordes, J. M. 1981, AJ, 86, 1098
Wu, X. H., Du, S., & Xu, R. X. 2020, MNRAS, 499, 4526
Xu, J., & Han, J. L. 2019, MNRAS, 486, 4275
Xu, R. X. 2003, ApJL, 596, L59
Xu, X., Wang, C., Han, J., & Hu, L. 2011, Science China Physics, Mechanics, and Astronomy, 54, 552
Xu, Y., Reid, M., Dame, T., et al. 2016, Science Advances, 2, e1600878
Yao, J. M., Manchester, R. N., & Wang, N. 2017, ApJ, 835, 29
Yuan, J. P., Wang, N., Manchester, R. N., & Liu, Z. Y. 2010, MNRAS, 404, 289
Zeng, Q., Chen, X., Li, X., et al. 2021, MNRAS, 500, 2969
Zhang, L., Li, D., Hobbs, G., et al. 2019, ApJ, 877, 55
Zhu, W. W., Berndsen, A., Madsen, E. C., et al. 2014, ApJ, 781, 117
Zhu, W., Li, D., Luo, R., et al. 2020, ApJL, 895, L6